공 학 박 사 학 위 논 문

Development of Effective Stem Cell Therapy by Cell Surface Modification

세포 표면 개질을 통한 효과적인 줄기세포 치료제 개발

2020년 7월

서울대학교 대학원

공과대학 화학생물공학부

김 현 범

Abstract

Development of Effective Stem Cell Therapy by Cell Surface Modification

Hyunbum Kim
School of Chemical and Biological Engineering
The Graduate School of Engineering
Seoul National University

Stem cell therapy has been emerged as a promising approach to treat various degenerative diseases and impaired organs. Transplantation and direct injection of stem cell have provided a viable solution for congenital defects treatment. However, decline in survival rate and therapeutic effect of administered cells due to physical stress and allogeneic host immune rejection substantially limits the broad applications of cell-based therapy. Consequently, a suitable strategy with general accessibility and versatility is required to determine the fate of stem cell prior to transplantation and

improve therapeutic outcomes.

According to this demand, cell surface modification with natural or synthetic biomaterials is extensively studied as a stem cell therapy technique. Cell functions can be modulated by modifying various bioactive functional groups introduced onto the cell surface through covalent conjugation, hydrophobic interaction and electrostatic interaction. Engraftment of exogenous materials on the cell surface guarantees more stable attachment to cells when they are transplanted into the complex biological environment. In addition, covering the cell surface with polymer chains to cover cell surface antigen provides camouflage effect against T cells, resulting in inhibition of adaptive immune response. Thus, cell surface modification strategies in this thesis will be useful to understand the critical cues for ideal stem cell therapy in the aspects of tissue engineering and translational medicine.

First, I present a facile and universal cell surface modification method that involves mild reduction of disulfide bonds in cell membrane protein to thiol groups. The surface reduced cells are successfully coated with biomacromolecules by maleimide-thiol chemical conjugation for an assortment of applications, including cell visualization, rapid cell assembly, layer-by-layering of cell layer, interaction with surrounding matrix, and localized cell-based drug delivery. No adverse effect on cellular morphology, viability, proliferation, and metabolism is observed. Furthermore, the activities of injected cells in mice can be enhanced via conjugation of polyethylene glycol and immunosuppressant-loaded nanoparticles on the cell surface to overcome acute immune rejection.

Second, I analyzed the biological effect of mesenchymal stem cells (MSC) in

cell surface protein reducing microenvironment. Reduction of surface protein receptors resulted in significant increase of focal adhesion without any adverse effect in cell viability. Eventually, elevation of focal adhesion enhanced early stage of osteogenic differentiation of MSC. Moreover, down regulation of TGF-β signaling pathway was detected as its fundamental cell membrane protein, endoglin, got reduced. Taken together, cell surface protein reducing microenvironment synergistically induced stem cell adhesion and internal cell signaling to up-regulate early osteogenic differentiation.

Finally, I constructed a multilayer hydrogel nanofilm formation strategy which protects cells from high shear stress and reduce immune response by interfering cell-cell interaction. A tough and elastic hydrogel nanofilm was fabricated by modifying two opposite charged polysaccharides to have monophenol functional groups that crosslink each other to form nano-thin hydrogel on the cell surface via tyrosinase mediated reactions. Hydrogel nanofilm encapsulation conducted on β-cell spheroids was applied in the field of islet transplantation. Thin, uniform, and compact film layers on β-cell spheroids achieved cytoprotective effect against physical stress and immune protective effect *in vitro*. Injection into type 1 diabetes mouse model showed blood glucose level regulation significantly effective compare to non-coated groups. Overall, we expect our novel enzymatic crosslinking-based hydrogel nanofilm coating method will provide a new platform for clinical applications of β-cell-based therapy.

Keyword: Cell surface modification, Biomacromolecules, Microenvironment, Cell differentiation, Cell encapsulation

Student Number: 2014-21517

Table of Contents

List of Figures

CHAPTER ONE:

INTRODUCTION

1.1 Overview

The field of stem cell therapies involving direct injection and transplantation have been highlighted in last decades. Although there are a few commercial products, many challenges remain to develop ideal stem cell therapy for each congenital defects and damaged tissues. One of the difficulties is host immune rejection against transplants. Additionally, transplanted cells to retaining biofunctionality and long-term success has not achieved yet. To this end, the final of this thesis is to establish efficient approaches to develop effective stem cell therapy by cell surface modification. Within this objective, surface modification by mild reductant utilized cell surface to achieve various functionality for cell therapy and modulate stem cell surface protein receptors to regulate internal cell signaling pathway. Moreover, encapsulation of cell with nature-derived biomaterials and enzyme was applied. Furthermore, the established surface modified cells area applied in the various animal model to approve functionality for stem cell therapy.

1.2 Organization of the thesis

This thesis consists of six chapters; chapter one is introductions of the thesis, chapter two is scientific background and research progress, and chapter three to five are introducing each strategy of cell surface modification, and concluding remarks are chapter six.

In Chapter one, the overall organization of the thesis is introduced.

In Chapter 2, the scientific background of cell surface modification is described. The materials and chemistry that are the prominent strategies for the development of stem cell therapy using surface modification methods are introduced to suggest rational of this thesis.

Following the background chapter, in Chapter three, I present a general and universal method for efficient labeling of therapeutic cells with multifunctional biomacromolecules. Disulfide bonds in cell membrane proteins are reduced to active thiol groups, and maleimide conjugated biomacromolecules are used to coat mammalian cells via chemical conjugation. Various applications were evaluated with this facile method.

In Chapter four, I investigated biological effects on mesenchymal stem cell in reduced microenvironment. Reduced microenvironment by mild reductant stimulates early osteogenic differentiation of T-MSCs incorporated with increment of focal adhesion and modulation of surface protein receptor mediated cell signaling.

In Chapter five, the synthesis and application of novel hydrogel nanofilm formed by enzymatic crosslinking using tyrosinase with superior reactivity to certain polysaccharide were evaluated. To demonstrate the potential of hydrogel nanofilm, surface coating on β-cell spheroids for blood glucose regulation of type 1 diabetic mice were performed. These will demonstrate the possibility of stem cell transplantation for clinical trial and translational medicine.

Finally, Chapter six illustrates further suggested research ideas from this thesis and summarizes with concluding remarks of the thesis.

CHAPTER TWO:

THE SCIENTIFIC BACKGROUND

2.1 Stem cell therapy in tissue engineering and regenerative medicine

2.1.1 Introduction

Stem cell-based therapies have significant therapeutic potential and present substantial benefits over conventional treatment strategies in various diseases [1]. Consequently, many studies have focused on the development of stem cell-based therapies and investigating their therapeutic potential for the treatment of devastating diseases [2, 3]. In general, stem cells used in stem cell therapies are classified into two categories namely, embryonic stem cells (ESCs) and adult stem cells (ASCs), which include mesenchymal stem cells (MSCs), hematopoietic stem cells (HSCs), and induced pluripotent stem cells (iPSCs) **(Figure 2.1)** [4]. In a group of various stem cell types reported so far, human pluripotent stem cells (hPSCs), including human embryonic stem cells (hESCs) and human induced pluripotent stem cells (hiPSCs), possess the most robust capabilities for self-renewal and differentiation into one or more specialized cell types for regenerating damaged tissue [5, 6]. Even though ESCs and iPSCs are pluripotent, their clinical application has been hindered by ethical issues. Rather than ESCs, ASCs has been considered as the gold standard cell candidate for stem cell therapy [7]. Among ASCs, MSCs can be derived from a patient's own tissue, including

their bone marrow, adipose tissue, cord blood, and tonsils, and show reasonable regenerative potential [8, 9], these cells are the most favored for clinical applications [10]. As the ultimate goal of stem cell-based therapies is to promote the regeneration of tissues/organs damaged by disease, injury, trauma, or aging-associated degenerative disorders [11]. Effective clinical application of stem cell-based therapies is dependent not only on the cell types themselves but also on the transplantation procedures [12]. Thus, establishing approaches to effectively promote stem cell prior to transplantation would greatly improve the outcomes of stem cell therapy.

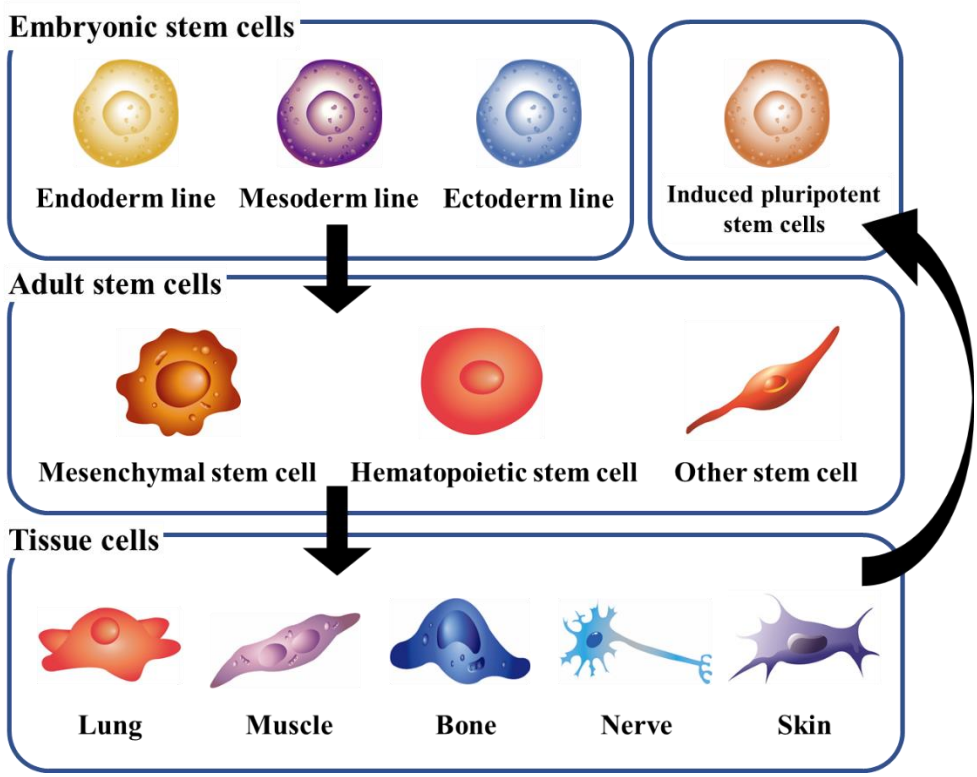

Figure 2. 1 Schematic illustrations of stem cell types used in stem cell therapies

2.1.2 Factors influencing the efficacy of stem cell therapy

As mentioned earlier, even with their pluripotency, clinical applications using ESCs and iPSCs have been hampered by several factors, including safety concerns such as immunological rejection and teratoma formation, as well as ethical issues [13]. Although hiPSCs can be derived from autologous patient-specific resources, and therefore could bypass most immunological and ethical concerns. However, their incomplete fate determination into target-specific cells upon *in vivo* transplantation may cause teratogenic risks due to their pluripotency and self-renewable nature, a problem which remains unsolved [14]. To bypass the risk of ESCs, ASCs with unlimited accessibility and low risk of tumorigenicity were favored [15]. MSCs with capacity to differentiate into various cell types and high expansion capability, generated a great interest as a stem cell source for stem cell therapy. Despite the impressive virtues of MSCs as a potential source for stem cell therapy, they have two main limitations to successful stem cell therapy. The primary limitation is the low survival rates and engraftment of MSCs in the transplanted site. Direct injection of cells causes mechanical stress against the injection pressure and fluidic shear forces, led to necrotic and apoptotic cell death with cell membrane rupture [16]. Even transplanted, MSCs might undergo anoikis as the transplanted MSCs are in single-cells with lack of ECM [17, 18]. Second, transplanted MSCs triggers vigorous inflammatory host immune response, hampering replacement of the damaged tissue cells by MSCs [19]. Therefore, to achieve higher efficacy and functionality of stem cell-based therapeutics, novel cell engineering strategy could be employed to effectively benefit the therapeutic outcomes of stem cell therapy.

2.2 Cell surface modification

2.2.1 Introduction

When stem cells are injected, transfused or transplanted to a patient without any prevention of the environmental stress, it might induce donor cell to death [20], which declares the importance of stem cell engineering to enhance viability, proliferation or differentiation ability to increase the efficacy of stem cell-based therapy. Following its trend, cell surface modification with natural or synthetic biomaterials is rapidly emerging as a cell engineering technique (**Figure 2.2**) [21]. It allows new opportunities in biomedical engineering by using a variety of functional groups and bioactive substances introduced on the cell surface. Cell functions can be modulated by cell surface engineering by modifying various bioactive functional groups on the cell surface such as cellular receptors and their ligands through covalent conjugation, hydrophobic interaction and electrostatic interaction [22]. One of the key applications includes cell adhesion and migration by exposing exogenous ligands into the cell membrane. Introduction of cell surface glycosylation can also regulate cell microenvironment (**Figure 2.3**) [23]. Coating biopolymer on the cell surface, it can work as a safeguard by camouflaging the donor cells against the donee's immune system, as it is especially important in stem cell-based therapies for prolonged *in vivo* persistence and functionality (**Figure 2.4**) [24]. Moreover, these biomolecules and components can enhance modified donor cell longevity, proliferation and therapeutic potential. Thus, cell modifications can be applied to enhance the therapeutic potential of cell products in clinic.

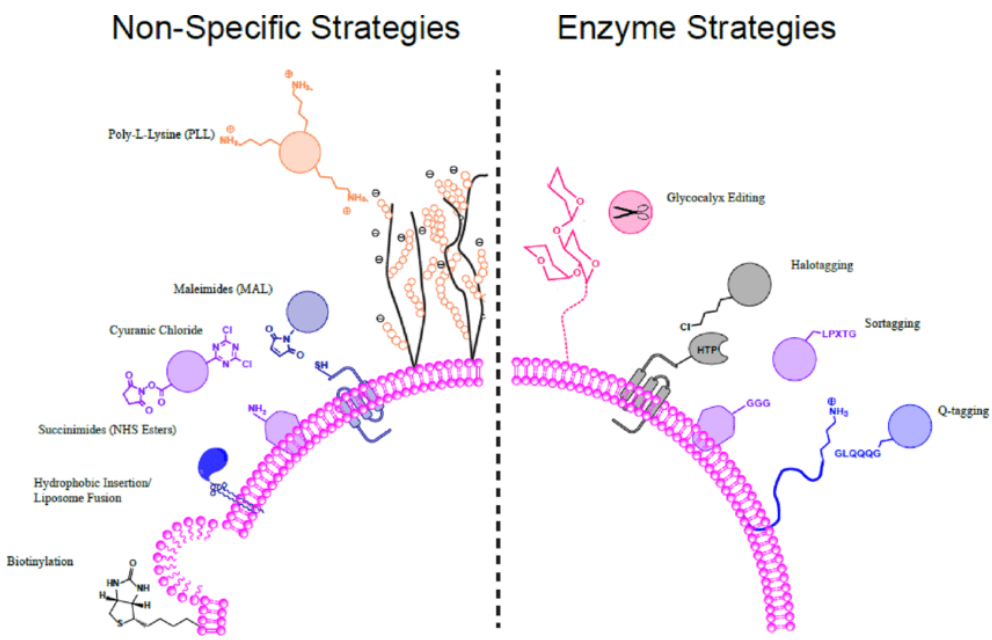

Figure 2. 2 Overview of non-specific and specific (Enzyme) strategies currently used in cell surface engineering.

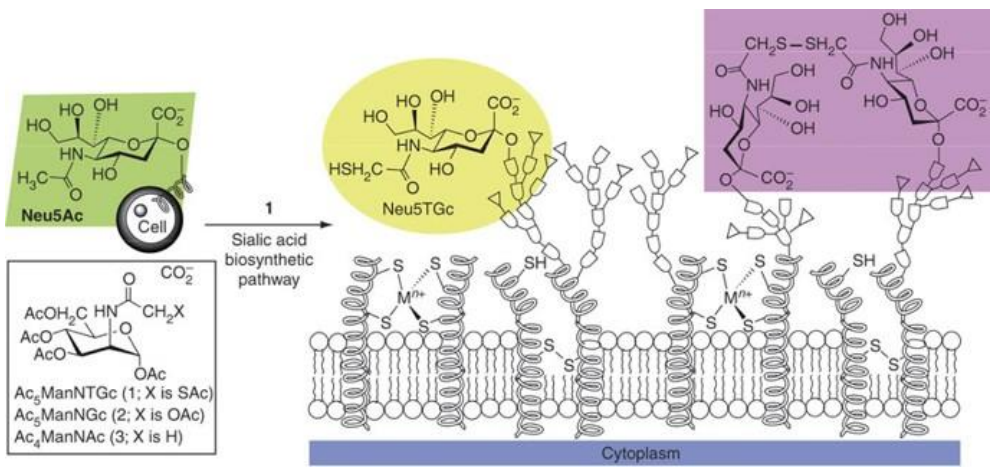

Figure 2. 3 Metabolic expression of thiols on cell-surface through the sialic acid biosynthetic pathway.

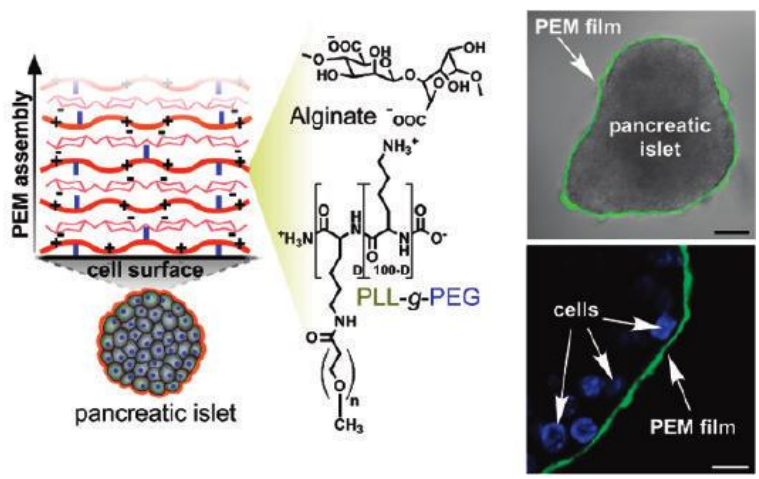

Figure 2. 4 Scheme illustrating the design of cell surface-supported PEM films. PLL-g-PEG copolymers simultaneously facilitating layer-by-layer self-assembly of PEM films directly on the surface of cells.

2.2.2 Types of cell surface modification in cells

For stem cell therapy applications, there are criteria for developing clinically available stem cell surface engineering strategies. As cell surface is not a static structure, but rather is dynamic state, modifying the cell surface is in fact, complicated [25]. At first, cell surface engineering should minimize alterations in microenvironment of engineering primary cells. Small changes in pH, temperature and serum starvation can effects on cell viability and differentiation ability [20]. Also, considering the complexity and membrane fluidity of the cell membrane, surface engineering without inhibiting or blocking the surface molecules by modifying cell membrane surface proteins, glycolipids and polysaccharides, can be a dilemma. Since cell functions, such as cell signaling, proliferation, adhesion and migration mainly depend on these parameters, several strategies [26], which are discussed in detail below **(Figure 2.5)**, have been established to stabilize and retain function of surface engineered stem cells to work as a suitable tissue regeneration therapy.

Among the strategies, cell surface proteins, which contain cysteine residues with thiol groups in their primary structures, exposed towards the extracellular matrix may be a useful active targeting site for modifying cell surface by covalently conjugating molecules to exofacial thiols [27]. Studies shown modified biomolecules can be attached to free thiols on the surface to create reducible disulfide bonds. The key advantage of chemical conjugation is the broad applicability. Biomaterials functionalized with cross-linkers can be used to modify variety of cells with more selective attachment. Even though conjugated biomaterials gradually disappear over time because of the proliferation and endocytosis of cells, modifications connected

through covalent conjugation are stable compare to other non-covalent methods. Additional concern will be difficulty in controlling the degree of modification, usually gets high degree of modification that may cause significant physiological alterations, such as reduction of membrane mobility and diffusion kinetics to the modified cells.

Representative for cell surface modification in non-covalent methods is using electrostatic interaction between the negatively charged cell surface and positively charged biomolecules. This method is beneficial as cells initially modified with cationic polymers can be engineered again via a layer-by-layer technique by sequentially applying anionic and cationic polymers **(Figure 2.6)** [28]. With the ability to add additional polymeric layer, it can reduce molecular recognition which has been often investigated in the cell transplantation research, which layered cells are protected from the sheer stress and immune response [29]. Moreover, thickness of the polymer layer can be controlled by changing the number of layers and the new surface properties of the modified cells rely on the polymer characteristics of the outermost layer. However, it should be noted that high charge density of cationic polymers significantly reduces the viability of modified cells which should be resolved in order to be used in cell therapy.

Lastly, through hydrophobic interaction, amphiphilic polymers composed with long alkyl chains, such as phospholipid-conjugated poly ethylene glycols and poly(vinyl alcohol), can be modified on the cell surface **(Figure 2.7)** [30]. Like chemical conjugation, hydrophobic interaction with lipid-conjugated biomaterials can modify a large number of different cell types. Commercially used cell membrane dye products such as Dil, DiD, DiR, and DiO are developed upon hydrophobic interaction.

Advantage of using hydrophobic interaction is that it allows membrane-anchored bioactive molecules to participate in the dynamic movement of cell membrane, which were embedded in the lipid bilayer able to diffuse laterally within the lipid bilayer, unlike covalent conjugation and electrostatic interaction. Most importantly, cells modified with lipid-conjugated biomaterials showed negligible toxicity with rapid modification, the modified cells resumed normal cellular activities. Although hydrophobic interaction seems reasonable, the fate of the lipid-conjugated bioactive molecules has not been fully understood, and the exclusion pathway requires further investigation.

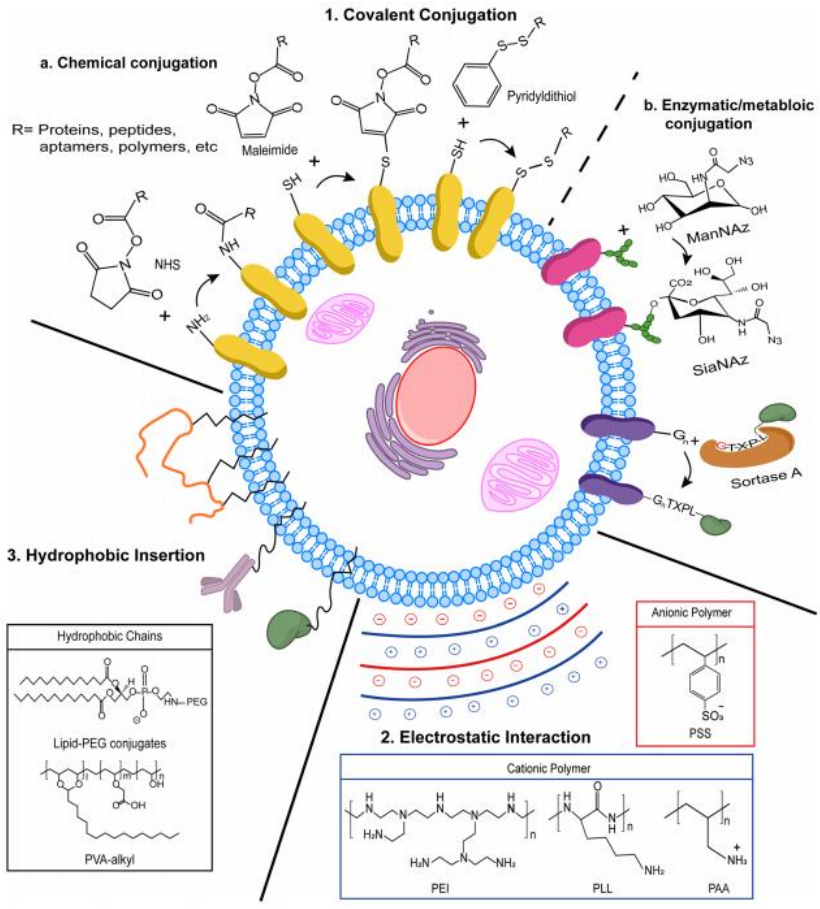

Figure 2. 5 Schematic illustrations of modes of cell surface modification techniques. Cell surface modification with biomaterials through chemical covalent conjugation, electrostatic interaction and hydrophobic interaction.

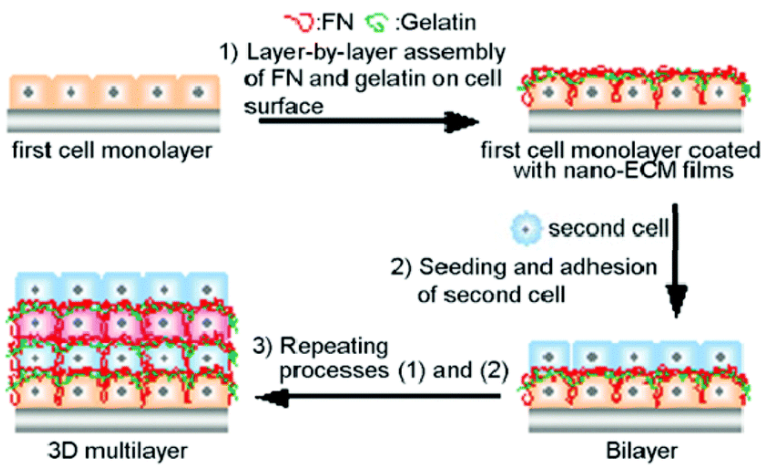

Figure 2. 6 Fabrication process of 3D cellular multilayers composed of cells and nano-ECM films. The nano-ECM films were composed of FN and gelatin, and the outermost surfaces of all films were FN, which allowed cell adhesion.

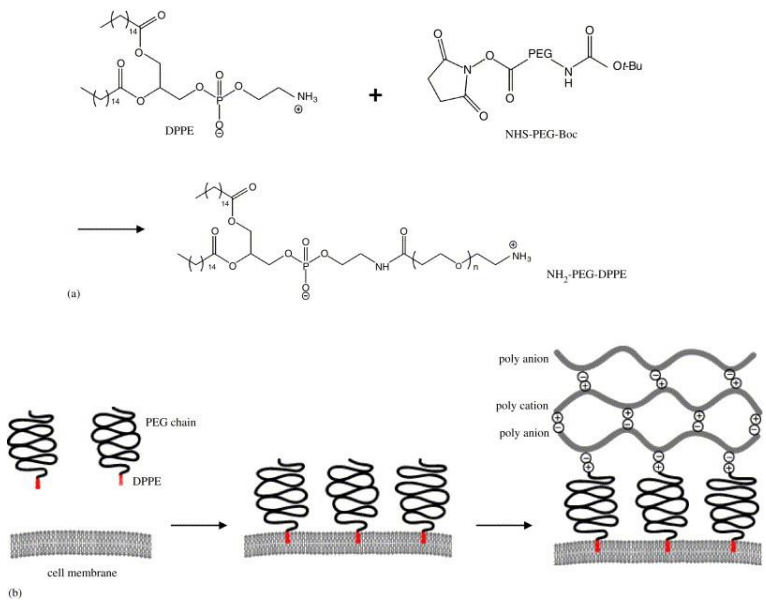

Figure 2. 7 Illustration of PEG-lipids and incorporation into the cell membrane. (a) Synthesis of PEG-lipids. (b) Incorporation of PEG-lipids into cell membrane.

2.2.3 Current cell surface modification systems and their limitations

Apart from molecular biological techniques to genetically engineer cells, modifying cell surfaces with natural or synthetic biomacromolecules become a powerful approach for expanding the structural repertoire and properties of cells **(Figure 2.8)**. In recent years, modifying cell membrane with bioorthogonal chemical groups have been devised for the control of ligand presentation on cell surfaces [31]. Taking advantage of metabolic labelling approach and bioorthogonal click reaction, tailoring cell membrane to achieve photo-driven host–guest recognition by enriching cell surface with the azide tag **(Figure 2.9)** [32]. The aggregation and dispersion of cells were mediated by a fully reversible photo-responsive molecular recognition process. Feature associated with this method was stimuli-responsive host-guest recognition. However, incubating cells to decorated cell surface with metabolic labelling takes longer time that it may not be suitable for primary cell transplantation whereas shortage of time is a major requirement. Also, as functional groups on the cell surface are stricted in one approach, limited application can be available.

To satisfy the time shortage and utility of the modification method, controlled radical polymerization (CRP) techniques have been shown to offer viable routes to polymer–biomolecule conjugates, especially for systems that are sensitive to chemical damage. By using the photoinduced electron transfer-reversible addition fragmentation chain-transfer polymerization (PET-RAFT) method [33], cell surface-initiated controlled radical polymerization could be obtained and coat the cell with polymer within 5 minutes **(Figure 2.10)** [34]. Well-defined high density glycopolymers could be directly

initiated from the cell surface without compromising cell viability. By controlling the spatial and temporal distributions of these glycopolymers, manipulating cell-cell interaction can be achieved.

Moreover, synthetic nanomaterials have a significant role to play in cell surface engineering, due to their unique properties and ability to provide functionality beyond that achievable by single molecules. Chemical modification of the nanoparticle (NP) surface can promote adhesion of NPs to cells. The interaction between NPs and cells is governed by the NP surface characteristics such as surface charge, polymer density, and nature of the inorganic NPs [35]. Because NPs are mainly internalized into the cells through endocytosis [36]. To overcome the internalization, carboxylates, amine, sulfate, or zwitterionic ligands contribute to the stable dispersion of NPs on the cell surface, for example, thiol groups on the T cell, B cell, and hematopoietic stem cell surface enable attachment of liposome NPs to the cell surface through a strong covalent bonding **(Figure 2.11)** [37]. Electrostatic and electrodynamic properties of NPs also can modulate NP adhesion. Most animal cells have a negatively charged surface that preferentially attracts positively charged NPs. The effective surface charge density of NPs determines their electrostatic interaction with cells [38].

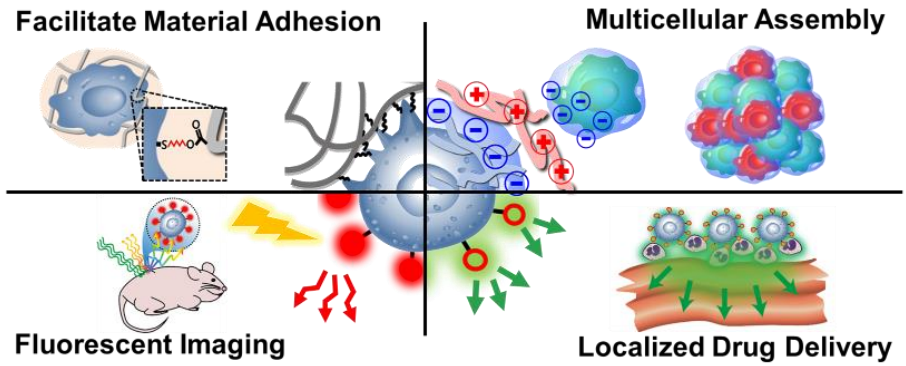

Figure 2. 8 Schematic illustrations of applications using cell surface modification.

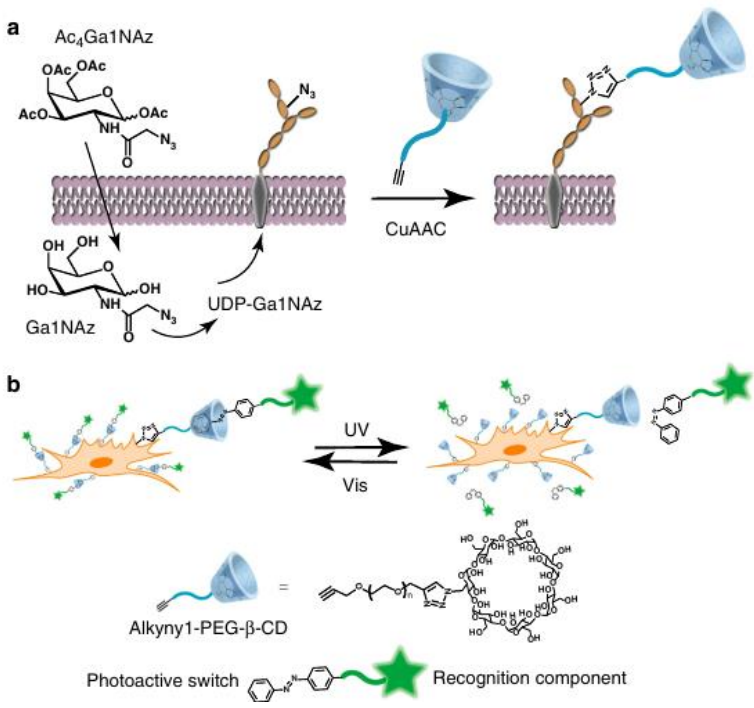

Figure 2. 9 Schematic illustration of engineering photo-responsive host-guest recognition on cell surfaces.

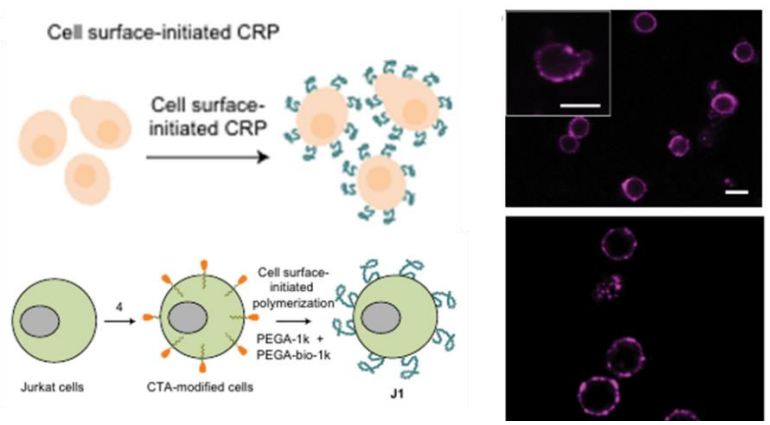

Figure 2. 10 Controlled radical polymerization method, a biocompatible technique for cell surface-initiated polymerization on cell surfaces.

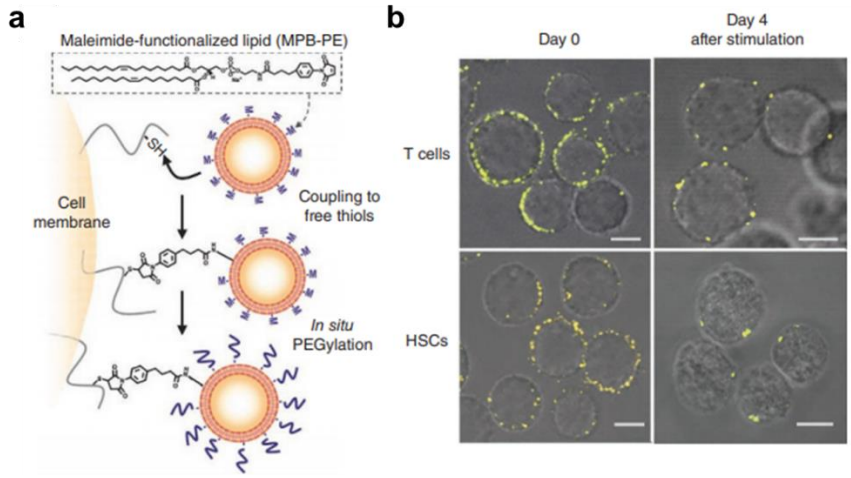

Figure 2. 11. Stable conjugation of NPs to the surfaces of cells via cell-surface thiols.

2.2.4 Application of cell surface modification *in vivo*

As described before, transplanted cells show poor engraftment and survival rate in the injected tissue. Thus, efficient *in vivo* delivery to the targeted tissue by cell encapsulation has been studied abroad. Encapsulation of single cells in a thin hydrogel layer could offer precise microscale control in assembly of complex tissue mimics and provide the appropriate matrix cues for producing desired biological phenomena of encapsulated cells [39]. Encapsulation with alginate microgels containing cells generated by a water-in-oil emulsion, resulted in uniformly coated single cells protected from shear force and immune clearance secreting factors into circulation in a more sustained manner **(Figure 2.12)** [40]. The injected microgels did not cause any adverse effect on overall health of the recipients after intravenous injection to mouse. The results suggest that decreasing material-to-cell volume ratio does not diminish steady-state cytokine diffusion from cells in gels, but rather enhances the reactivity to exogenous stimuli of transplanted encapsulated cells.

Imaging is another critical factor during transplantation for determining the location and quantity of stem cells as well as distribution during tissue repair [41]. Tracking implanted cells requires labeling prior to injection. Cells can be genetically modified to express fluorescent protein so that they can be distinguished within tissue, but these cells can only be tracked by fluorescence imaging. Moreover, cellular activity might be lost during transfection and exogenous protein expression. Imageable NPs can be bounded to chemical receptors on the stem cell surface specifically via bio-orthogonal copper-free click chemistry [42]. Then NP labeled stem cells could be continuously tracked by non-invasive optical imaging over 15 days. Furthermore, it

could be efficiently visualized using *in vivo* MR and CT imaging **(Figure 2.13)** [43]. This labeling method had no adverse effects on stem cell functions, such as viability, proliferation, and differentiation ability, and presented the high contrast at the transplanted site *in vivo*.

4

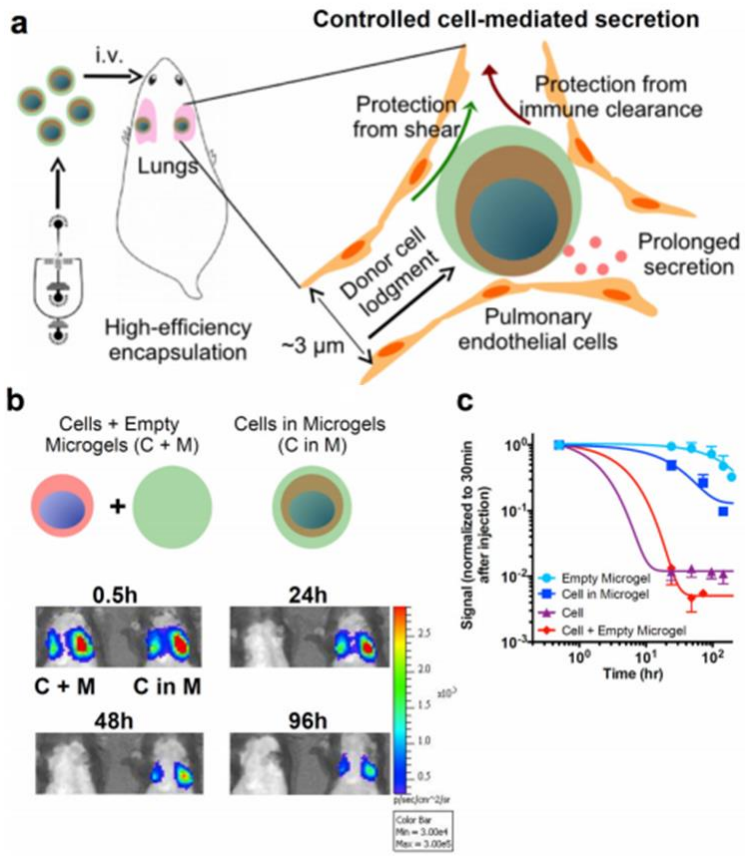

Figure 2. 12 Microgel encapsulation of single cell injected intravenously for demonstrating prolonging *in vivo* residence time of donor cells and systemic levels of secreted soluble factors after injection.

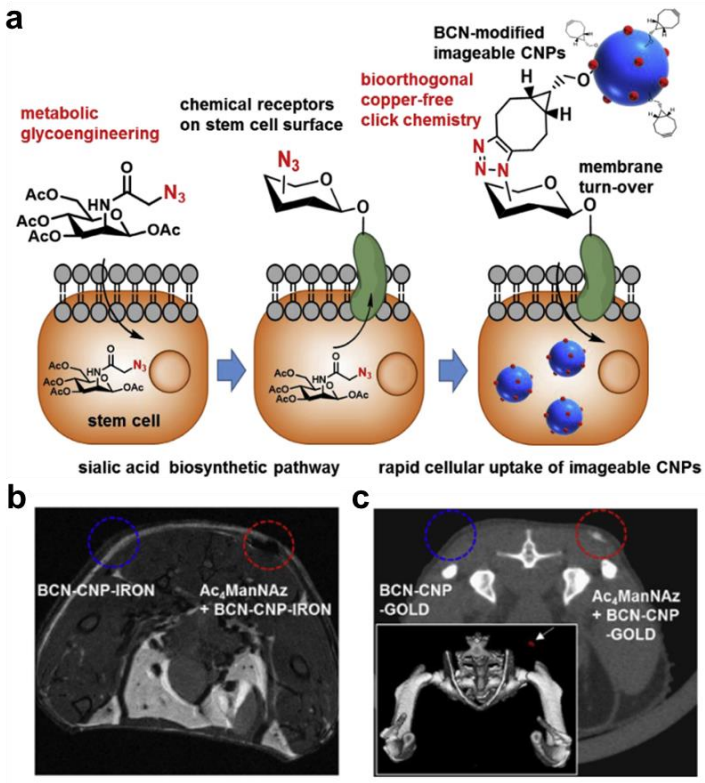

Figure 2. 13 Stem cell labeling and tracking strategy involving NP and bio-orthogonal click chemistry.

CHAPTER THREE:

CELL SURFACE MODIFICATION VIA REDOX REACTION OF DISULFIDE BONDS

3.1 Introduction

Cell-based therapies involving transplantation and direct injection have provided a viable solution for the treatment of congenital defects and damaged tissues [44, 45]. However, decline in survival rate and therapeutic effect of administered cells due to allogeneic host immune rejection substantially limits the extensive applications of cell-based therapy. Consequently, a suitable method is required to track and monitor the administered cells to evaluate the efficacy of cell therapy.

Hence, incorporation of biomaterials and nanomaterials in cells has been spotlighted in cell-based therapies as a strategy to provide therapeutic cells with a protective layer or to tag them with imaging probes [34, 40, 46-48]. In addition, incorporating drug-loaded nanoparticles is expected to enhance the efficiency of drug delivery because of their targeting capability [31, 49, 50].

One of the main approaches for the incorporation of exogenous materials is cell surface modification via chemical conjugation to functional groups in the cell membrane proteins [51-53]. Compared to other cell surface engineering methods, this

approach enables direct engraftment of various materials, and guarantees their stable attachment to cells when they are implanted into the complex biological environment. This conjugation-based surface engineering allows modifying individual cells uniformly and stabilizing them without aggregation, unlike electrostatically driven cell coating.

Because the approach does not involve hydrophobic interaction, it broadens the selection of available materials without compromising the solubility and stability of the exogenous materials [54]. On the basis of the well-established bioconjugation techniques, the procedure is generally accessible without additional preparation steps or special equipment such as microfluidic devices.

Despite the advantages of conjugation-based modification, the introduction of active functional groups on the cell surface remains challenging because most cell surfaces do not contain chemically reactive moieties [55]. Although amide coupling has been employed, cross-coupling between carboxylate and amine groups potentially decreases both efficiency and specificity of the reaction between coating materials and cell surface [56-58]. There are several reported methods to introduce non-natural functional groups such as ketone and azide on mammalian cell surfaces via glycoengineering [59-61]. However, this process takes several days to express these functional groups and to confirm their expression.

Herein, we report a facile and universal method for cell surface engineering that involves mild reduction of disulfides in cell surface proteins with tris(2-carboxyethyl)phosphine (TCEP) and subsequent thiol-maleimide conjugation. A

variety of cell types can be coated without any adverse effect on cell functions. This method can coat biomolecules and polymers to demonstrate rapid formation of multicellular assembly and facilitation of cell adhesion to a polymeric scaffold. Multifunctional nanoparticles can be attached to cell surface for tracking the administered cells and simultaneously delivering adjuvant drugs. Finally, synergistic enhancement of cellular activity is achieved through a dual coating of polymer and nanoparticles.

3.2 Materials and methods

3.2.1 Cell culture and preparation

Human bone marrow-derived mesenchymal stem cells (hMSCs) were purchased from Lonza (Walkersville, MD, USA). Induced neuronal stem cells were obtained from human fibroblast (C-013-5C, Thermo, USA) as previously reported [62]. HeLa, Jurkat, C2C12, and neuro-2A cells were purchased from the Korean Cell Line Bank (Korea). All cells, except induced neuronal stem cells, were cultured in tissue-culture plates with high-glucose Dulbecco's modified Eagle's medium (DMEM; Gibco-BRL, USA) containing 10% fetal bovine serum (FBS; Gibco-BRL), 1 % L-glutamine (200 mM, Gibco-BRL), and 1 % penicillin-streptomycin (10,000 U/ml of penicillin and 10,000 g/ml of streptomycin, Gibco-BRL). Induced neuronal stem cells were cultured in neurobasal medium (Gibco-BRL) containing 1 % penicillin-streptomycin, 1 % glutaMAX (Gibco-BRL), B27 supplement (Gibco-BRL), N2 supplement (Gibco-BRL), bFGF (20 ng/ml, PeproTech, USA), and EGF (20 ng/ml, PeproTech). The cells were incubated at 37 °C under a humidified atmosphere of 5 % CO_2. When the cells reached 80 % confluency, they were washed twice with phosphate-buffered saline (PBS; pH 7.4, Gibco-BRL). For experiments using detached cells, trypsin-ethylenediaminetetraacetic acid (EDTA) solution (0.25% trypsin, 380 mg/L EDTA-$^4Na \cdot 2H_2O$; Gibco-BRL) was added to the culture plate, which was then incubated at 37 °C for 3 min. After the cells were detached from the plate, growth media was added for neutralization. The cells were collected by centrifugation (266 x g for 5 min) and washed twice with PBS.

3.2.2 Tris(2-carboxyethyl)phosphine (TCEP) treatment

Cells at a density of 2×10^6 cells/ml were collected in 1.7-ml tubes by centrifugation at 300 x g and suspended in 1 ml of PBS containing 0.5, 1, 2, or 3 mM of TCEP (Sigma-Aldrich, USA). Then the samples were incubated at 37 °C for 20 min. After incubation, the cells were washed with PBS twice. For the certification of free thiols, Ellman's assay (5,5-dithio-bis-(2-nitrobenzoic acid), Thermo, USA) was performed following the manufacturer's procedure. The cell viability was measured by Live/Dead® viability/cytotoxicity kit (Thermo).

After treatment, Live/Dead assay was used to indicate live cells and dead cells. The cells were subsequently imaged via fluorescence microscopy (EVOS® Cell Imaging Systems, Thermo) and counted in separate 5 fields. For proliferation, cells were stained using the ClickiT® EdU Alexa Fluor® 488 Imaging Kit (Thermo). Prior to EDU assay, cells were cultured overnight in serum free media for the synchronization of cell growth. After synchronization, cells were treated with reductant and incubated in EdU containing growth media for 3 hrs. Then, EdU assay kit was applied to indicate cells in S phase and analyzed by flow cytometry. To assess cell metabolism, cells were incubated with the growth media containing the alamarBlue® Cell Viability Reagent (Thermo). The relative absorbance difference was measured on same time each day. For morphological analysis, cells were fixed with 4 % PFA (paraformaldehyde, Sigma-Aldrich) for 10 min and permeabilized with Triton X-100 (Sigma-Aldrich) for 10 min. Fixed cells were stained with DAPI (Thermo) for 10 min and Alexa Fluor® 594 Phalloidin (1:200 dilution, Thermo) for 2 hrs.

3.2.3 Maleimide Alexa Fluor 488 (MFluor) Coating

After TCEP treatment, HeLa cells were washed with PBS twice. Then, Alexa Fluor® 488 C_5 Maleimide (MFluor; 1 mg/ml, Thermo) was diluted in PBS solution (final concentration: 3 μg/ml) and added to the cells, which were then incubated for 20 min in an incubator at 37 °C. During incubation, the tubes were tapped every 5 min. After 20 min, the cells were washed with PBS twice and analyzed by confocal microscopy (LSM 780; Carl Zeiss) and flow cytometry (FACS Aria II; BD Biosciences, USA). For confirmation of surface coating, the PKH26 Red Fluorescent Cell Linker Kit (PKH26; Sigma-Aldrich) was used. For flow cytometric analysis, a fluorescein isothiocyanate (FITC) standard signal was set.

3.2.4 Cell differentiation and assay

For C2C12 differentiation, cells were cultured in a DMEM containing 2 % of horse serum (Gibco-BRL) and 1 % penicillin-streptomycin for a week. For neuro-2a differentiation, cells were cultured in low-serum (2 % FBS) DMEM medium with retinoic acid (0.1 μM) for a week. Both types of cells were fixed with PFA, permeabilized with TritonX-100, and stained with DAPI and Alexa Fluor® 594 Phalloidin (1:200 dilution). For osteogenic differentiation of hMSCs, cells were cultured in DMEM supplemented with 10 % FBS, 1 % penicillin-streptomycin, 50 mg/ml L-ascorbic acid (Sigma-Aldrich), 10 mM glycerol-2-phosphate (Sigma-Aldrich), and 100 nM dexamethasone (Sigma-Aldrich) for 14 days. For astrocyte differentiation, induced neuronal stem cells were cultured for 2 weeks in DMEM containing N2 supplement, 1 % glutaMAX, and 1 % FBS. For neuron differentiation, induced neuronal stem cells were cultured for 2 weeks in a 1:1 mixture of neurobasal medium and DMEM/F12 medium (Gibco-BRL) containing 1 % glutaMAX, B27 supplement, 1

µM of retinoic acid (Sigma-Aldrich), 200 µM of ascorbic acid (Sigma-Aldrich), brain-derived neurotrophic factor (20 ng/µl; Peprotech), glial-cell-line-derived neurotrophic factor (20 ng/µl; Peprotech) and forskolin (5 µM; Sigma-Aldrich).

3.2.5 Alkaline phosphatase (ALP) and Alizarin Red S (ARS) staining

After 14 days of culture, hMSCs were fixed, washed with distilled water, and stained for ALP (Sigma-Aldrich) as previously described [63, 64]. Diazonium salt solution was prepared by dissolving 0.2 mg Fast Blue RR Salt in 1 ml distilled water, after which 33 µl naphthol AS-MX phosphate solution was added. Cells were stained for 45 min and washed twice with distilled water. For ARS staining, 20 mg ARS (SigmaAldrich) was dissolved in 1 ml distilled water, and the pH was adjusted to 4.1–4.2 with 0.1 M ammonium hydroxide. hMSCs were fixed in neutral buffered 10 % formalin solution, stained with ARS solution for 40 min, and washed with distilled water 4 times ARS staining was quantified by measuring the absorbance at 405 nm with a microplate reader (Infinite® 200 PRO).

3.2.6 Immunofluorescence analysis

Differentiated C2C12, astrocytes and neuronal cells were fixed and subsequently immunostained with antibodies against CD325 (C2C12), GFAP (astrocyte) and TUJ1 (neuronal cells) (Abcam, UK). Immunoreactivity was visualized through FITC-conjugated secondary antibodies (Jackson Immuno Research Laboratories, West Grove, PA, USA). Nuclei were counterstained with DAPI, and F-actin was stained with Alexa Fluor® 594 Phalloidin.

3.2.7 Synthesis of maleimide chondroitin sulfate (MCS) and FITC-conjugated MCS (FMCS)

Maleimide-conjugated CS derivative (MCS) was synthesized by dissolving 500 mg of CS sodium salt (Tokyo Chemical Industry, Japan) in 24 ml of PBS. When the CS was fully dissolved by magnetic stirring, 46 mg of N-(3-dimethylaminopropyl)-N′-ethylcarbodiimide hydrochloride (Sigma-Aldrich) and 54 mg of N-hydroxysulfosuccinimide sodium salt (NHS; Sigma-Aldrich) were added, and the mixture was stirred for 20 min. Then, 124 mg of N-(2-aminoethyl)maleimide trifluoroacetate salt (Maleimide; Sigma-Aldrich) was dissolved in 1 ml of PBS and added to the mixture, which was then reacted for 5 h at room temperature. Next, the solution was dialyzed (SnakeSkin™ Dialysis Tubing, Mw cutoff 1 kDa; Thermo, USA) against distilled water for 48 h (distilled water was renewed every 12 h) and freeze-dried for 48 h. Synthesis was determined by ^{1}H-NMR, the proton peak at 6.663 ppm was examined (maleimide proton). ^{1}H-NMR spectra of the polymers were recorded in a base of deuterium oxide (D_2O; Sigma-Aldrich). FITC-conjugated MCS (FMCS) was synthesized in a similar fashion as MCS, except that 2 mg of 5-(aminomethyl) fluorescein, hydrochloride (Thermo) was also added at the time of maleimide addition.

3.2.8 Surface modification with MCS

For cell surface modification with MCS or FMCS, 1 mM TCEP primed HeLa cells were washed with PBS twice. Then, 1 mM (0.756 mg/ml), 5 mM (3.78 mg/ml) and 10 mM (7.56 mg/ml) of MCS (or FMCS) in 1 ml PBS were added to each tube and incubated for 30 min in an incubator at 37 °C, the tube was tapped every 5 min. After

30 min, the cells were washed with PBS twice. Then, 1 ml of MFluor (3 μg/ml) was added to the cells and incubated for another 20 min at 37 °C with tapping every 5 min. Imaging was performed using a confocal microscope (LSM 780; Carl Zeiss). MFluor-treated 1 mM TCEP-primed HeLa cells were imaged as a standard. The ζ-potentials of MCS-coated cells were measured with Nano ZS (Malvern Instruments, Germany). Cell metabolism was measured with alamarBlue® Cell Viability Reagent.

3.2.9 Formation of cell clusters

HeLa cells were labeled with the green 3,3′-dioctadecyloxacarbocyanine perchlorate (DiO) and the red 1,1'-dioctadecyl-3,3,3',3'-tetramethylindocarbocyanine perchlorate (DiI) (both from Sigma-Aldrich). The labeled HeLa cells were coated separately with MCS, and labeled 1.5×10^5 cells/100 μl were added into each well in a 6-well plate with 1:1 ratio into 1.8 ml of 0.005% poly-L-lysine (PLL; 0.05%, Sigma) dissolved in DMEM without serum. The wells had been coated with bovine serum albumin (1 %; MP Biomedicals, USA) to avoid cell attachment. The cells were subjected to shear stress at the rate of 30 rpm for 1 h. Samples without PLL were dispersed in DMEM without serum.

3.2.10 Layer-by-layer (LBL) cell stacking

For LBL cell stacking, a 20-mm-diamater confocal dish was pretreated with 0.1 % gelatin (Sigma-Aldrich) solution at 37 °C incubator for 12 h, and HeLa cells were seeded. When the cells reached 100 % confluency, they were washed twice with PBS. Then, 10 mM MCS solution with 1 mM TCEP was added, and the cells were incubated at 37 °C for 30 min. Then, the cells were carefully washed with PBS, 2 ml of 0.005%

PLL solution was added, and the cells were further incubated at 37 °C for 2 h after the medium was replaced with serum free medium to inhibit the proliferation of first layer of HeLa cells. For the next layer, HeLa cells (2×10^6 cells/ml) were collected in 1.7-ml tubes. The cells were treated with 1 ml of 1 mM TCEP and 10 mM MCS, seeded on top of the PLL-coated HeLa cell layer, and incubated at 37 °C overnight. For the third layer of HeLa cells, previous steps were repeated once more. Imaging was performed using a confocal microscope (LSM 780).

3.2.11 Quartz crystal microbalance (QCM)

Gold was deposited onto a silicon wafer by the thermal evaporation method. Then, a monolayer of thiol groups was deposited on top of the gold substrate by self-assembly using dithiothreitol (DTT, Sigma Aldrich) [65]. DTT (1 mM) in ethanol was heated to 60 °C and reacted with the gold substrate for 30 min. Then, the substrate was gently washed with ethanol, dipped into 10 mM of MCS solution for 30 min, and washed with PBS. Finally, the substrate was dipped into 0.005% PLL solution for 2 h. The substrate was analyzed by QCM (QCM200; SRS, USA) at each process.

3.2.12 Maleimide PEG (MPEG) coating

Maleimide and acrylate bifunctional polyethylene glycol (MPA, MW 2 k; Creative PEGWorks, USA) was coated on the reduced cell surface using 10 % (w/v) MPA solution for 30 min. Coated cells (5×10^5) were neatly dispersed in 50 µl of 10 % PEG-diacrylate solution (w/v) with 0.05 % (w/v) Irgacure 2959 radical photoinitiator (BASF, USA) and photopolymerized using UV light (3.5 mW/cm^2) for 5 min. The gel construct was then incubated in DMEM solution for stabilization of the encapsulated cells. For

cellular morphological analysis, gels were fixed with 4 % PFA for 30 min and permeabilized with Triton X-100 for an additional 30 min. The cells were stained with DAPI (1:200 dilution) and Alexa Fluor® 594 Phalloidin (1:100 dilution), and imaged under a confocal microscope (LSM 780).

3.2.13 Secondary coating

Reduced cells were treated with 10 % (w/v) maleimide-PEG-biotin (MPEGbiotin, 2 kDa; JenKem Technology, USA) solution and incubated for 30 min at 37 °C with tapping every 5 min. After 30 min, the cells were washed with PBS twice. Then, streptavidin-FITC (SigmaAldrich) was added to the coated cells, cell imaging was performed. Both before and after treatment with streptavidin-FITC, cells were imaged by confocal microscopy (LSM 780).

3.2.14 Real-time PCR

Apoptosis test groups were treated with Trizol® reagent and collected in 1.7-ml tube. Chloroform was added and the tube was vigorously shaken by hand for 15 s. After a 10 min incubation at room temperature, the cells were centrifuged (21,055 x g, 20 min, 4 °C). The clear aqueous phase on top was transferred to a new tube and isopropanol was added and mixed. After another incubation at room temperature for 5 min, the cells were centrifuged (21,055 x g, 20 min, 4 °C). The white RNA pellet was collected, washed with 75 % ethanol, dissolved completely in molecular grade water, and denatured for 10 min at 60 °C. The RNA concentration was measured and cDNA was prepared by reverse-transcription using the EZ006M kit (Enzynomics, Korea) according to manufacturer's instructions. Gene expression levels of mesenchymal

(CD73, CD105, and CD45), osteogenic (ALP, OCN, COL-1 and RUNX-2), and neural (MSI-1, Nestin, Pax-6, and Sox-2) markers were determined by real-time PCR using SYBR green PCR Mastermix on a StepOnePlus TM Real-Time PCR System (Applied Biosystems). Complementary DNA samples were analyzed for the gene for interest and for the reference GAPDH.

3.2.15 Preperation of fluorescent mesoporous silica nanoparticles (MSN)

Uniform MSN were synthesized as previously reported with slight modification [66]. Two grams of hexadecyl trimethyl ammonium chloride (cetyltrimethylammonium chloride solution 25 %, 8 ml, Sigma-Aldrich) and 80 mg of triethanolamine were disolved in 20 ml of distilled water. After the solution was heated at 95 °C for 1 h, 1.5 ml of tetraethyl orthosilicate (Acros Organics) was added dropwise. To prepare fluorescently labeled MSN, the pre-conjugated dye-silane derivatives were subsequently added. Reactions were proceeded for 50 min, resulting in turbid solutions, and 50 mg of APTES was added and reacted for 10 min for amino-functionalization of the MSN. The products were collected by centrifugation and re-dispersed with ethanol several times. For extraction of residual surfactant in MSN, the products were dispersed and stirred in 1 wt % of NaCl in methanol at 60 °C for 3 h, and the same extraction process was repeated twice. The final products were dispersed in ethanol at 10 mg/ml.

3.2.16 Attachment of the MSN to mammalian cells

After mild reduction of the cell surface with TCEP at 0.75 mM, the cell suspension was washed several times with PBS and incubated in 5 mg/ml of Mal-MSN solution for 20

min. Subsequently, mPEG2k-SH (methoxy PEG2k-thiol) dissolved in PBS was added to the suspention at a concentration of 1 mg/ml, and incubated for 10 min to deactivate the maleimide groups on the nanoparticles. The MSN-coated cells were separated from residual nanoparticles by centrifugation and then washed with PBS several times. Depending on the imaging device, FITC-, Cy5-, or Cy5.5-labeled MSN was used. For dual-coating with MSN and PEG, 5 mg/ml of mPEG 2 kDa maleimide dissolved in PBS was introduced to the MSN coated-cell suspension. The confocal microscope image were obtained using LSM 780 NLO and Cy5 conjugated MSN. The fluorescence signal difference of cells was measured by flow cytometry by using FITC conjugated MSN (BD Accuri TM C6 Plus Cytometer System; BD Biosciences, USA).

3.2.17 Electron microscopic imaging of coated cells

Electron microscopy samples were prepared by fixation and dehydration. Coated HeLa cells were fixed with 2.5 % of glutaraldehyde and 2 % of PFA in 0.1 M of sodium cacodylate buffer (pH 7.4), then rinsed with cacodylate buffer. Additional fixation was carried out with 1 % osmium tetraoxide in cacodylate buffer. After washing away the residual fixation reagent with distilled water three times, cells were stained overnight with 2 % uranyl acetate solution. Dehydration was done gradually by incubating the stained cells for 10 min in each of 30 %, 50 %, 70 %, 80 %, 90 % ethanol, absolute ethanol, and propylene oxide. The dehydrated cells were suspended in 50 % Spurr's resin with propylene oxide for 2 h, and in Spurr's resin overnight. After fresh Spurr's resin was added to the cell suspension, the resin was hardened in oven at 60 °C for 24 h. The embedded cells were sliced with an ultramicrotome (EM UC7; Leica, Germany). TEM images were obtained with JEM1010 (Jeol, Japan).

3.2.18 Animals and Cells

In this study, we used male BALB/c nude and Crl:CD-1 (ICR) mice weighing 28–30 g (Orient, Seoul, Korea). The animals were maintained at 22–24 °C under a 12-h/12-h light/dark cycle. The mice had at least 1 week of acclimation prior to experiments. The Institutional Animal care and Use Committee at the Korea Basic Science Institute (KBSI-AEC 1601) reviewed and approved this study. All animal procedures were in accordance with the Guide for the Care and Use of Laboratory Animals issued by the Laboratory Animal Resources Commission of KBSI. HeLa-Luc (Xenogen) human cervical adenocarcinoma cancer cells were grown at 37 °C in DMEM (Lonza) containing 10 % (v/v) FBS (Gibco-BRL).

3.2.19 Intravital imaging

For the implantation of a dorsal skin-fold chamber into mouse, two plastic frames were implanted into extended double layers of skin. One layer of the skin was removed in a circular area of approximately 13 mm in diameter. One milligram of rhodamine 123 were loaded to 5 mg of PEGylated MSN and the excess rhodamine dye were removed by washing procedure with PBS. One million of Hela cells were coated with rhodamine 123 loaded MSN using the same method described above. About 20 μl of rhodamine loaded MNP-coated HeLa cells (1×10^4) prepared was implanted at the center of the remaining layer (epidermis, subcutaneous tissue, and muscle). A cover glass (12 mm) was then placed on the chamber. Dorsal skin-fold chambers were examined with an intravital microscope (LSM 780 NLO; Carl Zeiss, Germany, KBSI Chuncheon Center, Korea).

3.2.20 In vivo imaging system

The in vivo fluorescence imaging to track the location of cells was obtained by whole body imaging system using Cy5.5 conjugated MSN coated HeLa-Luc cells. The cells were reduced by 0.75 mM TCEP and incubated in 5 mg/ml of Cy5.5 conjugated Mal-MSN solution for 20 min. About 1×10^6 HeLa-Luc cells were injected subcutaneously in each group. The fluorescence and luminescence were imaged by IVIS200 system (Xenogen Corporation, Alameda, CA, USA) for 0-8 days.

3.2.21 Implanting cells with drug delivery vehicle and protective polymer

The protection and immunosuppression with polymer/nanoparticle coating were evaluated with monitoring subcutaneous injected coated cells. For polymer coating, cells were reduced by 1 mM TCEP and treated with 10 % (w/v) maleimide-PEG (JenKem Technology, TX, USA) solution for 20 min and washed for several times. For MSN coating, after mild reduction of the cell surface with TCEP at 0.75 mM, the cell suspension was washed for several times with PBS and incubated in 5 mg/ml of (dexamethasone)-loaded Mal-MSN solution for 20 min. Dual-coating of cells was conducted with the mixture of 10% (w/v) maleimide-PEG and 5 mg/ml of (dexamethasone)-loaded Mal-MSN solution for 20 min after 0.75 mM TCEP reduction. For the subcutaneous primary tumor model, mice were anesthetized by exposure to 2–2.5% isoflurane, and 100 μl sterile Dulbecco's phosphate-buffered saline containing 1 × 10 7 HeLa-Luc cells were injected into the back of each mouse. To check viability of the Hela-Luc, luciferin was dissolved in PBS (30 mg/ml) and 150 μl of the luciferin

solution was intraperitoneally injected. Cellular activities were monitored on the IVIS200 system for 0–7 days, and the regions of interest were quantified with photon flux (p/s) using Living Imaging software v4.2 (Xenogen Corporation).

3.3 Results and Discussion

3.3.1 Exposure of thiol group on cellular surface

Figure 3.1 describes the surface modification method that consists of mild reduction of disulfides in cell surface protein with TCEP and subsequent thiol-maleimide conjugation. TCEP is nonvolatile and stable in aqueous solution at room temperature over a wide range of pH, and resistant to air oxidation [67]. It can selectively reduce disulfide bonds, but is essentially unreactive toward other functional groups in proteins [68]. Compared to typical thiol-based reducing agents such as dithiothreitol and 2-mercaptoethanol, TCEP does not react with active maleimide groups, retaining the efficiency of cell surface modification.

Fluorescent dye with a maleimide functional group (MFluor) was utilized to evaluate the coating method **(Figure 3.2)**. Fluorescence signals were distributed evenly over the cell surfaces without any evidence of internalization. When the cells were post-labeled with a membrane dye (PKH-26), MFluor signals co-localized with those of PKH-26, confirming that the conjugation takes place solely on the cell surface. Dose-dependent effects of TCEP on HeLa cells were evaluated by flow-cytometric analysis. The reduction reaction dramatically increased the fluorescence of attached MFluor on the cells, which was saturated after treatment with 1 mM TCEP. In quantitative analysis, the ratio of the amount of MFluor to cellular surface area is nearly identical in attached or detached state, indicating that the conjugation evenly occurs regardless of the cellular morphology. Most importantly, no adverse effect on cellular morphology, viability, proliferation, and metabolism was observed for TCEP concentrations equal or below 1

mM, and the reduced thiols are recovered in a single day. Thus, 1 mM of TCEP was designated as the optimal concentration for cell surface reduction.

We further examined the universal and innocuous character of the coating method in other cell types such as Jurkat T, C2C12, Neuro-2a (N2A), human mesenchymal stem cells (hMSC), and human induced neural stem cells (hiNSC) with different cellular morphology, potency, and tissue origins. All cell types were efficiently labeled with MFluor, and no sign of cytotoxicity was observed **(Figure 3.3)**. All cell lines retained their potency, differentiation capability, and functionalities during reduction and labeling steps as optimized for the HeLa cells. The C2C12 and N2A cells cultured in differentiation-inducing media were capable of forming multinucleated myotubes and neurite outgrowth, respectively. hMSC was able to differentiate into osteoblast, and hiNSC differentiated into both astrocyte and neuron **(Figure 3.4)**.

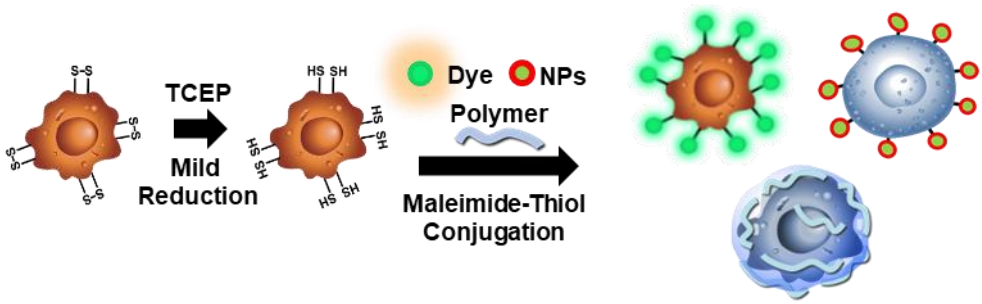

Figure 3. 1 Cell surface modification with fluorescent dye, polymer, and nanoparticles by mild reduction using TCEP.

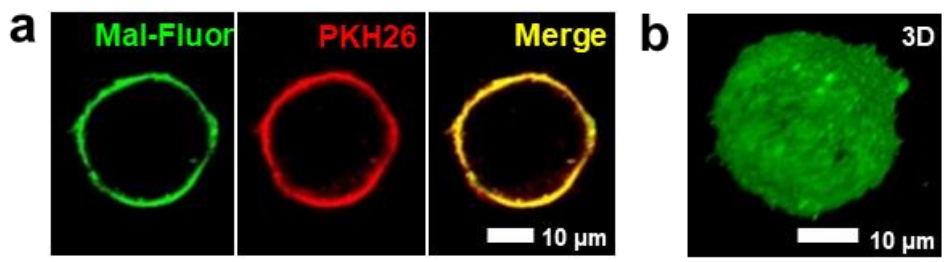

Figure 3. 2 Confocal image of HeLa cell surface coated with a) MFluor and PKH26. b) 3D-rendered image of MFluor-coated HeLa cells.

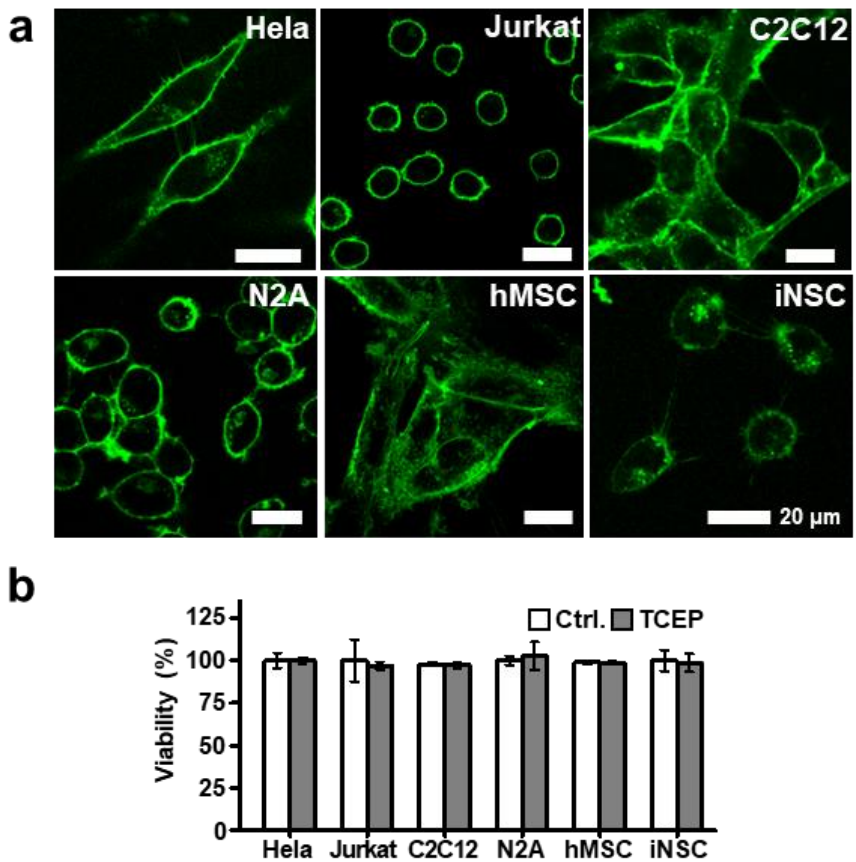

Figure 3. 3. MFluor coating in various types of cells. a) Confocal microscopic images of the indicated cell types coated with MFluor. b) Viability of reduced cells and nontreated cells.

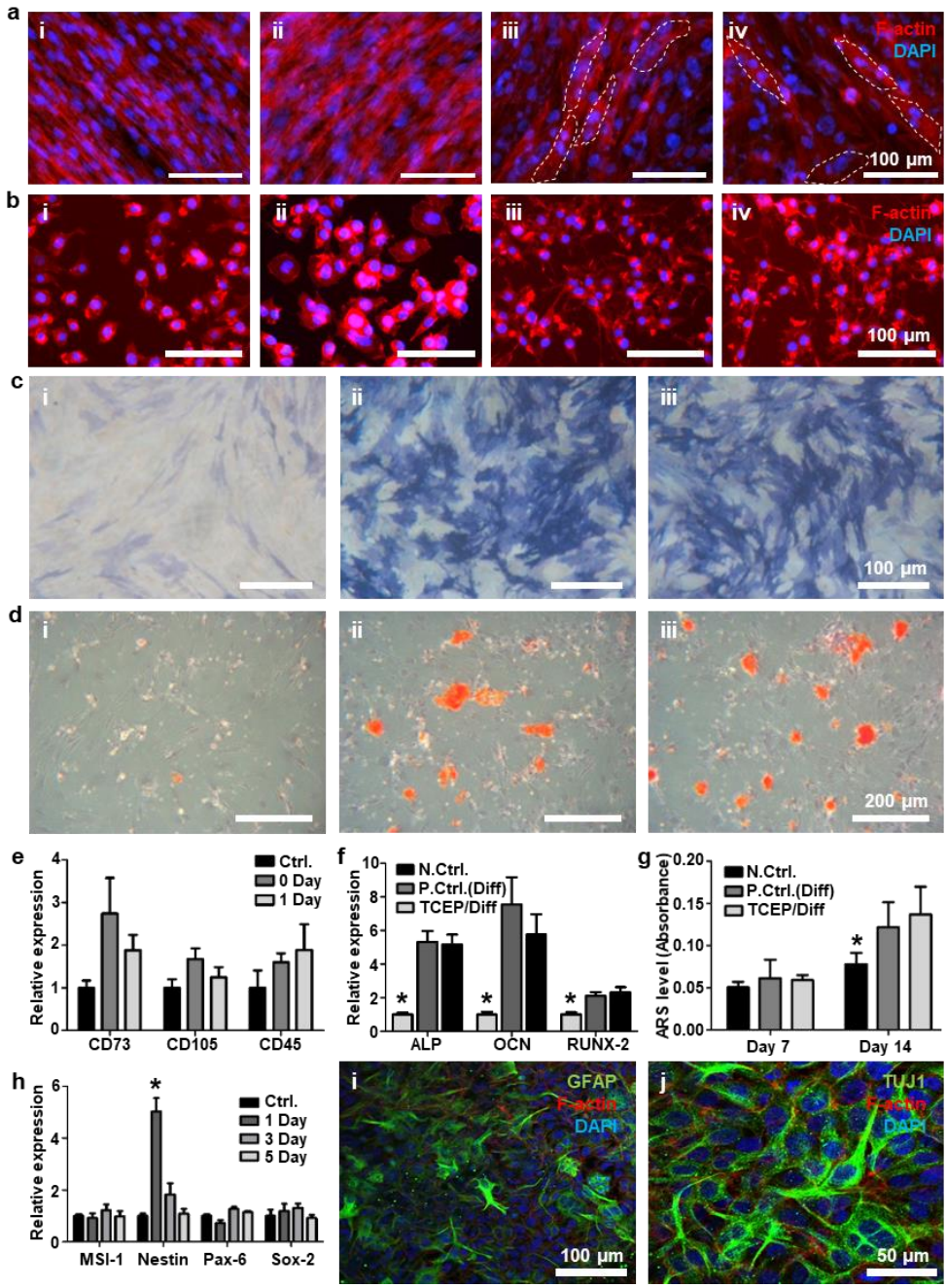

Figure 3. 4 Analysis of differentiation functionality of each type of cells after cell surface reduction. Fluorescence images of a) multinucleous myotube formation of C2C12 cells and b) neurite outgrowth of N2a cells i) non-treated group, ii) surface reduced undifferentiated group, iii) nontreated differentiated group, and iv) surface reduced differentiated group). c) Alkaline phosphatase and d) Alizarin Red S staining images of

hMSC differentiated into osteoblasts. One week of differentiation for Alkaline Phosphatase staining and two weeks of differentiation for Alizarin Red S staining i) non-treated group, ii) non-treated differentiated group, and iii) surface reduced differentiated group). e) qPCR analysis data of mesenchymal stem cell markers of hMSC (n = 4). f) qPCR data of osteogenic markers and g) quantitative analysis of deposited calcium as measured by Alizarin Red S staining of differentiated hMSC with/without surface reduction (*$p < 0.05$ vs. negative control group, n = 4 in (f) and n = 3 in (g)). h) qPCR data of neural stem cell markers of iNSC with/without surface reduction (*$p < 0.05$ vs. negative control group, n = 3). Confocal image of differentiation of iNSC into i) astrocytes and j) neurons. Glial fibrillary acidic protein (GFAP) was stained for astrocyte marker and neuron-specific class III beta-tubulin (TUJ1) was stained for neuron marker. Cells were also stained for F-actin (red) and with DAPI (blue) for cellular morphology.

3.3.2 Biomacromolecules attachment on the cell surface

We applied the method for coating cell surfaces with biopolymer including chondroitin sulfate (CS) and polyethylene glycol (PEG). The biopolymers grafted onto cell surface facilitated cell clustering, cell sheet construction, and manipulation of a scaffold−cell interaction. This modification technique promotes the formation of artificial tissues or complex scaffolds and is expected to induce cellular interplays and enhance adhesion onto polymeric matrices [69]. Reduced cell surfaces could be easily modified with maleimide-conjugated chondroitin sulfate (MCS), without compromising their viabilities **(Figures 3.5 & 3.6)**. MCS on the cell could be observed by fluorescence microscopy using fluorescein isothiocyanate (FITC)-conjugated MCS on HeLa cells **(Figure 3.7)**. MCS-coated HeLa cells retained a highly negative surface charge derived from the inherent characteristics of CS as confirmed by ζ-potential analysis. When cells were additionally treated with poly-L-lysine (PLL), the extra negative surface charge derived from MCS induced rapid cell clustering through electrostatic forces, offering a favorable environment for cell−cell interaction by shortening the distances between the cells **(Figure 3.8)**. In contrast, bare cells formed smaller clusters, with fewer cells being involved in the cluster formation. Without PLL, cells repelled each other via the highly negative MCS-derived charges, preventing aggregation. In addition, we were able to construct a 3-layered layer-by-layer structure by multiple rounds of MCS coated cell seeding and PLL covering as confirmed by quartz crystal microbalance analysis on gold substrate **(Figures 3.9 & 3.10)**. Cells can similarly be coated with functionalized PEG to enhance the cell−material interaction in a PEG hydrogel that is biologically inert, allowing efficient transport of external

nutrients to the encapsulated cells [70]. PEG itself does not provide sufficient cell adhesion to the substrate because of the lack of cell specific binding activity [71]. Therefore, maleimide-PEG-monoacrylate (MPA) was applied onto the cell surface and the cells were incorporated into a conventional PEG diacrylate (PEGDA)-based hydrogel. During scaffold polymerization, the MPA on the cell surface participates in polymerization and induces cell−material interaction. Uncoated cells exhibited globular morphology, whereas MPA-coated cells showed cellular protrusions into the surrounding PEG matrix promoted by the interaction between the acrylates of the MPA and PEGDA **(Figure 3.11)**. Not only single modification but also secondary modification could be achieved via specific bonding between the coated anterior material and the additional posterior material **(Figure 3.12)**.

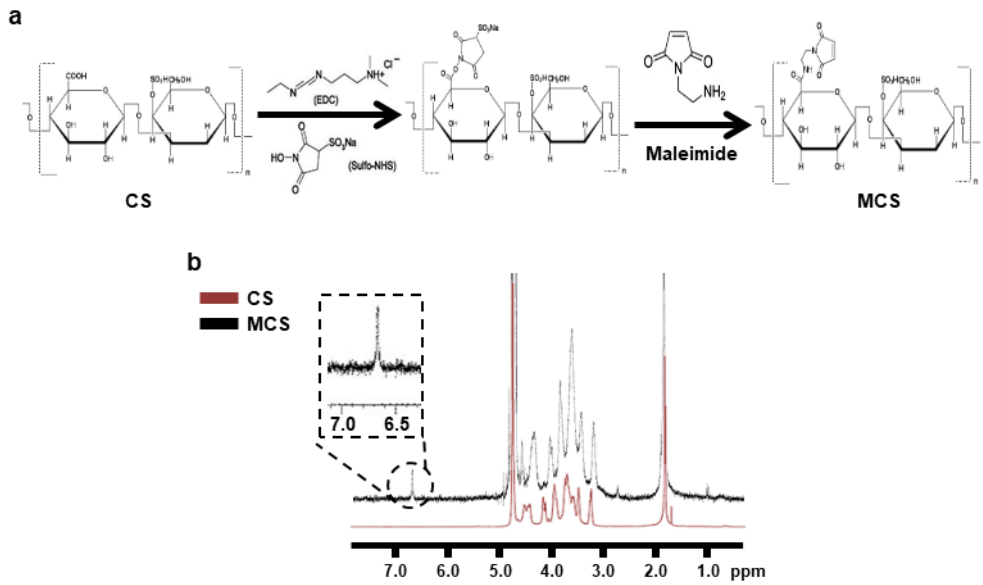

Figure 3. 5 Synthesis of maleimide conjugated chondroitin sulfate (MCS). a) Reaction scheme and b) ^{1}H-NMR spectra of chondroitin sulfate (CS) and MCS. The enlarged proton peak at 6.663 ppm indicates the presence of a maleimide moiety on the MCS.

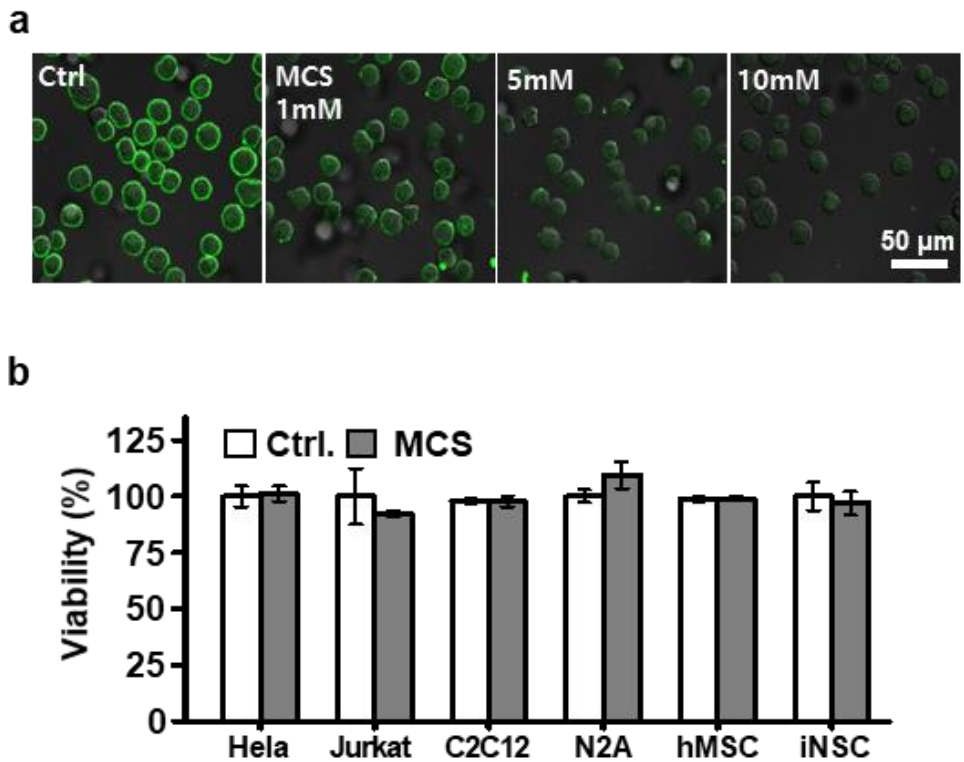

Figure 3. 6 Optimization of MCS coating. (a) Confocal microscopic images of dose dependent MCS coated HeLa cells after MFluor treatment. The fluorescent signals on images are from the MFluor that is attached to the thiol groups remained after MCS coating, and reduction of the fluorescent signals confirms that the coating procedure at 10 mM concentration guaranteed full coating of MCS on the cell surface. (b) Comparison of cell metabolism between with and without MCS coating by alamarBlue assay (n = 3).

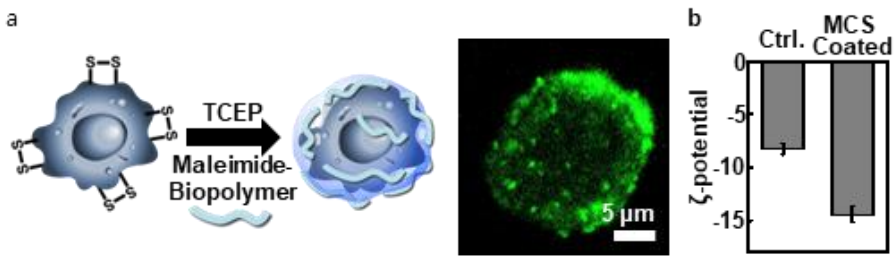

Figure 3. 7 Illustration and confocal image of a) MCS coating surrounding the reduced cell. b) ζ-potential difference between untreated cells and MCS-coated cells (n = 3).

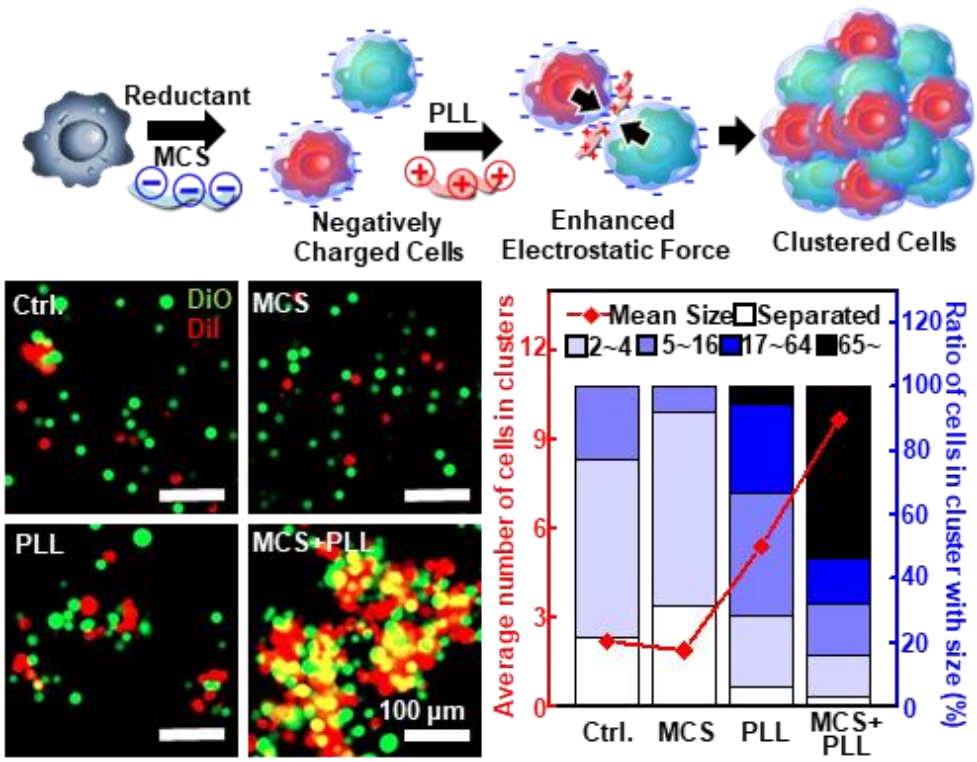

Figure 3. 8 Schematic and fluorescent images of facile development of cell cluster by anionic polymer MCS coated cells (iii,iv) interacting with cationic polymer PLL contrast to non-coated cells (I,ii) (ii and iv are enlarged image of white circle area of i and iii, scale bar: 400 μm).

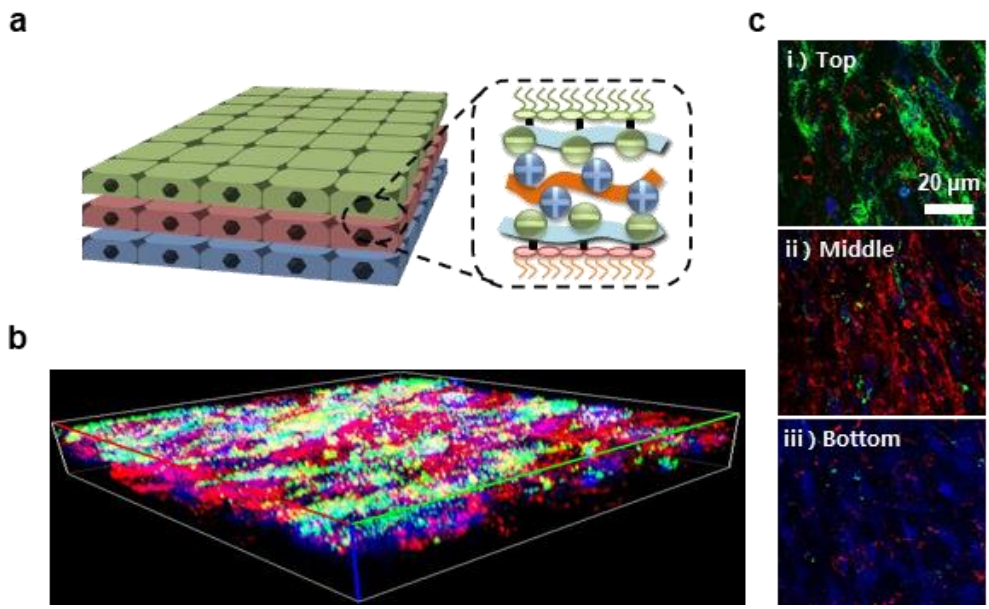

Figure 3. 9 Layer-by-layer (LBL) cell stacking through repeated rounds of biopolymer coating. a) Schematic drawing of an LBL stacked cell sheet formed by the strong electrostatic attraction between the CS and PLL coatings. b) 3D confocal image of the cell sheet. c) XY-plane confocal images of different layers (first layer is stained blue with cell tracker blue, second layer is stained red with PKH26 dye, third layer green fluorescence from GFP-producing HeLa cells).

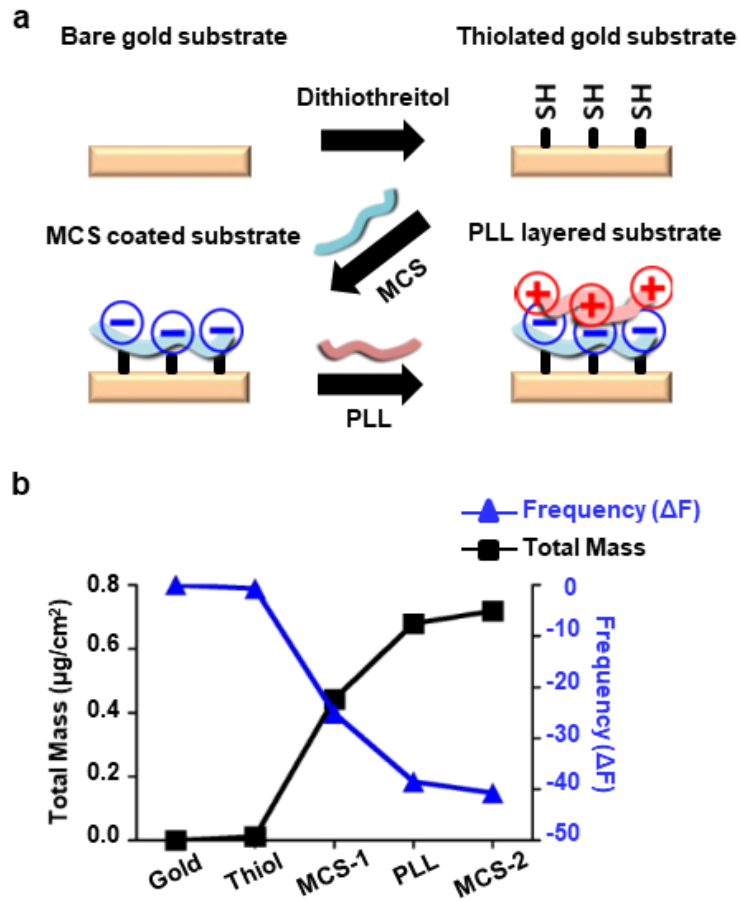

Figure 3. 10 Analysis with quartz crystal microbalance (QCM) a) Schematic images of coating and LBL procedure. b) QCM analysis of polymer LBL, supporting successful LBL generation through the processes of MCS coating and PLL stacking via thiol-maleimide conjugation and electrostatic forces. Accumulated mass was quantified by QCM. As MCS and PLL layers form on the substrate sequentially, the increase in mass was determined from the decrease of frequency, indicating the accumulation of molecules.

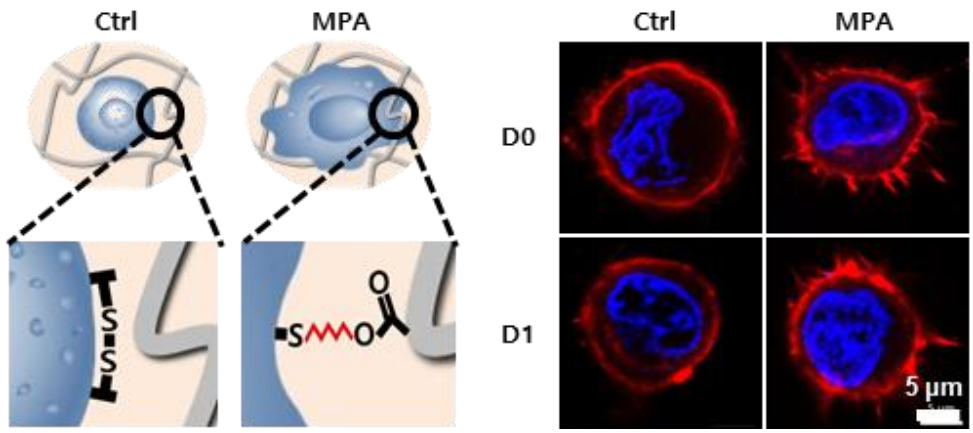

Figure 3. 11 Schematic representation and confocal microscopic images of MPEG-acrylate (MPA) coated HeLa cells individually encapsulated in PEG-diacrylate gel comparison to normal cell encapsulation. MPA coated cells represented cellular sprouting within hydrogel (Blue = DAPI, Red = F-Actin, scale bar: 5 µm).

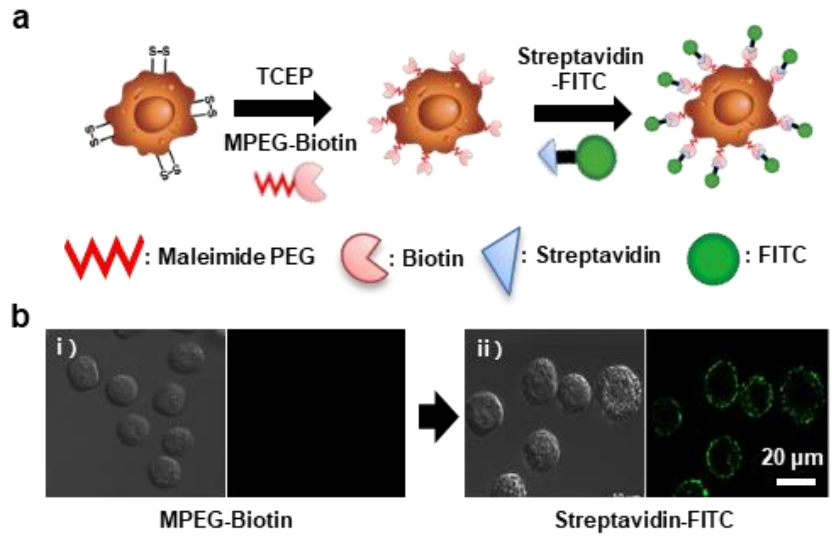

Figure 3. 12 Demonstration of secondary surface coating using additional functional groups attached to coated material. Secondary coating of streptavidin-FITC was able though the specific interaction with biotin modified maleimide-PEG-biotin (MPEG-Biotin). Before adding the streptavidin-FITC, fluorescent signal was not detected around the modified cell surface. Fluorescent signal was obtained after treatment of streptavidin-FITC. a) Schematic representation of secondary coating on the cell surface. b) Confocal microscopic image of MPEGBiotin coated cell before (i) and after (ii) additional streptavidin-FITC treatment.

3.4 Summary

In summary, we demonstrated a universal and innocuous method for cell surface modification to impart various properties of exogenous materials to cells. As this method does not require any additional stabilization and culture step and no adverse effect was observed, it is expected to be used for cell therapy using primary cells, such as cancer immunotherapy and hematopoietic stem cell transplantation. An examination of surface ligands and targeting capacity of cells will be necessary prior to practical therapeutic applications, considering the non-specificity of the reduction process using TCEP. Given the need for incorporation of various materials onto cell surface to monitor cell therapy and to produce artificial tissue, this versatile technique is anticipated to play a key role in next-generation cell-based therapies.

CHAPTER FOUR:

BIOLOGICAL EFFECT OF REDUCED MICROENVIRONMENT TO STEM CELL

4.1 Introduction

Mesenchymal stem cells (MSC) present a promising tool for tissue regeneration, as it holds the ability to self-renew and differentiate into mesodermal lineage [72, 73]. Several studies have been demonstrated to treat skeletomuscular tissue regeneration by utilizing MSCs [74-77]. For the efficacy of these studies, managing MSC differentiation is essential, which is tightly balanced by its microenvironments [78-80]. Regulating microenvironments composition *in vitro* systems of MSCs, such as soluble factors, extra-cellular matrix proteins, physical forces, and cell-cell interactions, have advances in understanding the signals that promote MSCs differentiation [81]. In particular, changes in cell shape, via mechanical cues, can switch MSCs between discrete fates of growth and differentiation [82-84]. Specifically, the cyclic mechanical stretch has been shown to commit MSCs to a myogenic phenotype [85], and also composition, texture, and topography of a material surface modification influence MSCs to differentiate into mature specialized cells, such as osteoblasts and adipocytes [86]. In addition, cellular interactions with neighboring cells have been known to enhance osteogenic and adipogenic differentiation, and the differentiation extends varies with cell-cell contact [87]. As described, researches inducing MSC differentiation by physicochemical control such as cell-cell interaction, designing

suitable mechanical environments, and applying noninvasive physical forces are widely established.

In recent years, our group has demonstrated that the mild surface reducing using TCEP can be achieved. TECP treatment on stem cells allowed reactive thiol groups to be exposed by breaking the disulfide bonds on cell surface proteins [88]. Furthermore, Cha and colleague have demonstrated that creating a reducing microenvironment on metastatic cancer cells activated focal adhesion kinase and prevented the cancer cells from spreading [89]. Therefore, we hypothesize that extended exposure of MSCs to reducing microenvironment can alter the cell fate changes by modulating the receptor activities. MSCs express CD29, CD44, CD90, CD49a-f, CD51, CD73, CD105, CD106, and CD166, which have a collective influence on the osteogenic differentiation [90, 91]. Moreover, cell surface receptors may influence the cellular biomechanics by utilizing both calcium-dependent and -independent pathways to alter gene expressions, modulate calcium oscillation, and reorganize cytoskeleton [92]. Nevertheless, the underlying mechanisms of osteogenic commitment induced by cell surface reducing microenvironment are not yet fully elucidated.

Herein, we examined the biological effects of reducing microenvironment on human palatine tonsil derived MSCs (hTMSCs) commitment [93-95] **(Figure 4.1)**. In particular, we examined the effect of reducing microenvironment on the early osteogenic commitment of hTMSCs as it by increment of FAK activation and cell surface protein mediated signaling modulation. Furthermore, we examined the *in vivo* commitment by seeding osteogenically committed hTMSCs on biodegradable PLGA/PLLA scaffolds and transplanting in a critical-sized cranial-defect model. This early osteogenic commitment strategy by applying reducing agent could be extended to bone tissue engineering.

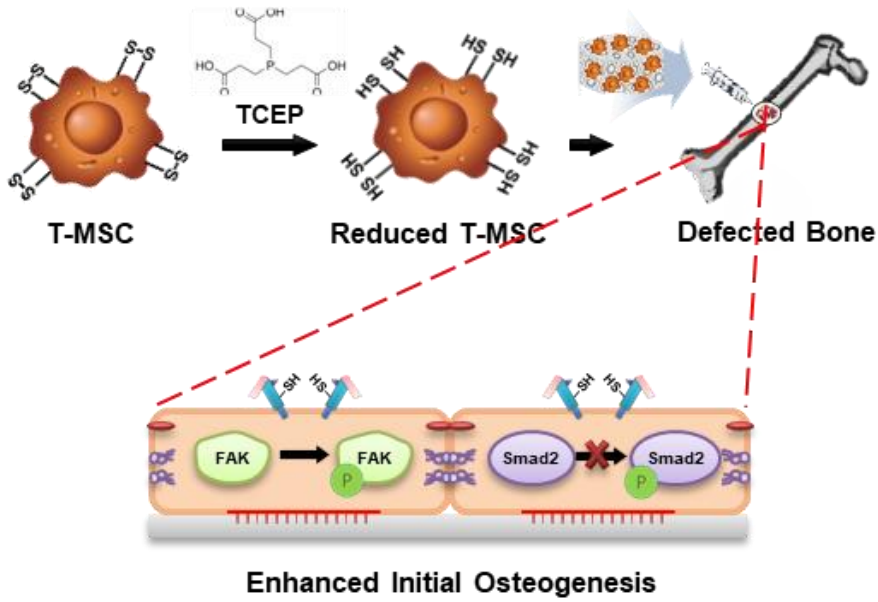

Figure 4. 1 Schematic representation of the surface disulfide bond reduction on T-MSC, and application to defected bone for osteogenic enhancement

4.2 Materials and methods

4.2.1 Cell culture

Tonsil-derived mesenchymal stem cells (T-MSCs) were cultured in DMEM containing 10 % (v/v) FBS, 1 % (v/v) penicillin-streptomycin, and 1 % (v/v) Antibiotic-Antimycotic (AA; Gibco-BRL) under a humidified atmosphere of 5 % CO_2.

4.2.2 Cytotoxicity of TCEP reductant treatment on T-MSCs

For reduction of attached cells, cells at a density of 1.2 x 10^5 cells/cm^2 were cultured in cell culture plate. To reduced cells, PBS containing 0.5 mM (14.3 μg/mL), 1 mM (28.6 μg/mL), 2 mM (57.2 μg/mL), and 3 mM (85.8 μg/mL) of TCEP were treated and incubated for 5 min in 37 °C. After incubation, cells were washed with PBS twice. Cell viability was analyzed after staining the cells with Live/Dead® viability/cytotoxicity kit (Live/Dead; Thermo) that contains calcein-AM and ethidium homodimer solution. After treatment of each concentrations of TCEP for 5 min, Live/Dead assay were used to indicate live cells and dead cells. Live cells were counted and divided by total number of cells, then normalized by negative control group. To examine the cellular proliferation rate, Click-iT® EdU Alexa Fluor® 488 Imaging kit (EdU; Thermo) was used and analyzed by FACS (FACS Aria II, BD Biosciences, USA). Prior to EdU assay, both cells were cultured overnight in serum free media for the synchronization of cell growth. After synchronization, cells were treated with reductant and 3 h incubation with EdU containing growth medium was followed. Then, EdU assay kit was applied to indicate cells in S phase by Alexa Fluor® 488. For the determination of doubling time of reduced cells, Cell Counting Kit-8 (CCK-8; Sigma-Aldrich Co.) was treated to each

reduced sample and measured the absorbance at 450 nm using a microplate reader (Infinite® 200 PRO, Tecan, Swiss). Each data was normalized by its absorbance data of day 0. Duration of reduction time of T-MSCs was measured by modifying T-MSCs with Alexa Fluor® 488 C_5 Maleimide (1 mg/ml, Thermo). Modified cells surface fluorescence intensity was measured by microplate reader (Infinite® 200 PRO) day by day with twice of PBS washing.

4.2.3 Immunofluorescence analysis

T-MSCs were fixed with 4 % PFA for 30 min and permeabilized with 0.1% TritonX-100 in PBS for 30 min. Then, subsequently immunostained with antibodies against Ki-67 (ab833, Abcam, UK), CD105 (ab11414, Abcam) and Vinculin (ab129002, Abcam). Immunoreactivity was visualized through FITC-conjugated secondary antibodies (Jackson Immuno Research Laboratories, West Grove, PA, USA). Nuclei were counterstained with Hoechst 33258, and F-actin was stained with Alexa Fluor® 594 Phalloidin. The cells were subsequently imaged via fluorescence microscopy (EVOS® Cell Imaging Systems, Thermo) and confocal microscopy (LSM 780; Carl Zeiss).

4.2.4 Scratch assay for migration of reduced Cells

T-MSCs were cultured in 6 well-plate to full confluency. Surface reduced groups were treated with various concentrations of TCEP. After reduction, by using cell scratcher, a straight line has been formed. Two times of washing step with PBS was performed to remove the debris and smooth the edge of the scratch. Samples were incubated at 37 °C in humid air with 5% CO_2. After the incubation, samples were imaged on each day same

timepoint and the distance of each scratch closure on the basis of the distances was measured.

4.2.5 Western blot analysis

Reduced cell lysates were prepared with cell/tissue lysis buffer (Cell Signaling, USA). Concentration of obtained protein was quantified with the Bradford protein assay (Sigma Aldrich Co.). Electrophoresis was carried out in a 10 % SDS-polyacrylamide gel to detect β-tubulin as a loading control and targeted proteins (t-FAK, p-FAK, CD105, t-Smad2, and p-Smad2) by loading 30 mg of the total protein per lane. Proteins were transferred to a nitrocellulose membrane by iBlot (Invitrogen ™, USA) and blocked by 3 % Bovine Serum Albumin (#9998, Cell Signaling, USA) in PBS-T (pH 7.5 with 0.1 % Tween®-20) for 1 hr. FAK (#3285, Cell Signaling Technology, USA), p-FAK (#3283, Cell Signaling Technology), CD105 (ab252345, Abcam), t-Smad2 (#5339, Cell Signaling Technology) and p-Smad2 (#3108, Cell Signaling Technology) were incubated with samples with suggested dilution rate overnight at 4 °C. To detect primary antibody binding, HRP-conjugated secondary goat anti-mouse antibody (170-5047, Bio Rad, USA) and HRP-conjugated secondary goat anti-rabbit antibody (170-6515, Bio Rad) was applied in a 1:10,000 dilution for 1 h. Visualization of proteins was preceded by incubating the membrane in a 1:1 ratio of a luminol/enhancer solution from an Immun-Star™ HRP Substrate kit (170-5040, Biorad®, USA).

4.2.6 Osteogenic differentiation and chemical staining of T-MSCs

For osteogenic differentiation of T-MSCs, each cell samples were cultured in DMEM supplemented with 10 % FBS, 1 % Pen/Strep, 50 mg/ml L-ascorbic acid (Sigma), 10

mM glycerol-2-phosphate (Sigma), and 100 nM dexamethasone (Sigma) for 21 days. Differentiation medium was changed every other day. After 14 days and 21 days of differentiation, differentiated T-MSCs were fixed, washed with distilled water, and stained for alkaline phosphatase (ALP; Sigma-Aldrich Co.) followed by the protocol previously described. Diazonium salt solution was prepared by dissolving 0.2 mg Fast Blue RR Salt in 1 ml distilled water and then 33 μl naphthol AS-MX phosphate solution was added. Cells were stained for 45 min and washed twice with distilled water. For Alizarin Red S (ARS) staining, 20 mg ARS (Sigma-Aldrich Co.) was dissolved in 1 ml distilled water, and the pH was adjusted to 4.1~4.2 with 0.1 M ammonium hydroxide. hMSCs were fixed by neutral buffered 10 % formalin solution and stained with ARS solution for 40 min and washed with distilled water 4 times. Images were observed under a light microscope (IX71 inverted microscope, Olympus).

4.2.7 Real-time PCR analysis

Osteogenic markers (RUNX-2, ALP, COL-1, and OCN) were quantified by treating each cell samples with Trizol® reagent to obtain RNA. Chloroform was added and the tube was vigorously shaken for 15 seconds by hand. After incubating at room temperature for 10 min, centrifugation (15,000 rpm for 20 min) was performed at 4 °C. The clear aqueous phase at the top was transferred to new tube and isopropanol was added and mixed. After incubating at room temperature for 5 min, centrifugation (15,000 rpm for 20 min) was held at 4 °C. Then white pellet of RNA was collected. RNA pellet was washed with 75 % ethanol, dissolved completely in molecular grade water and denatured for 10 min at 60°C. RNA concentration was measured and reverse-transcriptional PCR was performed with cDNA kit (EZ006M, Enzynomics, Korea)

according to manufacturer's instructions. PCR with osteogenic markers (RUNX-2, ALP, COL-1, and OCN) were done to observe gene expression levels of the cells. The real-time PCR was performed using SYBR green PCR Mastermix and StepOnePlus™ Real-Time PCR System (Applied Biosystems). Complementary DNA samples were analyzed for gene for interest and for the reference GAPDH.

4.2.8 Calcium assay

To quantify calcium amount in media of differentiating T-MSCs, Calcium Liquid Reagents (Pointe Scientific™, USA) were used. Cells were seeded in scaffold and cultured in differentiation media for 6 weeks. Small amount of media was collected every week, and the calcium amount was measured followed by the manufacturer's protocol.

4.2.9 Scaffold fabrication and cell attachment

Porous poly(L-lactide) (PLLA) / poly(lactide-co-glycolide) (PLGA) scaffolds were fabricated. An equal amount PLGA and PLLA was dissolved in chloroform (Daejung Chemical) to make a final concentration of 5 % (w/v) solution. NaCl (300 mg; Merck) was placed into a mold (300 μm in diameter), and 250 μl PLGA/PLLA solution was added to make 7 mm width and 2 mm height disc-shaped scaffolds. Scaffolds were completely dried and immersed in 500 ml distilled water for 3 days to leach out NaCl residue in the polymer scaffold. The distilled water was exchanged every 12 h at least 6 times. Cells were seeded at 3 x 10^6 cells per scaffold. The Quant-iT PicoGreen dsDNA Assay Kit (P11496, Invitrogen) was used to evaluate cell attachment after 6 h of seeding. Papain solution was prepared by adding 1.58 mg cysteine and 25 mg papain type III

(Worthington) in PBE buffer. The samples were breaking down and digested with papain solution at 60 °C for 16 h. DNA contents were measured with PicoGreen agent by using an Infinite M200pro (TECAN) microplate reader at 485 nm (excitation) and 535 nm (emission). Control scaffold without any modification was utilized as a control.

4.2.10 In vivo cranial-defect model

All experiments were maintained and managed in accordance with the Guide for the Care and Use of Laboratory Animals by the Seoul National University. Six-week-old female BALB/c athymic mice (Orient Bio, Korea) were used for the critical-sized calvarial defects. Mice were anesthetized using 30 mg/kg Zoletil 50 (Virbac) and 10 mg/kg Rompun® inj (Bayer) and all endeavors were established to minimize animal suffering. Two 4-mm-diameter defects were formed by using a hand drilling machine, STRONG106 (SAESHIN), on the both sides of the mouse skull, and 4-mm diameter scaffolds were implanted in the defect sites. After 8 weeks of transplantation, the animals were euthanized by CO_2 asphyxiation and mouse skulls were collected for analysis of bone formation.

4.2.11 μ-CT

Collected skull samples were fixed with 4 % PFA, and μ-CT images were taken with a Skyscan1172 (Bruker). The source current was 167 μA and the operation source voltage was 59 kV. Each image was stacked by the CTvox program (Bruker), and the regeneration area of samples was evaluated by Image J software (USA).

4.2.12 Histological assessment and immunostaining analysis

The harvested skull samples were fixed in 4 % PFA for 24 h, decalcified with 0.5 M EDTA at pH 7.4 for 2 weeks, and embedded in optimal cutting temperature compound (O.C.T. compound, Scigen, USA) and longitudinally sectioned at a thickness of 10 μm. The sections were stained with Hematoxylin & Eosin staining method and Masson trichrome staining method for light microscopic analysis. Stained Samples were observed under light microscope with a 4-objective lens (CKX41, Olympus, Japan) and a digital camera (ProgRes C14, Jenoptik, Germany).

4.2.13 Statistical Analysis

Quantitative data were expressed as the means ± standard deviation (SD). The statistical analysis was determined using one-way analysis of variance (ANOVA). A value of *$p < 0.05$ and **$p < 0.001$ was considered as statistically significant.

4.3 Results and Discussion

4.3.1 Biological Effect of MSC in Cell Surface Reducing Microenvironment

To investigate the non-cytotoxic microenvironment by mild reductant TCEP on MSCs, we thoroughly assessed cellular morphology, cell viability, doubling time, and proliferation rate for optimal concentration of reductant. While typical MSCs exhibited a shape of long spindle, morphology of MSCs in higher concentration of reductant than 1mM was changed into shrunk shape **(Figure 4.2)**. Similarly, cell viability and doubling time showed no significant difference observed in MSCs up to 1 mM. However, all of these parameters were dramatically decreased in higher dose above 1 mM **(Figure 4.3)**. Cell proliferation in protein level was visualized by Ki-67 immunostaining. Consistent with the data on cell viability and doubling time, we observed that the number of Ki-67 expression cells were noticeably decreased at higher dose of reductant **(Figure 4.4)**. We lastly evaluated the duration of cell surface disulfide bond reduction by attaching fluorescent dye conjugated maleimide functional group onto 1 mM TCEP treated MSCs and cultured for days **(Figure 4.5)**. After 1 day in growth media, fluorescent signal formed by reduction was significantly increased by 48%, and these free-thiols represented by fluorescent dye were mostly recovered to disulfide bond within 2 days. By summing up these results, we designated the targeting reductant concentration below or equal to 1 mM suitable for forming cell surface reducing microenvironment for the subsequent studies.

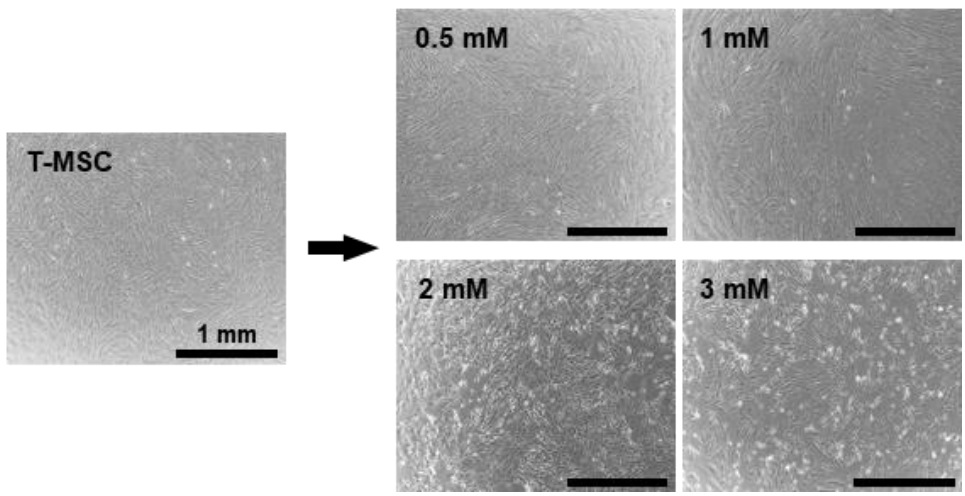

Figure 4. 2 The representative microscopic images of T-MSCs before treatment and after treatment of various concentrations of reductant.

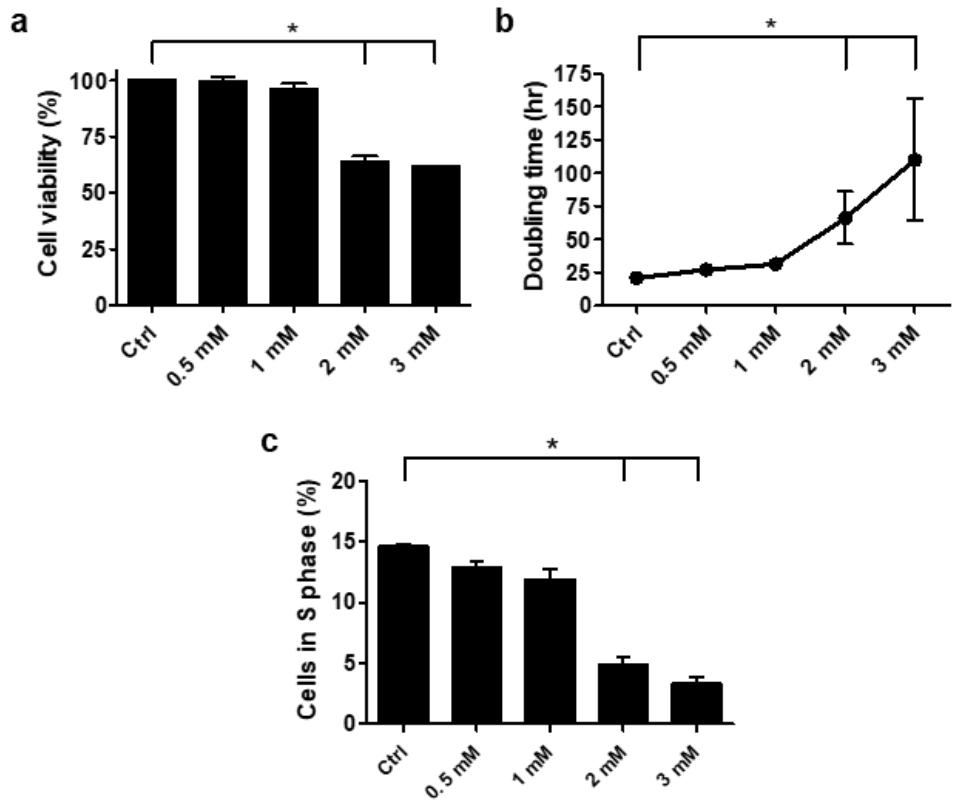

Figure 4. 3 Cell viability and proliferation rate test. a-b) Relative percentage of cell viability and doubling time at the treatment of given dose. The data were obtained using Live/Dead® viability/cytotoxicity kit. c) The number of cells in S-phase was obtained by flow cytometry analysis of EDU-stained cells for determination of cell proliferation rate. Statistical analysis—bars indicate means; error bar represents SD; unpaired t tests were performed. Statistical significance is marked by asterisks (*).

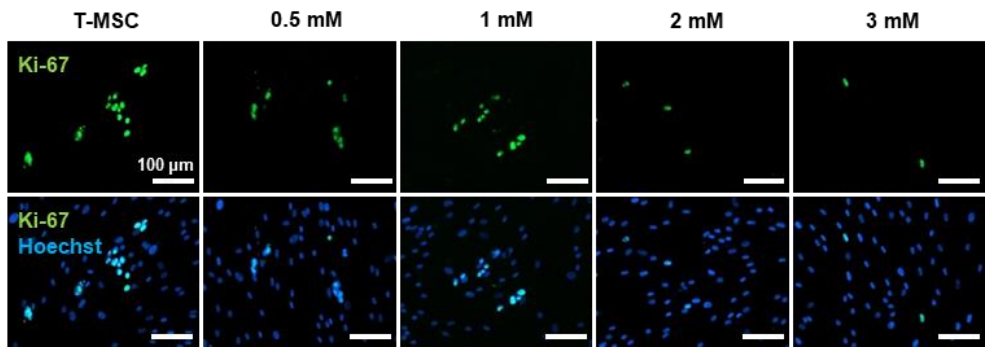

Figure 4. 4 Immunofluorescent images of Ki-67 (green) and cell nuclei (blue) after various concentration of TCEP treatment to T-MSCs.

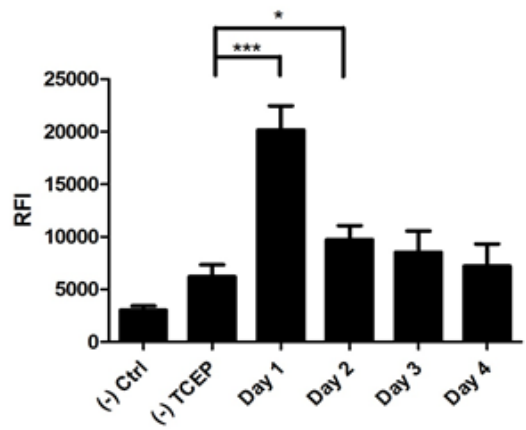

Figure 4. 5 Analysis plot of surface reduction duration of T-MSCs. Relative fluorescence intensity was measured daily after modifying cell surface with fluorescent molecule that reacts with free thiol groups.

4.3.2 Focal Adhesion Enhancement in Cell Surface Reducing Microenvironment

Then, we analyzed the mobility of MSC in cell surface reducing microenvironment by wound area coverage of scratch assay **(Figure 4.6)**. Although all of groups successfully recovered scratched area on day 4, higher dose of reduction gradually decreased the rate of cell mobility along with proliferation. Moreover, F-actin and vinculin, which is closely related to focal adhesion of cell, were simultaneously immunostained. As cells surfaces are reduced, increased signaling of vinculin was observed at the tip of actin fibers **(Figure 4.7)**. Also, focal adhesion kinase (FAK) protein activity was measured by western blotting of total FAK protein (t-FAK) level and its activated phosphorylated form (p-FAK) level **(Figure 4.8)**. When FAK protein activity level was quantified by a ratio of p-FAK to t-FAK, cells in reducing microenvironment elevated p-FAK protein level, while t-FAK protein level was similar in all groups.

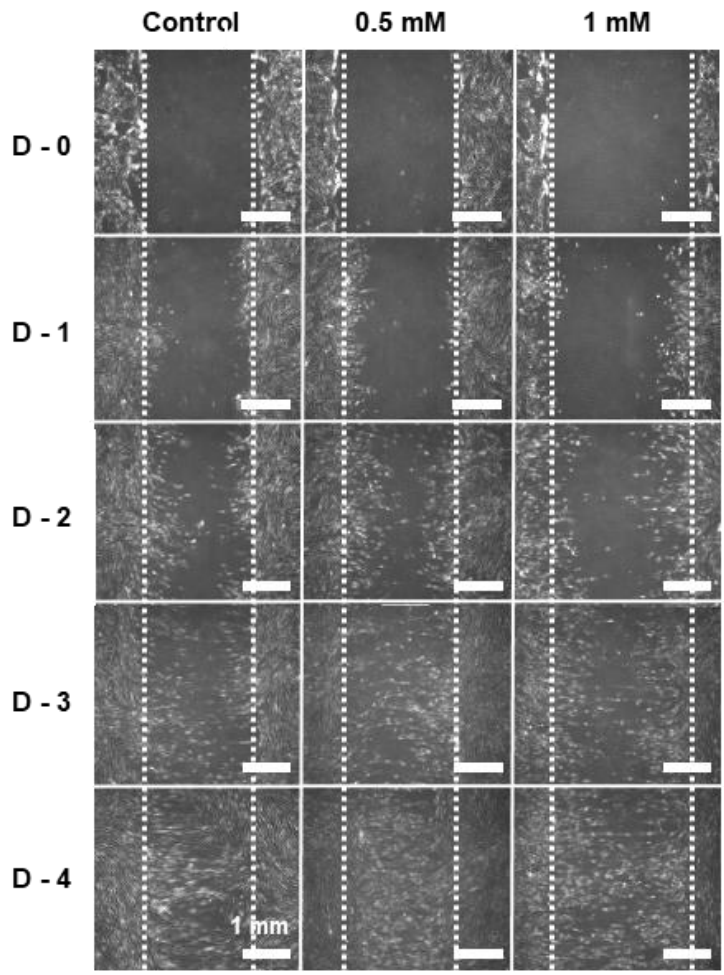

Figure 4. 6 Image-based monitoring of wound scratch assay of non-reduced and surface reduced T-MSCs groups. Imaging was performed daily at the fixed time, started at the experiment day (D - 0) until 4 days (D - 4), using phase contrast microscope with 4x magnification.

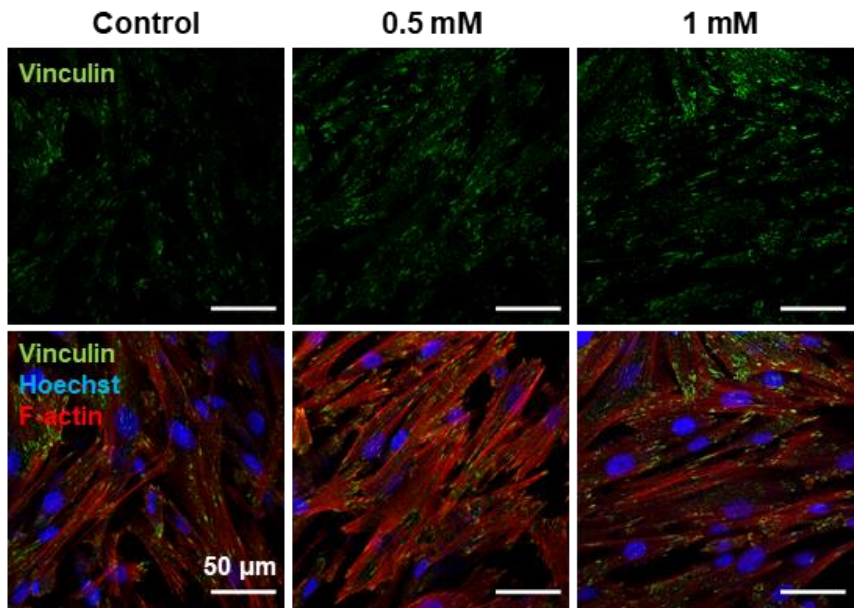

Figure 4. 7 Immunofluorescent images of vinculin (green), F-actin (red), and cell nuclei (blue) for visualization of focal adhesion of T-MSCs.

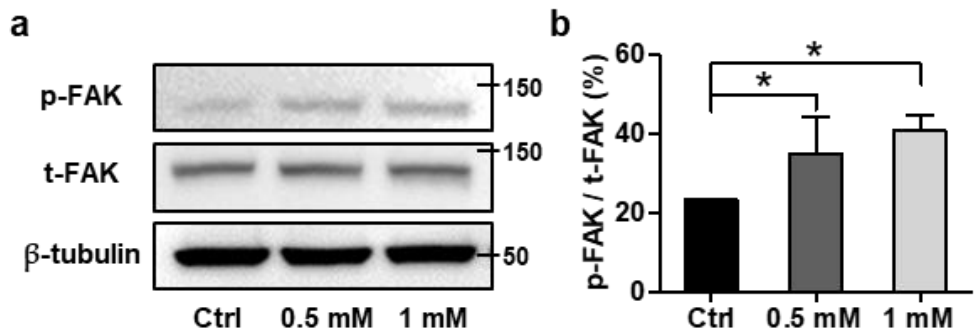

Figure 4. 8 Western blot image and plot demonstrating comparative amount of focal adhesion kinase and its phosphorylated form between non-reduced group and surface reduced group by given reductant dose. Statistical analysis - bars indicate means; error bar represents SD; unpaired t tests were performed. Statistical significance is marked by asterisks (*).

4.3.3 Enhanced Osteogenic Commitment of MSCs in Reducing Microenvironment

We sought to investigate whether increased FAK activity could actually induce osteogenic commitment of MSCs upon reducing microenvironment. After 1- and 2-weeks culture in osteogenic media, all groups were analyzed by real-time PCR to quantify the level of osteogenic mRNA expression of early genes (RUNX-2 and Alkaline Phosphatase (ALP)) and late genes (collagen type 1 (COL-1) and osteocalcin (OCN)) **(Figure 4.9)**. Notably, gene expression levels of early osteogenic genes were higher than it of late genes in surface reduced MSC groups, especially 0.5 mM group. As MSCs were differentiated into osteoblasts, calcium content in differentiation media in all groups were gradually increased at every week **(Figure 4.10)**. However, accumulation of calcium contents was conspicuously higher in groups committed by surface reducing microenvironment. Additionally, ALP and Alizarin Red S (ARS) staining assays were performed to further validate osteogenic differentiation **(Figure 4.11)**. In both assays, after 3 weeks of osteogenic commitment, ALP expression and calcium depositions were substantially higher in reduced groups than in other group. These results were consistent with previous studies reporting that elevation of focal adhesion in MSC can enhance osteogenic differentiation [96-98].

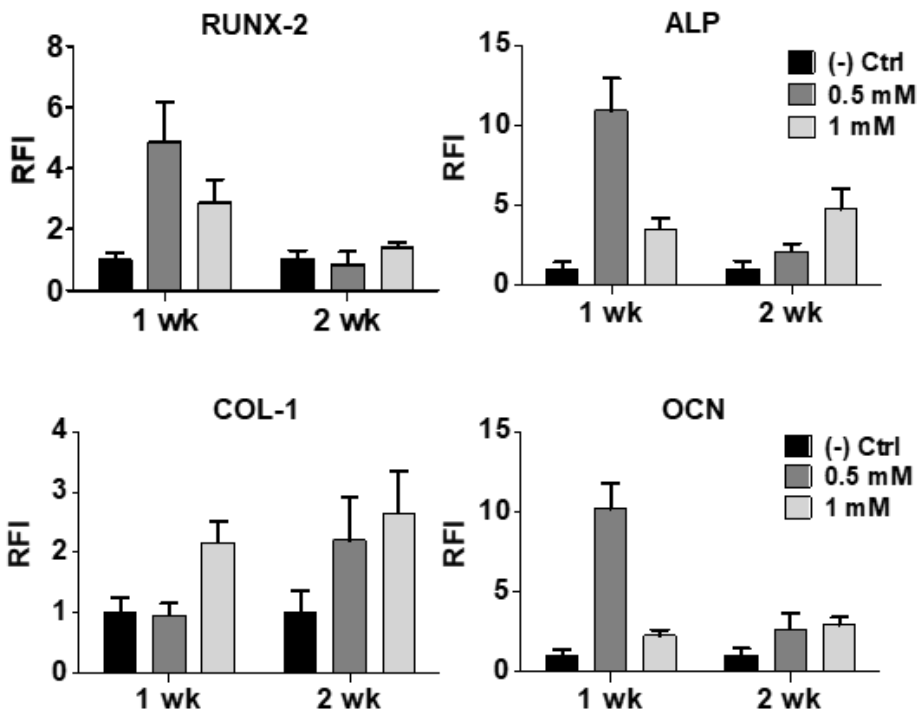

Figure 4. 9 mRNA expression by real-time PCR analysis of osteogenic factors in T-MSCs cultured in differentiation media of given weeks with or without surface reduction before differentiation.

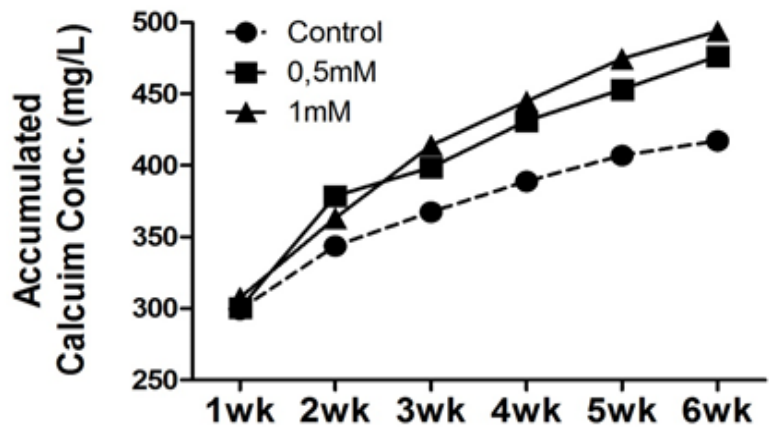

Figure 4. 10 Measurement of calcium concentration accumulation during osteogenic differentiation of T-MSCs groups. Calcium amount in differentiation media was measured to compare.

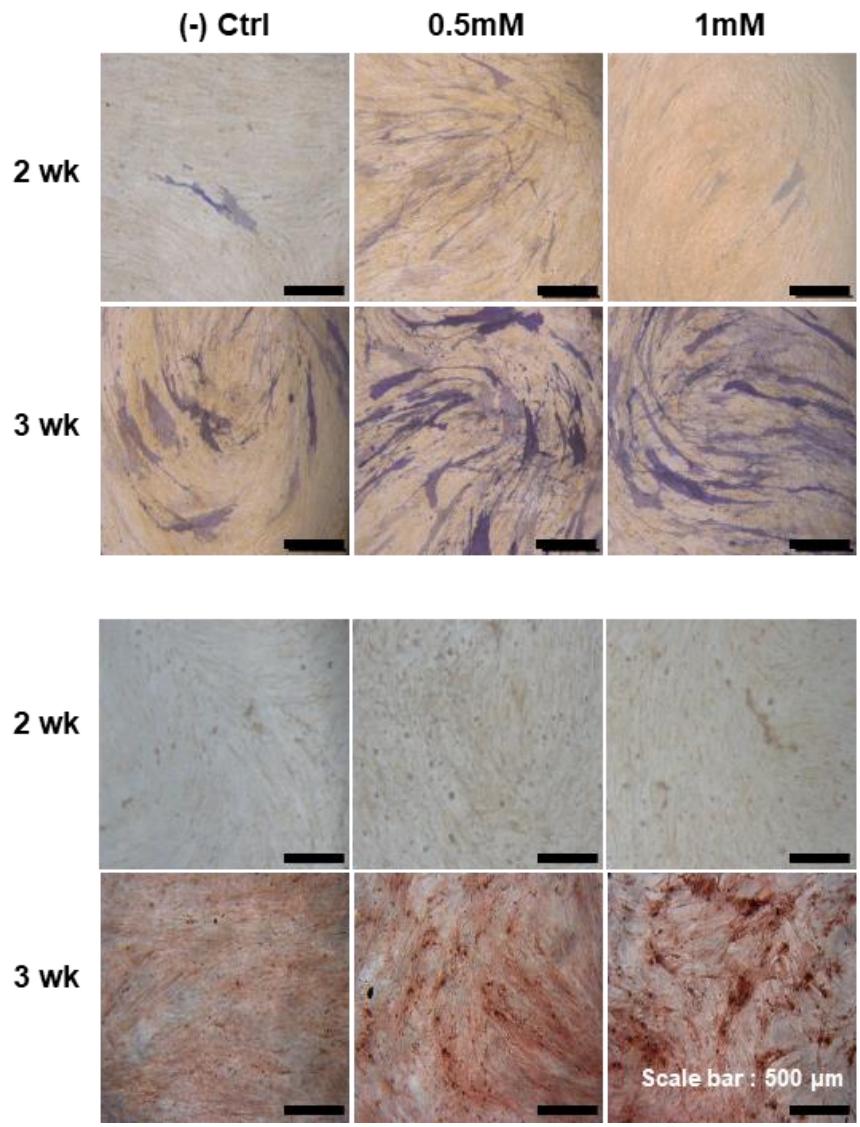

Figure 4. 11 Alkaline phosphatase (ALP) staining for relative ALP activity and Alizarin Red S (ARS) staining for calcium deposition of differentiated T-MSCs with or without surface reduction before differentiation.

4.3.4 Identification of Internal Cell Signaling Pathway for Inducing Early Osteogenic Commitment

Then, we investigated internal cellular signaling pathway related to both osteogenic differentiation and focal adhesion, related to inducing osteogenic commitment of MSC, have been influenced in cell surface reducing microenvironment. MSC surface differentiation markers such as CD73, CD90, and CD105 are known to be essential for osteogenic commitment [90, 99]. In one of candidates, TGF-β signaling pathway assisted by endoglin cell surface receptor, known as CD105 which get activated by dimerization, was chosen [100, 101]. While dimeric form of endoglin inhibit osteogenic differentiation by TGF-β signaling pathway, however when deactivated, endoglin monomer induces an opposite effect [102]. Endoglin receptor on MSCs in cell surface reducing microenvironment got separated into monomers by reductant which broke down the disulfide bond in between two monomers **(Figure 4.12)**. To evaluate the effect of osteogenic commitment by modulating TGF-β signaling pathway via real-time PCR, we set up the experimental groups into following groups: normal (negative control), TGF-β treated or TGF-β inhibitor treated group, non-reduced or 0.5/1 mM reducing groups. When analyzed RUNX-2 gene expression on these groups, the TGF-β inhibitor increased RUNX-2 expression by ~3 fold compared to normal group as predicted **(Figure 4.13)**. Also, gene expression level of RUNX-2 in reducing microenvironment were comparable to it of TGF-β inhibitor treated group, indicating that inhibition of endoglin monomers dimerization resulted from cell surface reducing microenvironment could successfully suppress TGF-β signaling pathway.

Moreover, as phosphorylation of Smad2, one of the downstream molecules in TGF-β signaling pathway, can be triggered to eventually block the RUNX-2 expression, we measured protein levels of endoglin monomer, dimer, Smad2, and phosphorylated Smad2 (p-Smad2) by western blot analysis **(Figure 4.14)**. The amount of endoglin monomer was unchanged as shown in western blot and immunofluorescence confocal image **(Figure 4.15)**. Especially in 0.5 mM reducing group, although the amount of dimeric endoglin was significantly decreased right after surface reduction, endoglin started to recover its disulfide bonds after 4 hours from reduction. A ratio of dimer to monomer of both 0.5 mM and 1 mM reducing groups, represented the same trend as the level of endoglin dimer got gradually increased at 1 hr time interval. As predicted, we could observe the inverse relationship between the level of p-Smad2 and endoglin dimer. We further analyzed the level of p-Smad2 if additional TGF-β was treated onto surface reduced MSCs **(Figure 4.16)**. When surface reduction was conducted after treating TGF-β on MSCs, reduction did not invoke any change in trend of TGF-β signaling pathway, even though dimer form of endoglin diminished. On the other hand, signal transduction decreased when TGF-β treated after surface reduction. Along with the focal adhesion data, reduction of surface receptor endoglin elevates early stage of osteogenic commitment of MSC.

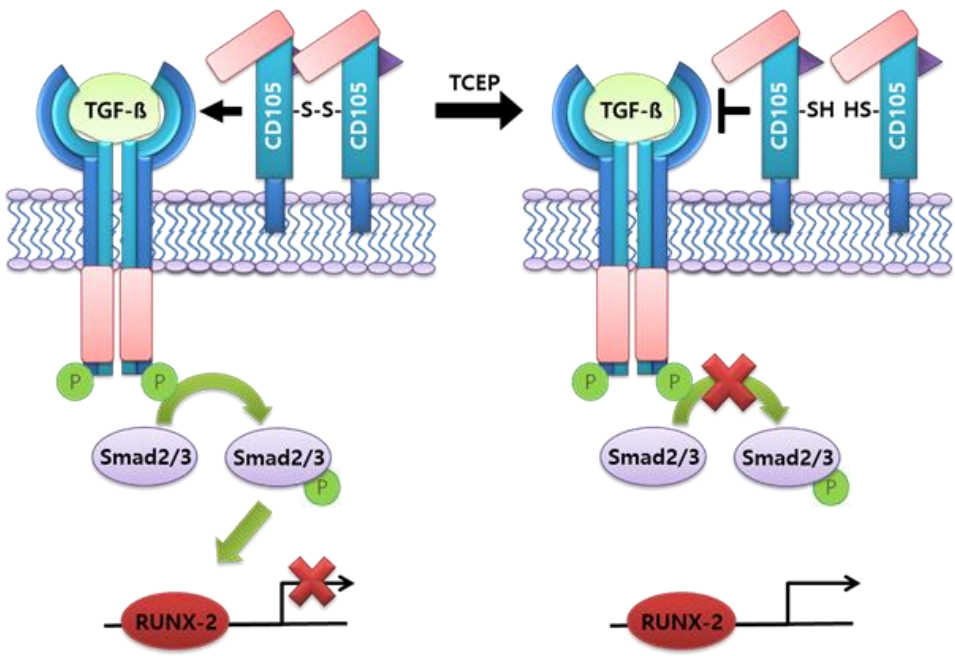

Figure 4. 12 Schematics representation of how reduction of disulfide bond in endoglin dimer influences TGF-β signaling pathway.

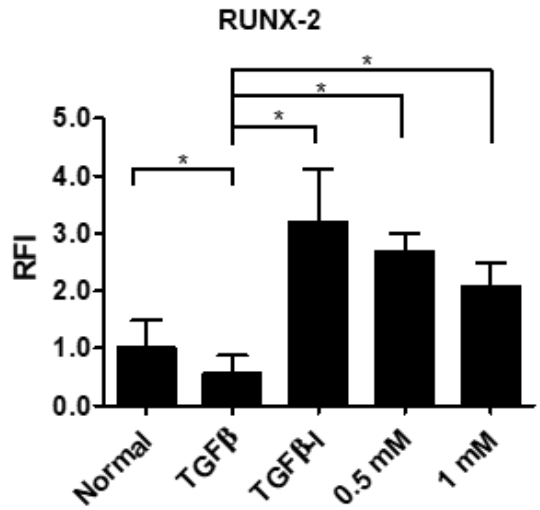

Figure 4. 13 mRNA expression by real-time PCR analysis of osteogenic factor, RUNX-2.

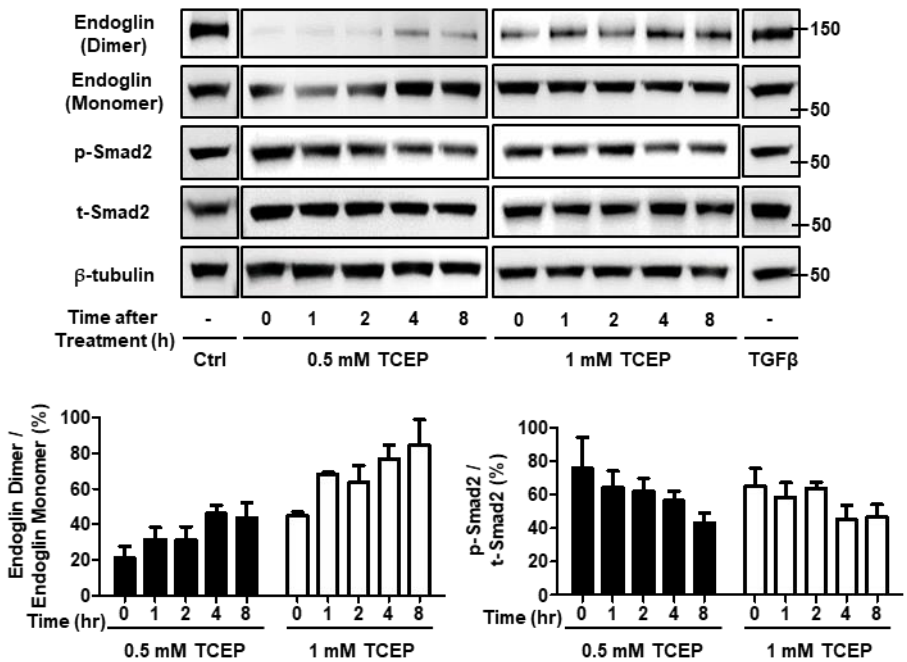

Figure 4. 14 Western blot images and plot showing amounts of dimer and monomer form of endoglin and activated Smad2 (p-Smad2) relative to total Smad2 (t-Smad2) protein. Surface reduced T-MSC by given doses were analyzed in time frames. Non-reduced T-MSC and TGF-β treated T-MSC were analyzed as negative and positive control group, respectively.

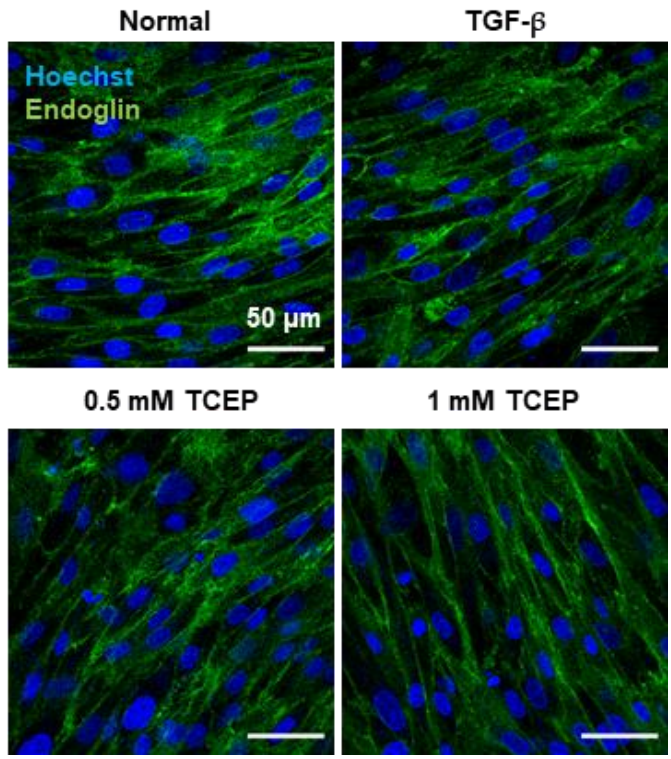

Figure 4. 15 Immunofluorescent images of endoglin (green) on cell surface and cell nuclei (blue) in cytoplasm of non-reduced T-MSC as negative control group, TGF-β treated T-MSC as positive control group, and surface reduced T-MSC by given doses for experimental group.

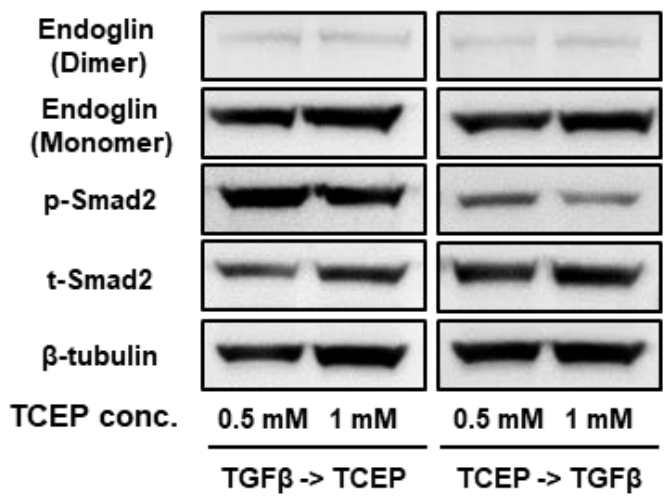

Figure 4. 16 Western blot images showing amounts of dimer and monomer form of endoglin and activated Smad2 (p-Smad2) relative to total Smad2 (t-Smad2) protein in T-MSCs primarily treated with TGF-β before reduction, or vice versa, treatment of TGF-β after reduction.

4.3.5 Application in Mouse Cranial-Defect Model with MSC in Cell Surface Reducing Microenvironment

After confirming the capability of osteogenic commitment of MSCs in surface reducing microenvironment in vitro, we demonstrated in vivo bone formation of surface reduced MSCs incorporated into PLLA/PLGA biodegradable scaffolds in mouse cranial-defect model **(Figure 4.17)**. After 8 weeks of implantation, when we compared the bone regeneration of non-reduced and surface reduced groups by micro-computed tomography (micro-CT), 0.5 mM group showed the highest bone regeneration of 62% while non-reduced group still presented some level of regeneration **(Figure 4.18)**. At the same time, we conducted several immunohistochemistry analyses to validate the implanted tissue organization. Hematoxylin & Eosin (H&E) staining indicated that MSCs in both non-reduced and reduced groups were well-distributed on the implanted scaffold throughout bone tissue regeneration. Likewise, Masson's Trichrome staining (MTS) revealed that lamellar-like bone formation and organization of the collagen in the reduction group were more discernable than in the non-reduced group **(Figure 4.19)**. Overall, these results demonstrated that reduced MSCs implanted scaffold could successfully function as native bone-tissue when it was incorporated into mouse cranial defect model. By summing up both in vitro and in vivo assessments, elevating early osteogenic efficiency of MSCs could be achieved by culturing cells in cell surface reducing microenvironment **(Figure 4.20)**.

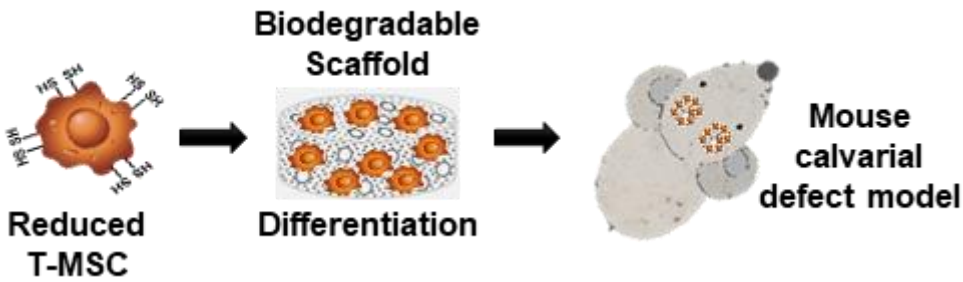

Figure 4. 17 Schematics of application to calvarial defect mouse models for enhanced bone regeneration by surface reduction.

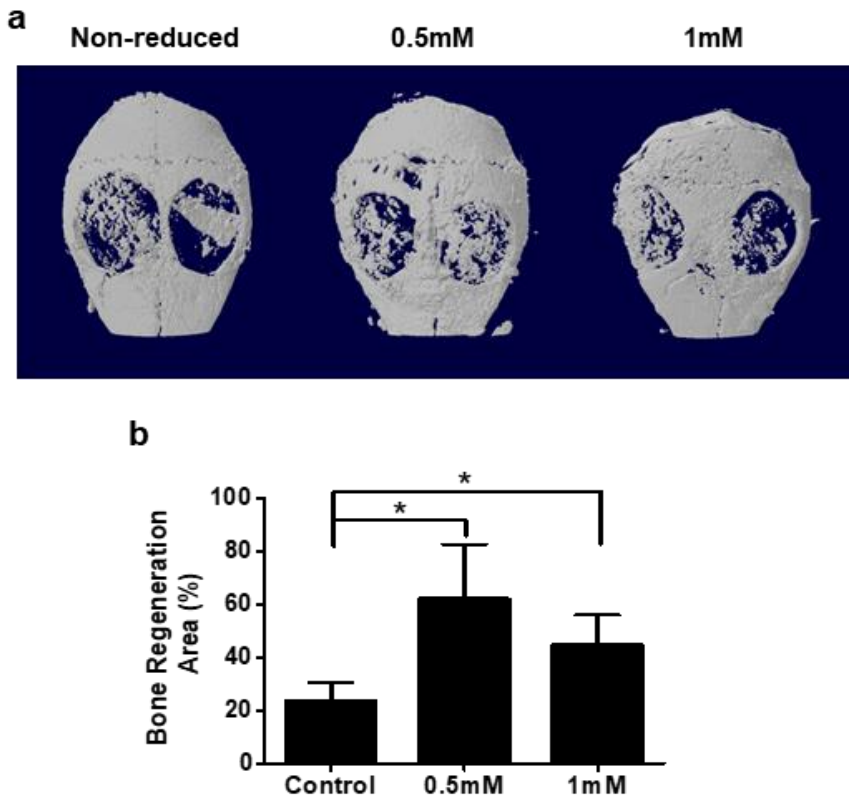

Figure 4. 18 Regeneration calvarial defect mouse models. a) Micro-computed tomography images representing regeneration area on calvarial defect models after 8 weeks of implantation with biodegradable scaffold with non-reduced T-MSCs and surface reduced T-MSCs groups. b) Quantification of bone regenerated area in defect sites via implanting biodegradable scaffold with non-reduced T-MSCs and surface reduced T-MSCs groups.

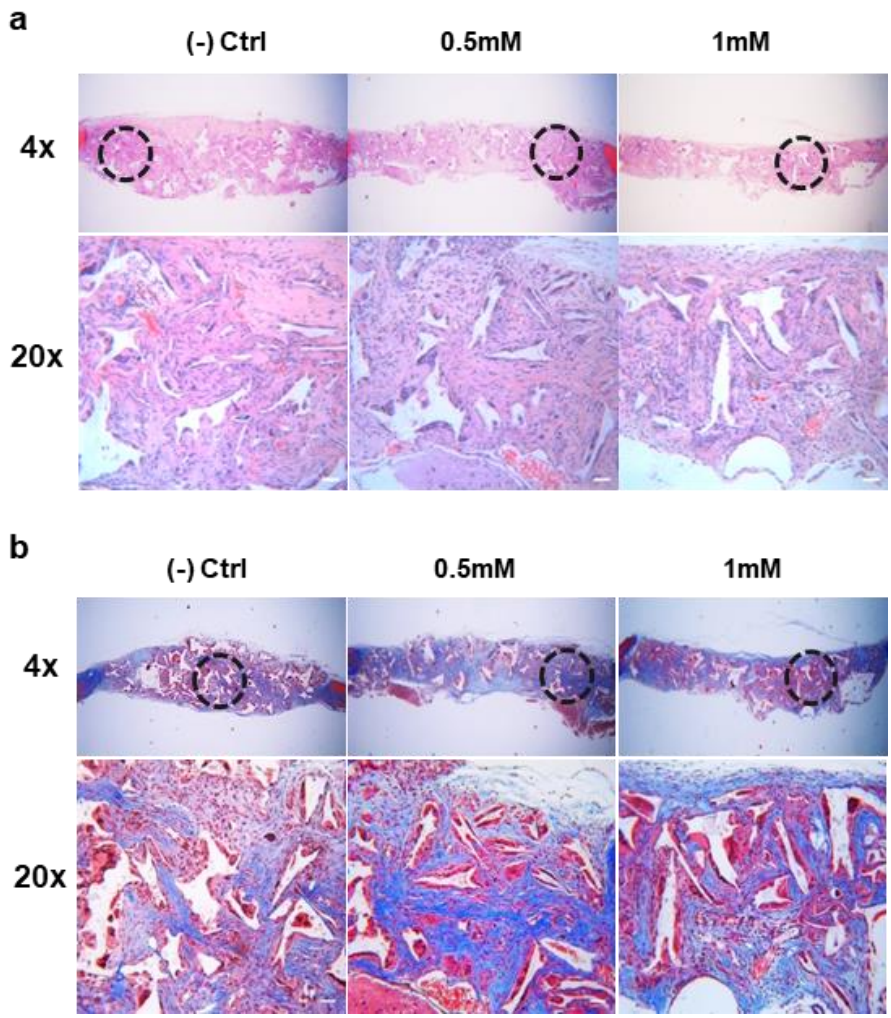

Figure 4. 19 Histological analysis a) Hematoxylin and Eosin, and b) Masson's Trichrome staining images of calvarial defected sites with scaffolds.

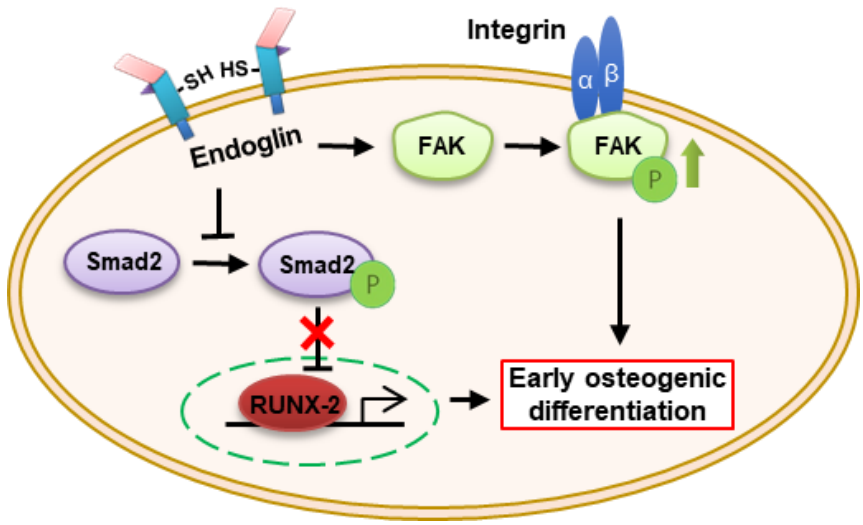

Figure 4. 20 Schematic model of endoglin protein receptor reduction induced early osteogenic differentiation enhancement.

4.4 Summary

In summary, reduced redox microenvironment by mild reductant TCEP stimulates early osteogenic differentiation of T-MSCs incorporated with surface receptor endoglin without causing cellular toxicity. Reduction of disulfide bond of endoglin dimer breaks down into monomers, causing cell focal adhesion heighten that leads to enhanced osteogenic differentiation. The differentiation efficiency was much superior compared to naïve T-MSCs. Additionally, due to the endoglin depletion, internal TGF-β signaling pathway was restricted showing suppression in phosphorylation of Smad2, which resulted in transcription of RUNX-2 early osteogenic marker. Examination by μ–CT and histological analysis in the critical-sized defect animal model, T-MSCs differentiated through reduction showed much higher efficacy in bone tissue regeneration than naïve T-MSCs. Thus, synergistic effect of increased focal adhesion and decreased TGF-β signaling by surface protein receptor endoglin reduction allowed enhancement of early osteogenic differentiation that may serve as a promising modality in clinical use for bone tissue engineering and bone regenerative therapies.

CHAPTER FIVE:

HYDROGEL NANOFILM ENCAPSULATION CROSSLINKED BY ENZYMATIC REACTION

5.1 Introduction

Cell transplantation, emerging as a promising strategy in the field of regenerative medicine, consists of delivering live cells or organoids to a patient as a therapeutic drug, in order to repair, reinforce or replace the biological functions of damaged tissues [88, 103, 104]. Currently, incurable diseases, such as diabetes, myocardial infarction, osteoarthritis and spinal cord injuries have been fundamentally treated via cell transplantation to actively ameliorate disease conditions [31]. Despite the benefits, challenges remain including poor viability of injected transplants and vigorous host immune response [105-107]. Direct injection of transplants causes mechanical stress against the injection pressure and fluidic shear forces, led to necrotic and apoptotic cell death with cell membrane rupture [16]. Moreover, allogeneic or xenogeneic cell transplantation triggers inflammatory host immune response through direct and indirect immune recognition [108-110]. Many efforts have utilized biomaterials to overcome the low survival rate and vigorous immune rejection of transplantation. Among them, encapsulation with biomaterials shed a light to solve the challenges above [111, 112]. Working as a protective sacrificial layer and supportive matrix, encapsulation thereby improve the cell viability against the external stress and host immune system.

Type 1 diabetes (T1D), one of the global epidemic diseases, is an autoimmune disease characterized by the destruction of pancreatic β-cells by the patient's immune system, resulting in high blood glucose level due to the deficiency of insulin [113-115]. Since T1D patients have few functional pancreatic β-cells, external supply of insulin or addition of functional pancreatic β-cell is required for glycemic control [116]. Clinical trials of islet transplantation using biomaterials have increased in number and vindicated its safety and effectiveness for T1D. Islets are encapsulated in biocompatible devices or hydrogel microbead composed of alginate and polyelectrolytes prior to transplantation to avoid the need for lifelong immunosuppression. However, the conventional encapsulation methods possess several challenges: large volume ratio of cell to polymer [117], poor diffusion of oxygen and nutrients [118], heterogeneous coverage due to random trapping [119], and fibrosis around transplantation site [120]. Recently, layer-by-layer cell encapsulation methods with polyelectrolytes have widely studied due to its simple and rapid manufacturing process [121-123]. Yet, limitations of these approaches include that numerous layers are required to form feasible thickness for transplantation, durable layers against shear force, and prevent immune response to the biomaterials. Therefore, new islet encapsulation method with nano-thin, porous, and durable film, which are sufficiently permeable to nutrient/waste exchange, long-term glycemic control, and immune-camouflage effect without immunosuppressive therapy, is highly desired.

Herein, we fabricated a new concept of pancreatic β-cells spheroid encapsulation by enzymatic crosslinking-based hydrogel nanofilm with high stability and cytoprotective property **(Figure 5.1)**. Hydrogel nanofilm is composed of biocompatible polysaccharide layers of glycol chitosan (GC) and hyaluronic acid (HA). Layers were crosslinked by the monophenol residues conjugated on each

polysaccharide, via Streptomyces avermitilis derived tyrosinase (SA-Ty) mediated reaction as previously studied [124]. Oxidation of monophenols rapidly interact with organic and inorganic substrates via hydrogen bond interaction, Michael addition reaction, and Schiff base reaction [125, 126]. In this respect, SA-Ty was able to rapidly crosslink polysaccharides to form hydrogel nanofilm on cell surface. We established hydrogel nanofilm on the surface of single cell and spheroid. Gradual accumulation of polysaccharide layers was analyzed by various approaches. In addition, demonstration of our hydrogel nanofilm as a physical barrier against external environment was validated by the long-term hydrogel nanofilm conservation, endurance against external pressure, and reduction of cell-cell interaction with natural killer cell. Finally, hydrogel nanofilm formed by SA-Ty on pancreatic β-cells spheroids were able to return T1D mouse to normoglycemia, unlike native spheroids. The successful engraftment and therapeutic efficacy of transplanted spheroids were confirmed by long-term blood glucose measure, intraperitoneal glucose tolerance test and immunohistochemistry.

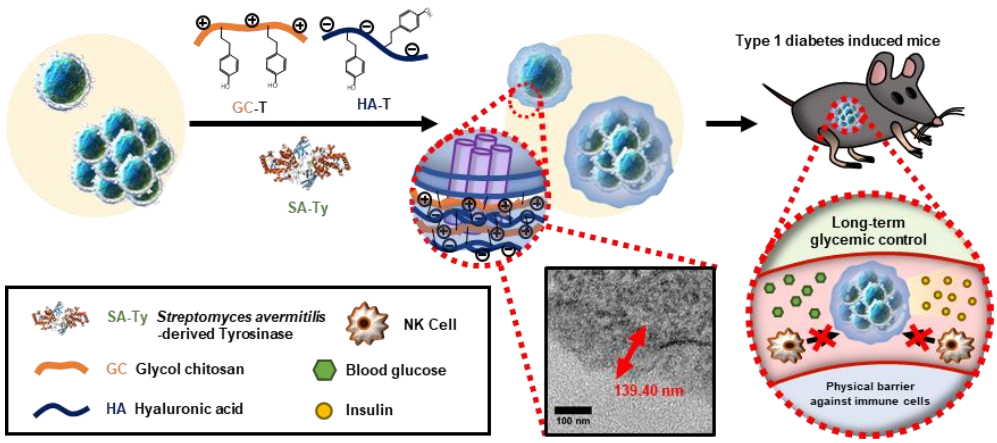

Figure 5. 1 Representative scheme of β-cell spheroids transplantation with enzymatic crosslinking-based layer-by-layer hydrogel nanofilm encapsulation.

5.2 Materials and methods

5.2.1 Cell culture

Jurkat cells (Jurkat Clone E6-1, ATCC® TIB-152™) were cultured in 75 cm^2 tissue culture flasks with cell culture growth medium at 37 °C under humidified atmosphere containing 5 % CO_2. The cell culture growth medium was RPMI 1640 containing 10 % FBS and 1 % P/S. Cells were harvested by centrifugation for subculture or experiments. Media was changed every 2 days. MIN6 cells were cultured in high-glucose D-MEM containing 15 % FBS, 1 % P/S, and 55 μM 2-ME and incubated in 5 % CO_2 at 37 °C. Media was changed every 2 days. K562 cells were cultured in RPMI 1640 media (Gibco) supplemented with 10 % FBS (Gibco) and 1 % P/S (Gibco). NK-92 cells were cultured in MEM alpha media (Gibco) supplemented with 12.5 % FBS, 12.5 % horse serum (Gibco), 1 % P/S and 20 ng/mL of human IL-2 (Peprotech). All cells were maintained at 37 ℃ with 5 % CO_2 in humidified incubator.

5.2.2 Synthesis of GC-T, HA-T, GC-T-RITC and HA-T-FA

4-Hydroxyphenylacetic acid (HPA) was conjugated to glycol chitosan (GC) via EDC/NHS coupling reaction. Firstly, 200 mg of GC were dissolved in 10 ml of 0.1 M pH 4.7 MES buffer at 70 °C until fully dissolved. 160.82 mg of HPA were dissolved in 10 ml MES buffer, and 202.64 mg of EDC and 114.76 mg of NHS were added to the solution and stirred for 5 min. Then, two solutions were mixed and reacted overnight at room temperature (RT). Next, the solution was dialyzed (SnakeSkin™ Dialysis Tubing, Mw cutoff 1 kDa, Thermo Fisher Scientific) against distilled water for 72 h and lyophilized for more than 72 h. In the same manner, HA-T was synthesized by conjugating tyramine hydrochloride to hyaluronic acid (HA). 200 mg of HA was dissolved in 20 ml of MES buffer, and 197.452 mg of EDC and 111.822 mg of NHS

was added, stirred for 5 min. Then, 178.85 mg of tyramine hydrochloride was added and reacted overnight at RT. Subsequently, the final solution was dialyzed and lyophilized. 1 ml of 10 mg/ml RITC and FA solution, dissolved in N,N-dimethylformamide (DMF), was added to the reacting solution of GC-T and HA-T, respectively, to obtain GC-T-RITC and HA-T-FA.

5.2.3 Expression and purification of recombinant tyrosinase from Streptomyces avermitlis (SA-Ty)

The recombinant plasmid for tyrosinase was constructed and provided by Professor Byung-gee Kim (Seoul National University, Seoul, Korea). Briefly, the gene of tyrosinase (Ty) was extracted from Streptomyces avermitlis (SA) and His-tag was introduced at the C-terminal of Ty. For the protein expression and purification of SA-Ty, the plasmid was transformed into E.coli BL21 (DE3) by heat shock and selected on Luria-Bertani (LB) agar plate containing 100 μg/ml of ampicillin. A single colony was inoculated into 5 ml of LB broth with ampicillin and cultured overnight in a 37 °C shaking incubator at 200 rpm. Then, 2 ml of cell culture was transferred into a flask with 200 ml of fresh LB containing 100 μg/ml of ampicillin. The cells were grown to an OD600 of 0.6 and protein expression induced by adding 0.2 mM isopropyl β-D-1-thiogalactopyranoside (IPTG) and 1 mM $CuSO_4$. After 20 h at 18 °C, cells were harvested by centrifugation at 4,000 rpm for 10 min at 4 °C. Cell pellets were washed once and resuspended in 50 mM Tris-HCl buffer, pH 8.0, and disrupted by ultrasonication. Cell lysates were centrifuged at 15,000 rpm for 30 min at 4 °C to remove debris. The supernatant was collected and filtered through a sterilized 0.2 μm polyethersulfone membrane (Acrodisc® Syringe Filter with Supor® Membrane, Pall Life Sciences, USA). The enzyme was purified by the general His-tag purification using

Ni-NTA agarose column (QIAGEN). The final enzyme solution was aliquoted and kept at -20 °C in pH 8.0 Tris-HCl buffer containing 25 % glycerol. The concentration of purified SA-Ty was determined by bicinchoninic acid (BCA) assay.

5.2.4 Measurement of the enzymatic activity of SA-Ty

2.5 μM SA-Ty, 5 μM $CuSO_4$, and the substrate (1 % (w/v) GC-T, 1 % (w/v) HA-T or 200 μM of L-tyrosine) were prepared in a total volume of 200 μl of 50 mM Tris-HCl buffer, pH 8.0. The absorbance at 475nm (εdopachrome = 3600 $M^{-1}cm^{-1}$) at 37 °C was measured every 1 min for 30 min with microplate reader (Infinite M200 PRO, TECAN, Switzerland). The initial rate of SA-Ty reaction was defined as the slope of a plot of the product concentration and the reaction time. The enzyme activity is quoted in units per ml (U/ml), where 1 unit (U) is the amount of SA-Ty that catalyzes the reaction of 1 μmol of L-tyrosine per minute.

5.2.5 Attenuated total reflection-fourier transform infrared spectroscopy (ATR-FTIR)

0.1 % GC-T and 0.1 % HA-T solution was reacted with 0.05 U/ml SA-Ty for 30 min at RT. Then, reaction solution was frozen and lyophilized. The solid sample was directly placed on the zinc selenide ATR crystal surface of ATR-FTIR (Spectrum 100 FT-IR Spectrometer, PerkinElmer, USA). The bare ATR crystal was used as a background. The FTIR spectra was obtained by scanning the transmittance at 700-4000 cm^{-1}.

5.2.6 Hydrogel formation and swelling ratio

Bulk hydrogels were formed by using high concentration of polysaccharides. 5 % (w/v) GC-T and HA-T individually formed hydrogel crosslinked by adding 0.05 U/ml of SA-Ty for crosslinking. Also, mixture of 2.5 % (w/v) of GC-T and HA-T formed hydrogel

by the same procedure. To measure the swelling ratios of GC-T and HA-T hydrogel, dry weight of each hydrogel groups was measured after freeze-drying. Then, dried hydrogels were incubated in PBS at at 37 °C for 1 day. The swollen samples were measured after drying excess solution on the surfaces of the samples. The swelling ratios were calculated by the following equation: swelling ratio (%) = $(W_s - W_i) / W_i \times 100$, where W_s indicates the wet weight of the samples and W_i indicates the initial dried weight of the samples.

5.2.7 Diffusion test of L6 hydrogel nanofilm

To evaluate the porosity and porous structures of L6 hydrogel nanofilm, the diffusion test was performed in a Transwell system, a common experimental tool for measuring permeability and molecular diffusion. Prior to L6 hydrogel nanofilm formation, Transwell insert was treated with plasma for negative charge. Then, L6 hydrogel nanofilm was formed on a Transwell insert (6.5-mm diameter of polycarbonate membrane with 0.4-μm pore size; Corning, USA), and 200 μL of fluorescein isothiocyanate (FITC)-dextran solutions (0.5 mg/mL; Sigma) with different molecular weights (20 and 70 kDa) were added on top of Transwell insert. Then, the insert was loaded into a 24-well plate containing 800 μL of distilled water. The diffusion profiles of FITC-dextran molecules through L6 hydrogel nanofilm were determined by collecting solutions in the 24-well plate at each time points and measured the fluorescence intensity using a microplate reader (Infinite M200; TECAN, Switzerland).

5.2.8 Cell coating with polysaccharides and SA-Ty

MIN6 β-cells were seeded on tissue culture plate and cultured for 3 days. Firstly, cells were washed twice with PBS. Then, GC-T-RITC solution and SA-Ty were added. After incubation, cells were washed twice with PBS. The degree of coating was confirmed

by measuring red fluorescence of GC-T-RITC at λ_{ex} = 543 nm / λ_{em} = 580 nm (RITC). Similarly, green fluorescence at λ_{ex} = 495 nm / λ_{em} = 525 nm (FA) was measured to detect HA-T-FA. For suspension cells, cells were collected in conical tube by centrifugation for every step.

5.2.9 Quartz crystal microbalance

Cr/Au (Chromium/gold) crystal (5 MHz, 1 inch-diameter, AT-cut, plano-plano) was used to deposit GC-T/HA-T layers. Before the deposition, the crystal was treated with piranha solution (H_2SO_4/H_2O_2 = 3:1) for 5 min and oxygen plasma for 5 min to clean and set negative charge on the surface. Next, the crystal was dipped into the 0.1 % GC-T solution with 0.05 U/ml SA-Ty. After 10 min, the electrode was rinsed twice with PBS for 1 min. To eliminate remaining PBS, the crystal was dried with air blower. Layer-by-layer (LbL) deposition was proceeded with 0.1 % HA-T solution until 5 bilayers were stacked. The hydrogel film deposited crystal was analyzed by QCM (QCM200, Stanford Research Systems, USA) for each layer. The accumulative mass can be calculated by following equation.

$\Delta f = -C_f * \Delta m$

where

Δf = the observed frequency change in Hz

Δm = the change in mass per unit area in g/cm^2

C_f = the sensitivity factor for the crystal (56.6 Hz μg^{-1} cm^2 for a 5 MHz AT-cut quartz crystal at RT)

5.2.10 LbL encapsulation of single cells

Prior to each encapsulation process, the activity of SA-Ty was measured. Lyophilized GC-T and HA-T was dissolved at 10 mg/ml in 0.1 % acetic acid and PBS, respectively. After fully dissolved, the solutions were diluted 10 times with PBS, making final concentration of 1 mg/ml, and filtered through sterilized 0.2 μm membrane. Jurkat cells were collected, washed twice with PBS and prepared at the density of 1×10^7 cells per 1 ml of PBS. 100 μl of cell suspension were seeded into a 3.0 μm polycarbonate membrane (Transwell® 6.5 mm insert, 24-well plate, Corning®). After 600 μl of 1 mg/ml GC-T solution and 0.05 U/ml SA-Ty was added into a well of a 24-well plate, the cell-containing membrane was dipped for 10 min at RT. During incubation, the plate was tapped every 2 min. After 10 min, the membrane was transferred to the next well with 500 μl of media for 30 sec once and 500 μl of PBS for 1 min twice on a shaking incubator. Subsequently, HA-T and GC-T were applied alternatively in the same manner. When the last layer was finished, the cells were dispersed into cell culture medium.

5.2.11 Characterization of the encapsulated cell surfaces

ζ-potential Cells were fixed with 4 % PFA for 10 min and prepared at a density of 1×10^6 cells per 1 ml of PBS. The ζ-potential of native or encapsulated cells were measured with Nano ZS (Malvern Instruments, Germany).

Flow cytometry (FACS) Cells were encapsulated with GC-T-RITC and HA-T-FA. After fixing, cells were prepared at 1×10^6 cells per 500 μl of PBS. Fluorescence of RITC and FA was measured by a flow cytometry (FACS Aria II, BD Biosciences, USA) using lasers of wavelength of 488 nm and 633 nm. 1-layer encapsulated cells with GC-T-RITC and HA-T-FA were used as positive controls for gating.

Confocal laser scanning microscopy (CLSM) After encapsulated with GC-T-RITC and HA-T-FA, cells were fixed with 4 % PFA for 15 min at RT. Cells were placed on a 20 mm confocal dish and imaged via confocal microscope (LSM 780, Carl Zeiss, Germany)

Transmission electron microscopy (TEM) To confirm the nano thin hydrogel on the cell surface, TEM (Talos L120C, 120kV, FEI, Czech) image was analyzed. For the preparation of TEM sample, native and encapsulated cells were fixed with Karnovsky's fixative. Cells were treated with 1% osmium tetroxide in cacodylate buffer for 1 h, 0.5% uranyl acetate overnight at 4 °C. After dehydrated in ethanol, the samples were embedded in Spurr's resin. The specimens were sectioned by using ultramicrotome (EM UC7, Leica, Germany).

5.2.12 LbL encapsulation of pancreatic β-cell spheroids

To fabricate β-cell spheroids, MIN6 pancreatic β-cells were detached from tissue culture plate with 0.25 % trypsin-EDTA. Then, the cells were seeded into an ultra-low attachment 96-well plate (Corning, USA) at a density of 5×10^3 cells/well in 100 ul of culture medium and incubated in 5 % CO_2 at 37 °C for 3 days. The assembled spheroids were collected in 15 ml conical tubes and washed twice with PBS. 100 spheroids were placed on the 3.0 μm polycarbonate membrane and proceeded LbL encapsulation in the same manner as single cell encapsulation. After encapsulation, β-cell spheroids were transferred to a sterile 35 mm dish in culture medium. Cell viability was measured by staining cells with Live/Dead® Viability/Cytotoxicity Kit that contains calcein-AM and ethidium homodimer-1 (EthD-1). After imaged with fluorescence microscope (EVOS® Cell Imaging Systems, Thermo Fisher Scientific), cells were counted in separate 4 fields. The viability was calculated by dividing the live cell number by total cell number.

5.2.13 Functional analysis of β-cell spheroids

Glucose-stimulated insulin secretion (GSIS) test was performed to evaluate the β-cell functionality. β-cell spheroids were washed twice with D-PBS and incubated in 500ul of D-PBS for 1 h in 5 % CO_2 at 37 °C. After 1 h, low-glucose solution (3.3 mM glucose in D-PBS) and high-glucose solution (20 mM glucose in D-PBS) was treated to different groups and incubated for 2 h in a 37 °C incubator. The supernatants of glucose solution, which contain secreted protein of insulin, were collected from each well. The amount of insulin was measured via mouse insulin enzyme-linked immunosorbent assay (Mouse Insulin ELISA, ALPCO, NH, USA) according to the manufacturer's instructions. β-cell spheroids were lysed with 0.2 % triton X-100 in TE buffer for 30 min with vertexing every 5 min. PicoGreen® assay was performed to quantitate dsDNA of the cells in whole. The insulin level was obtained by dividing the total amount of secreted insulin by the amount of DNA. The stimulation index (SI) was calculated as the amount of the insulin level at high-glucose condition divided by the insulin level at low-glucose condition.

5.2.14 Real-time PCR

Samples were prepared treating Trizol® reagent and collected in 1.8-ml tube. Chloroform was added to the tube and vigorously shaken by hand for 10 s. After a 5-min incubation at RT, the cells were centrifuged (21,055 x g, 20 min, 4 °C). The clear aqueous phase on top was transferred to a new tube. Then, isopropanol was added and inverted several times. After another incubation at RT for 5 min, the cells were centrifuged (21,055 x g, 20 min, 4 °C). The white RNA pellet was collected by eliminating the top aqueous phase, and washed with 75 % ethanol, dissolved completely in molecular grade water, and denatured for 10 min at 60 °C. The RNA concentration was measured and cDNA was prepared by reverse-transcription using the EZ006M kit

(Enzynomics, Korea) according to manufacturer's instructions. Gene expression levels of pancreatic β-cell markers, GLUT-2, insulin-1 (Ins1), and insulin-2 (Ins2) were determined by real-time PCR using SYBR green PCR Mastermix on a StepOnePlus™ Real-Time PCR System (Applied Biosystems). Complementary DNA samples were analyzed for the gene for interest and for the reference housekeeping gene GAPDH.

5.2.15 Physical stress test

For physical stress test, β-cell spheroids were dispersed in 500 μl of PBS in 1.7 ml Eppendorf tube after washing twice in PBS. Tabletop centrifuge (MiniSpin Plus, Eppendorf, Germany) was used to centrifuge spheroids at 1,100 and 4,000 rpm for 5 min. Between each step of centrifugation, clustered spheroids were resuspended without changes in PBS. After 3 times, residual cell traces are stained with calcein-AM and EthD-1 and imaged with fluorescence microscope.

5.2.16 Prevention of Cell-Cell interaction between L6 encapsuled cell/spheroid and NK cell

After preparation of K562 cell or T-MSC spheroid with L6 encapsulation and labeling with CellTracker™ Green (Invitrogen), NK-92 cells were washed twice with serum free media, and labeled with 1 mM cellTrace Far-red (Invitrogen) at 37 ℃ for 10 min. Then, the labeled cells were washed with complete medium containing FBS, and used for experiment. For fluorescence image of interaction between NK-92 cell and K562 cell, the labeled cells were loaded on 18 μm clean coverslips (NK-92 0.5×10^6 cells/mL & K562 0.1×10^6 cells/mL) and incubated for 2 hours at 37 ℃ with 5 % CO_2 in humidified incubator. Then, fluorescence images were acquired at that time. For spheroid, each spheroid was load on flat 96 well plate (SPL, Korea). To measure the initial size (t = 0 h) of the spheroid, fluorescence images were acquired without NK-92 cells. After

acquiring the initial images, NK-92 cells (0.15×10^6 cells/well) were added to the each well. Then, the flat 96 well plate was mounted on a microscope stage equipped with a Chamlide TC incubator system (Live cell Instrument, Korea), which maintains a cell culture condition (37°C, 5 % CO_2). Fluorescence images were acquired every 3 h for 24 h. The size of the spheroid was measured through the acquired fluorescence image. A modified Olympus IX 83 epi-fluorescence microscope with a 10 X (UPlanFLN, NA=0.30) objective lens and an ANDOR Zyla 4.2 sCMOS camera was used for imaging experiments. A U-LH75XEAPO Xenon lamp, 75W (Olympus) and GFP (EX BP 470/40, BS 495, EM BP 525/50), Cy5 (EX BP 620/60, BS 660, EM BP 770/75) filter sets were used for fluorescence imaging. The microscope was automatically controlled by Micro-manager. Acquired images were analyzed and processed with Image J.

5.2.17 Flow cytometry for NK-92 cytotoxicity

K562 cells labeled with CellTracker™ Green (10^5 cells/well) and NK-92 cells (10^5 cells/well) were added in 96 wells. After incubating 4 h, Cell suspension was prepared in PBS containing 2 % FBS, 0.1 % sodium azide (Sigma) and 1 mM EDTA (Sigma) for staining and flow cytometry analysis. To assess cytotoxicity, dead cells were labeled with CYTOX Red (Invitrogen) staining. Cytotoxicity was measured by the percentage of CFSE+CYTOX+ cells. Flow cytometry was performed using FACS CantoII (BD Bioscience), and data was analyzed using FlowJo (FlowJo, LLC).

5.2.18 Isolation of primary splenocytes

Isolated mouse spleen was washed with PBS twice, and placed on petri dish. Then, spleen was mashed by the cap of 1.8 mL tube. After fine grinding, cap and dish were rinsed and gathered the mashed spleen into 50 mL conical tube. Pour additional PBS to

reach total volume to 30 ml. Centrifugation with 800 x g for 3 min, discard supernatant and resuspend pellet with red blood cell lysis buffer (Sigma) following the manufactures' procedure. After the red blood cell lysis, solution was place into 40 μm cell strainer and washed with 30 ml PBS twice. Count the cell with hemocytometer.

5.2.19 Induction of type-1 diabetes mellitus in mice

8-week-age BALB/C mice were purchased from DaeHan-Bio link (Chungcheongbuk-do, Republic of Korea). All animal procedures were ensured by Institutional Animal Care and Use Committee (IACUC). Streptozotocin was dissolved in sodium citrate buffer adjusted to pH 4.5 before use. Streptozotocin (80 mg/kg weight) was administered to BALB/C mice that were fasted overnight. Diabetes was considered to be induced when non-fasting blood glucose levels were maintained over 300 mg/dL for 3 consecutive days.

5.2.20 β-cell transplantation into diabetic mice

MIN6 insulinoma cells were formed into spheroids (5K cells/spheroid) and transferred to polyethylene tubes before transplantation. BALB/C mice were anesthetized intraperitoneally by a 4:1 mixture of zoletil and rompun. After the removal of hair, a small incision of skin was made to extrude the kidneys. The capsule membranes were carefully cut with needles for the entrance of cell-containing tubes. PBS (sham), 150 non-coated spheroids (native), 150 non-crosslinked spheroids (crosslink-x), or 150 crosslinked spheroids (crosslink-o) were transferred from the PE tubes to the kidneys with a Hamilton syringe. The cut membranes were closed with a cautery, and the kidneys were returned to the body. After the skin closure with suture, the mice were moved to pre-warmed cages. Weight and non-fasting blood glucose levels of the mice were measured daily until day 7, and once every two days thereafter until day 30. On

day 30, BALB/C mice were anesthetized intraperitoneally by a 4:1 mixture of zoletil and rompun. After the removal of hair, a small incision of skin was made to extrude the kidneys. The blood vessels directly connected to the kidneys were tied tightly with threads to prevent bleeding. The kidneys were cut with surgical scissors and fixed in 10 % neutral-buffered formalin (NBF). After the skin closure with suture, the mice were moved to pre-warmed cages. Weight and non-fasting blood glucose levels of the mice were measured for a couple of days after nephrectomy. The mice were sacrificed after the blood glucose levels of all groups increased over 300 mg/dL.

5.2.21 Intraperitoneal glucose tolerance test

The fasting (16 h) blood glucose levels of MIN6 spheroids transplanted mice were measured before the administration of glucose. The blood glucose levels were measured at 15, 30, 60, 90, 120, and 240 m after the intraperitoneal injection of 20 % D-glucose(2 g/kg mouse) dissolved in PBS.

5.2.22 Histological evaluation of kidney capsule sections

After fixation in 10 % NBF for 3 d, kidneys were transferred to tissue cassettes and rinsed with running tap water. The kidneys were dehydrated and infiltrated with paraffin using a tissue processor. The tissues were embedded in paraffin blocks and sectioned at 5 um thickness on microscope slides. After the hydration, the antigens of the tissues were unmasked with sodium citrate buffer (pH 6.0) at 100 °C. The sections were blocked with goat serum (Abcam, UK) for 1 h and bound to rabbit anti-insulin primary antibody (Cat no. ab63820, Abcam) overnight at 4°C. After washing, the sections were bound to goat anti-rabbit secondary antibody Alexa Fluor 594 (Invitrogen) at dark room for 1 h. The tissues were washed several times and mounted with coverslips. The stained tissues were examined immediately with fluorescence microscope.

5.2.23 Statistical analysis

Experiments were carried out at least triplicated for statistical analysis. All data are expressed as mean ± standard deviation (SD). Statistical significance was determined by paired student's t-test with * $p < 0.05$, ** $p < 0.01$, *** $p < 0.005$.

5.3 Results and Discussion

5.3.1 Characterization of GC-T, HA-T and SA-Ty.

To fabricate the multilayer hydrogel nanofilm, two oppositely charged polysaccharides, GC and HA, are chosen as building blocks for layer-by-layer (LbL) assembly. Additionally, tyrosinase-reactive monophenol residues are introduced to each polysaccharide to provide an enzyme-mediated crosslinking reactivity. By the EDC-NHS coupling reaction, monophenol residue conjugated glycol chitosan (GC-T) and hyaluronic acid (HA-T) were synthesized, respectively **(Figure 5.2)**. ^{1}H-NMR spectra of GC-T showed peaks at 6.791 and 7.100 ppm, whereas that of HA-T at 6.847, 7.161, 7.272, 7.447 ppm, which are corresponding to protons of phenols (Figure S1). Degree of substitution (DS) was calculated as a ratio of integrated areas of a proton of monophenol to 3 protons of N-acetyl group. DS of GC-T was 10.66 % and that of HA-T was 17.50 %. ζ-potential of GC-T and HA-T was measured to be 7.962 ± 1.457 mV and -17.392 ± 3.763 mV, respectively, indicating that both polysaccharides maintained their original charges regardless of monophenol conjugation **(Figure 5.3)**. Then, the enzymatic reactivity of SA-Ty with the modified polysaccharides was measured. The initial oxidation rate, V_0, of SA-Ty on GC-T was 2.779 ± 0.046 μM min^{-1} and HA-T was 1.423 ± 0.023 μM min^{-1} when 0.0028 U/ml of SA-Ty and 0.1 % of each substrate were applied. The reaction solutions turned its color to brown within time. After full reaction, the FT-IR spectra was obtained using lyophilized samples. The broad peak of O-H bond at 3100-3500 cm^{-1} increased and the peak of aromatic C=C bond decreased at 1500-1800 cm^{-1}, indicating that diphenol and o-quinones were increased due to monophenol oxidation mediated by tyrosinase. The mechanisms of the hydrogel nanofilm formation involves enzymatic oxidative reaction mediated by SA-Ty and

crosslinking reactions of o-quinone with amine, thiol, and another quinone **(Figure 5.4)**. The catalysis of monophenols to o-diphenols(catechol) and o-quinones by the tyrosinase requires two-step oxidation previously described [126]. These o-quinones on both polysaccharides form covalent bonds with amines, thiols, and other quinones on cell surface molecules and other polysaccharides via Michael addition, Schiff base reaction, and aryloxyl coupling reaction [124]. To verify the crosslinking formation by SA-Ty with GC-T and HA-T, we demonstrated bulk hydrogel formation using high concentration of polysaccharides **(Figure 5.5)**. 5 % (w/v) GC-T and HA-T individually formed hydrogel crosslinked by 0.05 U/ml of SA-Ty. Interestingly, half and half mixture of GC-T and HA-T (2.5 % (w/v) each) formed more stable hydrogel than other two individual hydrogels, which aroused from additional electrostatic interaction between GC-T and HA-T. Swelling ratio of each hydrogels represented its polysaccharide characteristic. Hydrophilic HA-T based hydrogel swelled the most, in contrast, GC-T, which is known to be hydrophilic in acidic condition, did not swell as much in PBS, and hydrogel mixed with both polysaccharides showed the intermediate swelling ratio. Moreover, to analyze the porosity and porous structure of LbL formed hydrogel nanofilm, the diffusion profiles of fluorescein isothiocyanate (FITC)-conjugated dextran across the nanofilm were examined. Diffusion test of FITC-dextran molecules (20 and 70 kDa) was conducted in a Transwell system with membrane insert with 6-layered hydrogel nanofilm on it **(Figure 5.6)**. Diffusion profile showed that FITC-dextran (20 kDa) with a lower molecular weight diffused much faster and in larger quantities through the Transwell and nanofilm than FITC-dextran (70 kDa) with a higher molecular weight. The amount of diffused FITC-dextran molecules (20 and 70 kDa) across the hydrogel nanofilm was significantly less than that of Transwell itself.

This result may suggest again that GC-T and HA-T hydrogels formed by SA-Ty possesses dense internal polymer networks comprising nanofibrillar structures.

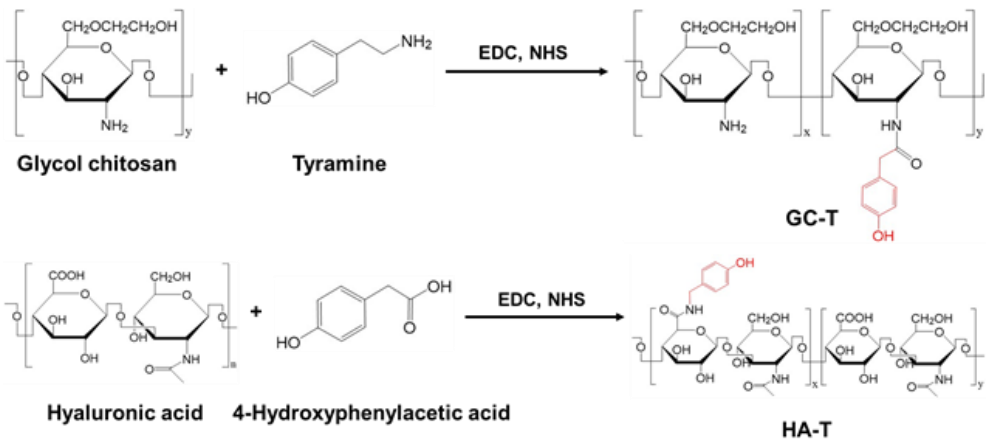

Figure 5. 2 Synthesis of GC-T and HA-T by conjugation of monophenols to GC and HA.

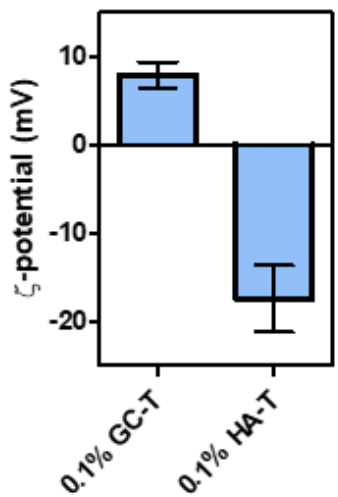

Figure 5. 3 ζ-potential of 0.1 % (w/v) GC-T and 0.1 % (w/v) HA-T.

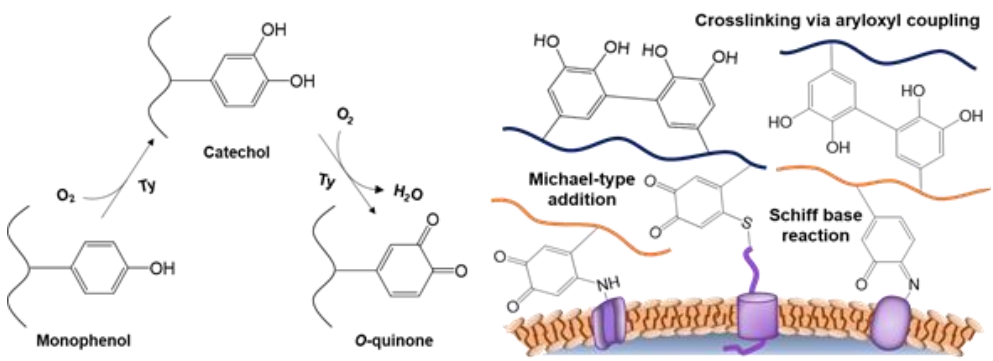

Figure 5. 4 Schematic illustration of enzymatic 2-step oxidative reaction mediated by tyrosinase and nonenzymatic crosslinking reactions of o-quinone.

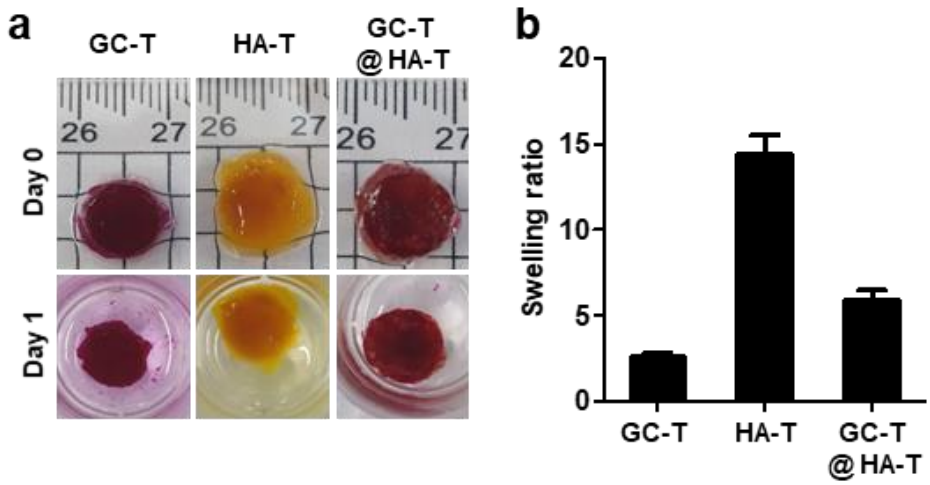

Figure 5. 5 Hydrogel formation by enzymatic crosslinking. a) Images of between 5 % (w/v) GC-T, 5 % (w/v) HA-T, and 2.5 % (w/v) GC-T and 2.5 % (w/v) HA-T hydrogel crosslinked by tyrosinase at Day 0 and Day 1 in PBS. b) Comparison of swelling ratio between 5 % (w/v) GC-T, 5 % (w/v) HA-T, and 2.5 % (w/v) GC-T and 2.5 % (w/v) HA-T hydrogel.

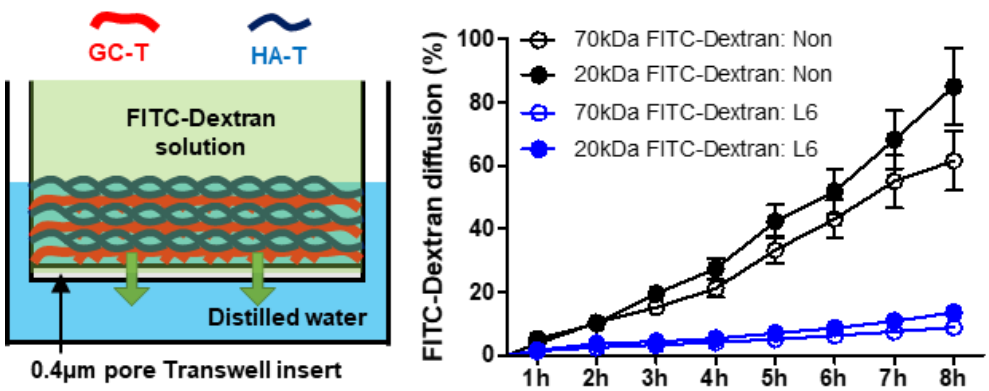

Figure 5. 6 Diffusion test. Schematic illustration of the experimental set-up and the diffusion profile of FITC-dextran (20 and 70 kDa) across 6-layers of GC-T and HA-T (L6) crosslinked by SA-Ty.

5.3.2 Optimization of hydrogel nanofilm formation.

Prior to form hydrogel nanofilm on the cell surface, the cytotoxicity of SA-Ty was assessed by incubating Jurkat cells in SA-Ty containing media upto 60 min long and 5 μM dose. On the basis of the cytotoxicity, the optimal molar concentration of SA-Ty used in this study was ranged from 2.5 to 5 μM, where it had no adverse effect on cell viability. To optimize the formation condition of hydrogel nanofilm on cell surface, the degree of coating was investigated with various parameters as follows: the concentration of SA-Ty, reaction time, and the concentration of polysaccharide. Mouse pancreatic β-cell line MIN6 cultured on cell culture plate was coated with single layer of RITC conjugated GC-T (GC-T-RITC). The fluorescence intensity of GC-T-RITC increased upto 0.05 U/ml of SA-Ty but decreased at higher concentrations. It is interpreted that polysaccharides react more with each other rather than attaching to cell surface at high concentration of SA-Ty. The coating efficiency was augmented in accordance with the reaction time and concentration of polysaccharides. Longer reaction time and higher concentration of polysaccharide increased the coating efficiency in constant 0.05 U/ml SA-Ty treatment. With the optimized SA-Ty treatment, the effect of SA-Ty on cell coating with GC-T-RITC and fluoresceinamine isomer I conjugated HA-T (HA-T-FA) was investigated. Fluorescence intensity differs in each polysaccharide as normal cell surface naturally exposes negative charge, GC-T with positive charge tends to be more attracted than negatively charged HA-T. In addition, as external GC-T tends to be in close proximity to the cell surface, treatment of SA-Ty greatly increased the intensity of GC-T-RITC upto 2.9-fold, while HA-T-FA showed less dependency in SA-Ty. Moreover, the coating efficiency of negative charged HA-T-FA substantially increased 2.4-fold when GC-T-RITC had been coated prior to HA-T-FA **(Figure 5.7)**. To inspect the feasibility of LbL assembly of hydrogel nanofilm,

frequency changes were measured in each stacked layer on O_2 plasma treated Cr/Au electrode by quartz crystal microbalance **(Figure 5.8)**. In the 6th layer, the cumulative mass per area of hydrogel film was 90.16 μg/cm^2 without SA-Ty, but increased to 148.50 μg/cm^2 with SA-Ty treatment in every step. The film was deposited average 1.6-fold with SA-Ty than without. In consequent data of mass increment, layers treated with SA-Ty gradually increased upto 10-layers but the increasing amount decreased after 6-layers, in contrast, layers formed only by electrostatic force have shown its mass increment became plateau after 6-layers. Thus, we designated 6-layers of polysaccharides as the optimal layers of hydrogel nanofilm on the cell surface.

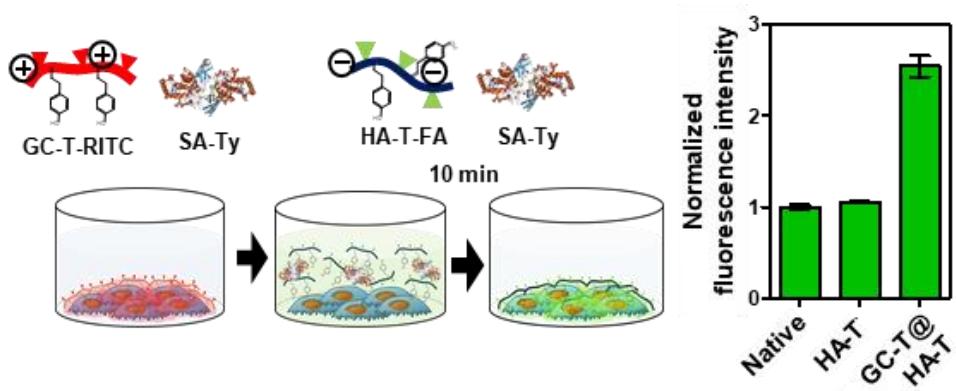

Figure 5. 7 The efficiency difference of HA-T-FA coating on different cell surface charges.

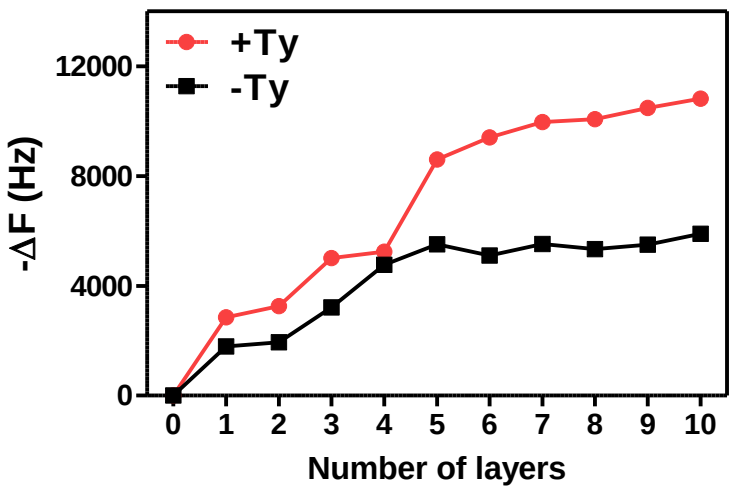

Figure 5. 8 Quantitative analysis of layer-by-layer deposition of GC-T and HA-T on cell surface.

5.3.3 LbL single cell encapsulation with hydrogel nanofilm.

Verification of the electrostatical and enzymatical coating of GC-T on the mammalian cell surface was analyzed by using Jurkat cells, suspension cells with cell clumping characteristics when incubated overnight. Cells were coated with 1 layer of GC-T-RITC and cultured. Impressively, cells with 0.1 % GC-T-RITC coated showed more dispersed locations and made only a few clumps while cells coated with less than 0.05 % GC-T-RITC solution and non-treated (native) showed normal clumping phenomenon. The result demonstrated that the positive charge of the GC-T hydrogel nanofilm formed on the cell surface induced slight repulsion between the cells to disperse. We then increased the coating layer to 6-layers by dipping the cell-loaded 3.0 μm polycarbonate transwell membrane into the coating solutions, medium, and PBS, sequentially, to minimize cell damage due to common centrifugation method (**Figure 5.9)**. GC-T was applied for the 1st and odd layers and HA-T was applied for even layers. Here, non-coated cells were termed 'Native' and (n)-layer encapsulated cells were termed 'L(n)'. Change in ζ-potential of the cell surface was measured in accordance with the deposition of positively and negatively charged polysaccharides. Similarly, in flow cytometry analysis performed on each (n)-layer, the cell population shifted to the right as layers were increased indicating increment of fluorescent signal in coated cells. Precisely, cell membrane before and after encapsulation was visualized by transmission electron microscopy images. Hydrogel film was densely fabricated on cell membrane with the thickness of average 139.40 ± 7.73 nm when 6-layers were stacked, which is remarkably thicker than previously reported electrostatic force based LbL cell encapsulation methods without any adverse effect to the cell viability.

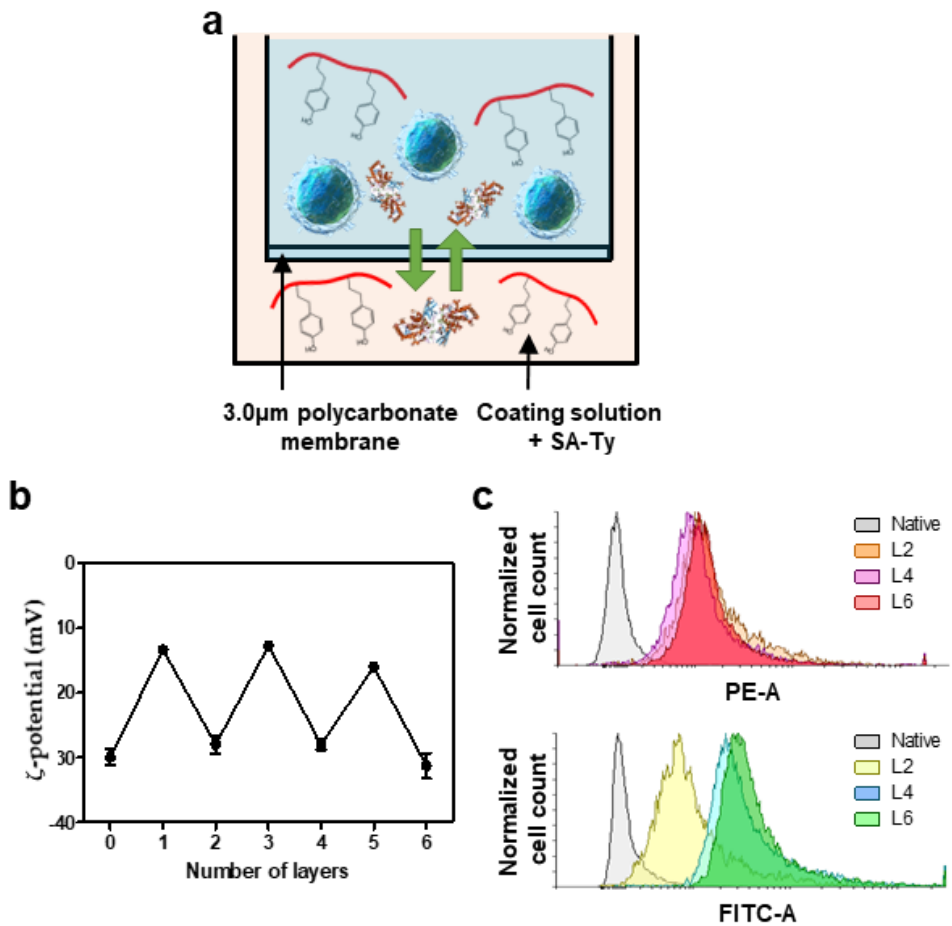

Figure 5. 9 Single surface nanofilm coating. a) Schematic image of single cell layer-by-layer hydrogel nanofilm formation. b) Changes in ζ-potential of encapsulated cell surface by the increment of layers. c) Flow cytometry analysis of encapsulated cells base on the increasing numbers of layers. GC-T-RITC and HA-T-FA were detected using PE channel and FITC channel, respectively.

5.3.4 Hydrogel nanofilm encapsulation of MIN6 β-cell spheroids.

LbL cell encapsulation method constructed above for single cells was applied to β-cell spheroids **(Figure 5.10)**. MIN6 β-cells were cultured in spheroid form prior to encapsulation, since connectivity and cell-cell interactions in β-cell clusters are essential for the glycemic control [127, 128]. β-cell spheroids were found to be average 350.0 ± 24.5 μm in diameter, as measured for 20 spheroids at 4 locations each. Hydrogel nanofilm on the spheroids was visualized using fluorescence labeled polysaccharides. Cell viability was evaluated on the day of encapsulation **(Figure 5.11)**. Base on the Live/Dead assay images, most cells were alive in both groups of Native and L6, maintaining its spheroid shape. To assess the cellular functionality after L6 encapsulation, glucose-stimulated insulin secretion (GSIS) assay was performed for Native and L6 groups. The β-cell spheroids were induced to secrete insulin in response to the two different concentrations of glucose solution in PBS. Insulin levels at low-glucose solution of Native and L6 were similar, in contrast, L6 expressed higher amount than Native at high-glucose solution. Stimulation index (SI), calculated by dividing the insulin level at high-glucose solution by the insulin level at low-glucose solution, was 4.1-fold higher in L6 compare to the Native. The expression level of mRNA related to β-cell function was evaluated by RT-PCR **(Figure 5.12)**. Among three β-cell function-related genes (GLUT2, Ins-1, and Ins-2), only Ins-1 expression was elevated in L6 group compared to Native β-cell spheroids when they were incubated in high-glucose medium for 24 h after encapsulation. According to these data, insulin expression of encapsulated β-cells was improved, probably by the additional interaction between membrane proteins and hydrogel nanofilm via electrostatic interactions and/or SA-Ty mediated covalent bonding. As known, transmembrane proteins, including GLUT2 transporter, ATP-sensitive K+ channel (K+ATP), voltage-dependent Na+ channel

(VDNaC), voltage-dependent Ca2+ channel (VDCC), voltage-dependent K+ channel (K+V), and gap junction channels, play a pivotal role in the mechanism of glucose responsive insulin secretion, and well influenced by the environmental factors [129]. Along with TEM and confocal images, we assumed that firmly formed hydrogel nanofilm on the cell membrane may affect β-cell function via inducing subtle structural changes on membrane channels without cytotoxicity or functional impairment. Overall, encapsulation of spheroids with hydrogel nanofilm did not hindered the β-cell glucose sensitivity.

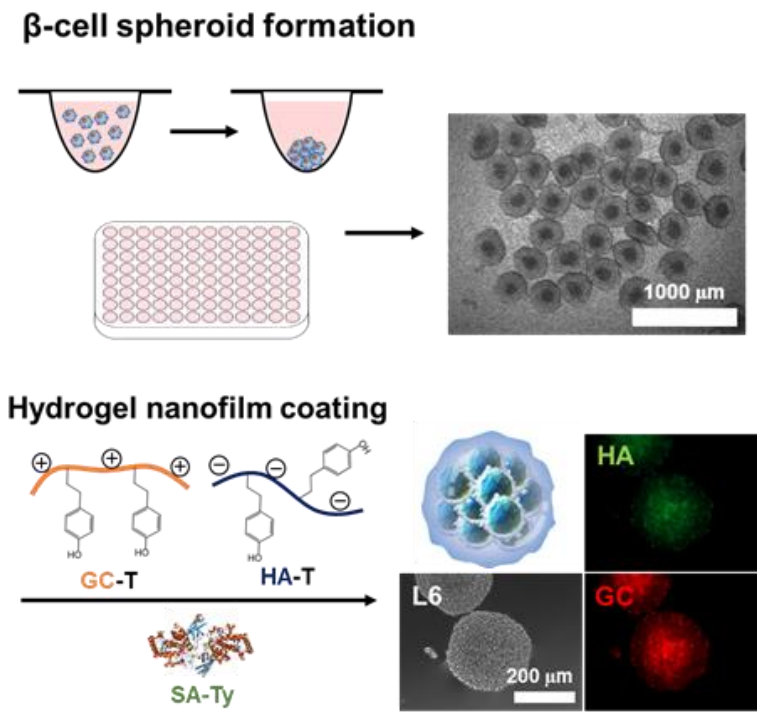

Figure 5. 10 Schematic and fluorescence images of β-cell spheroid encapsulated with hydrogel nanofilm (HA-T-FA in green, GC-T-RITC in red).

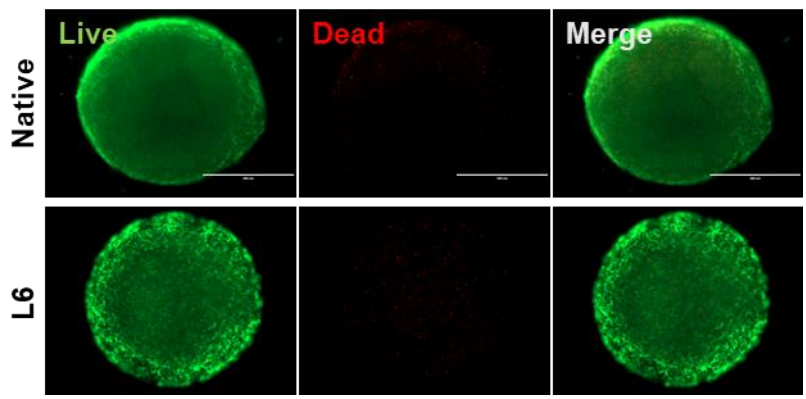

Figure 5. 11 Live/Dead assay images of Native and L6 encapsulated β-cell spheroids. Live cells were represented in green, and dead cells were in red. Scale bar, 200 μm.

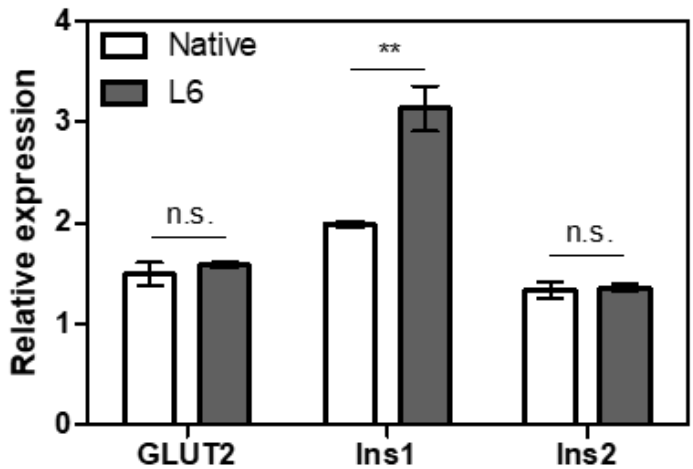

Figure 5. 12 Comparative Realtime PCR data analysis of pancreatic β-cell markers between Native and L6 β-cell spheroid.

5.3.5 Hydrogel nanofilm as a physical barrier against external environment.

Cell damage and apoptosis caused by the external physical stress such as syringe pressure and blood fluidic shear force are the major challenges in cell transplantation. By the stability and crosslinking advantage of hydrogel nanofilm driven by SA-Ty, we assumed our hydrogel nanofilm can overcome these challenges. To analyze the enhanced sustainability of nanofilm compare to common LbL with polyelectrolytes, L6 encapsulated β-cell spheroids, with/without SA-Ty derived crosslinking, were incubated for 6 days and imaged each 2 days **(Figure 5.13)**. Images represented that the hydrogel nanofilm crosslinked by SA-Ty was able to be sustained longer time. In contrast, the fluorescence of the LbL formed without SA-Ty dwindled as time goes by, indicating crosslinking with SA-Ty reinforce the interaction between polysaccharides to persist against exogenous environment. To investigate whether the hydrogel nanofilm protect β-cell spheroids from physical stress, both Native and L6, were repeatedly centrifuged at low speed (81 x g) and high speed (1073 x g). Spheroids in both Native and L6 group maintained its spherical shape at low centrifugal speed, however, at high speed, Native collapsed while L6 withstood the high pressure, proving durability of hydrogel nanofilm. In addition, hydrogel nanofilm to approve as a physical barrier, inhibition of cell-cell interaction between spheroid and NK cell were tested, as recognition of peptides or sugars on cell surface of antigen presenting cells is a priority to active immune system in T cells at transplantation **(Figure 5.14)** [130]. Prior to validate β-cell spheroids, we co-cultured L6 encapsuled K562 cell, a human myelogenous leukemia cell line that are easily killed by NK cells, with NK-92 cell, a natural killer cell line. Firstly, verification of single K562 cell coating with GC-T-RITC and HA-T-FA was demonstrated **(Figure 5.15)**. Then, green labeled L6 encapsuled K562 cells

were co-cultured with blue labeled NK-92 cells **(Figure 5.16)**. Significant decrease of binding frequency of NK-92 cell was detected in L6 encapsuled K562 cells compare to native K562 cells. Based on the successful inhibition effect in K562 single cell data, L6 encapsuled β-cell spheroids were co-cultured NK-92 cells. Numerous NK92 cells were detected on the surrounding surface of Native group, but notably less coverage was gained in L6 group **(Figure 5.17)**. By the interaction of NK-92 cell to β-cell spheroids, native β-cell spheroid size depleted in time lapse as NK cell dissociated β-cells off from spheroid starting from its surface. However, L6 encapsuled spheroids conserved its size, representing the reduction of cell-cell interaction with NK cells. Additionally, co-culture with primary splenocytes for 24 h showed the same loss of cell-cell interaction results in L6 encapsuled β-cell spheroids **(Figure 5.18)**. After 24 h, peripheral β-cells on the surface of Native group were observed to protrude outward from spheroids. In contrast, L6 retained the integrity of spheroidal form. Thus, with the properties of long-term conservation, endurance against external pressure, and reduction of cell-cell interaction, characteristic of physical barrier was achieved.

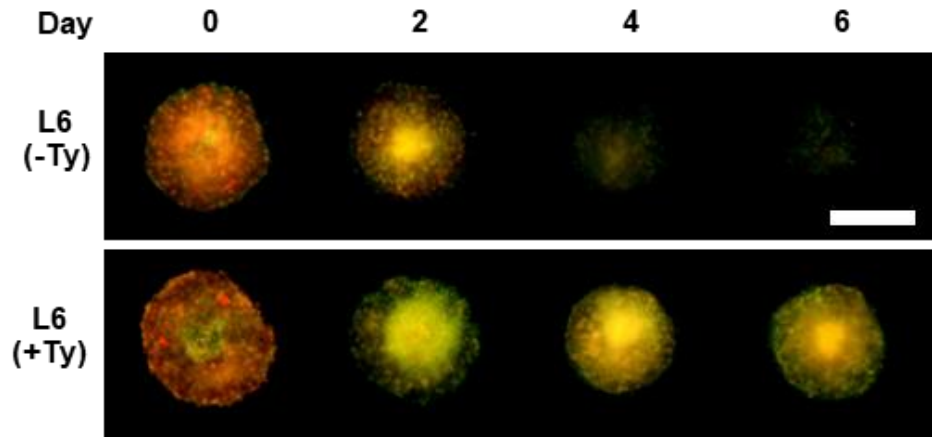

Figure 5. 13 Stability test of hydrogel nanofilm until 1 week. Treatment of SA-Ty prolonged the stability of hydrogel nanofilm.

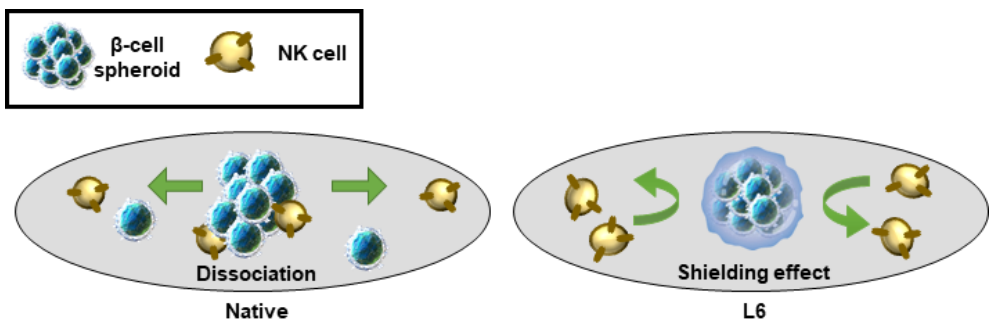

Figure 5. 14 Schematic images of immune protection by L6 hydrogel nanofilm.

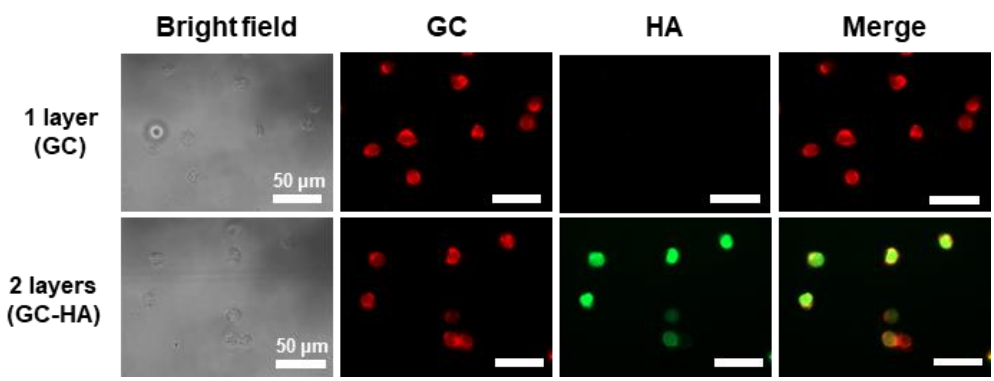

Figure 5. 15 Surface coating of K562 cell with GC-T-RITC and HA-T-FA.

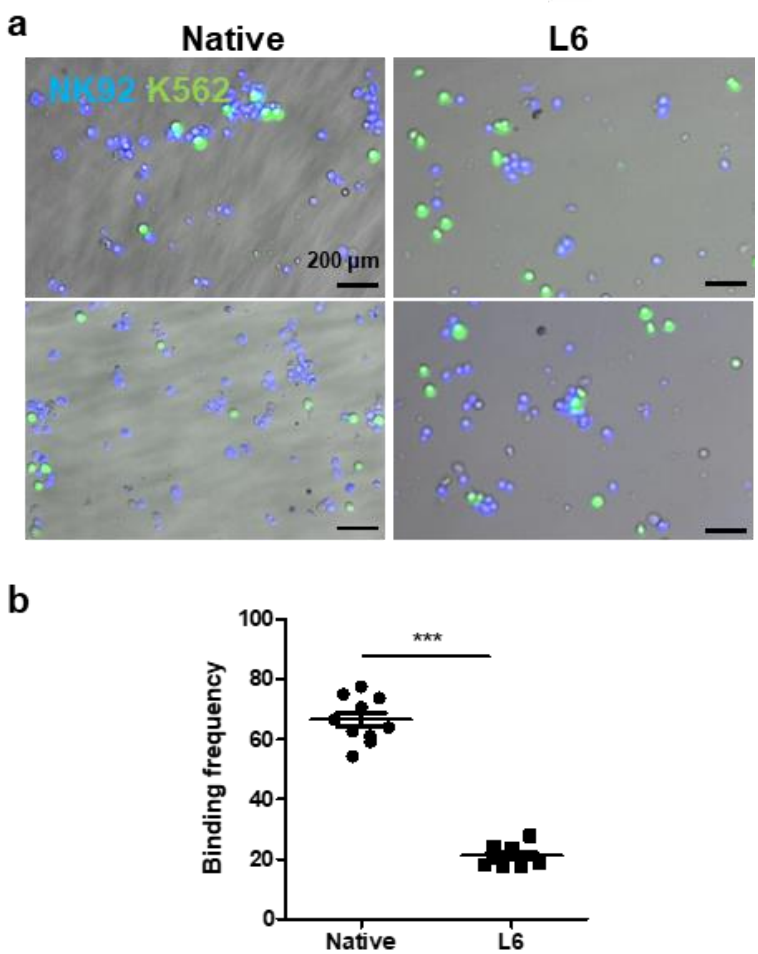

Figure 5. 16 Cell-cell surface interaction between NK92 cell to Native or L6 coated K562 cell. a) Fluorescent microscopic images of cell-cell interaction between NK92 cell and K562 cell with/without hydrogel nanofilm coating. b) Comparison of NK92 cell binding frequency to K562 cell with/without hydrogel nanofilm coating.

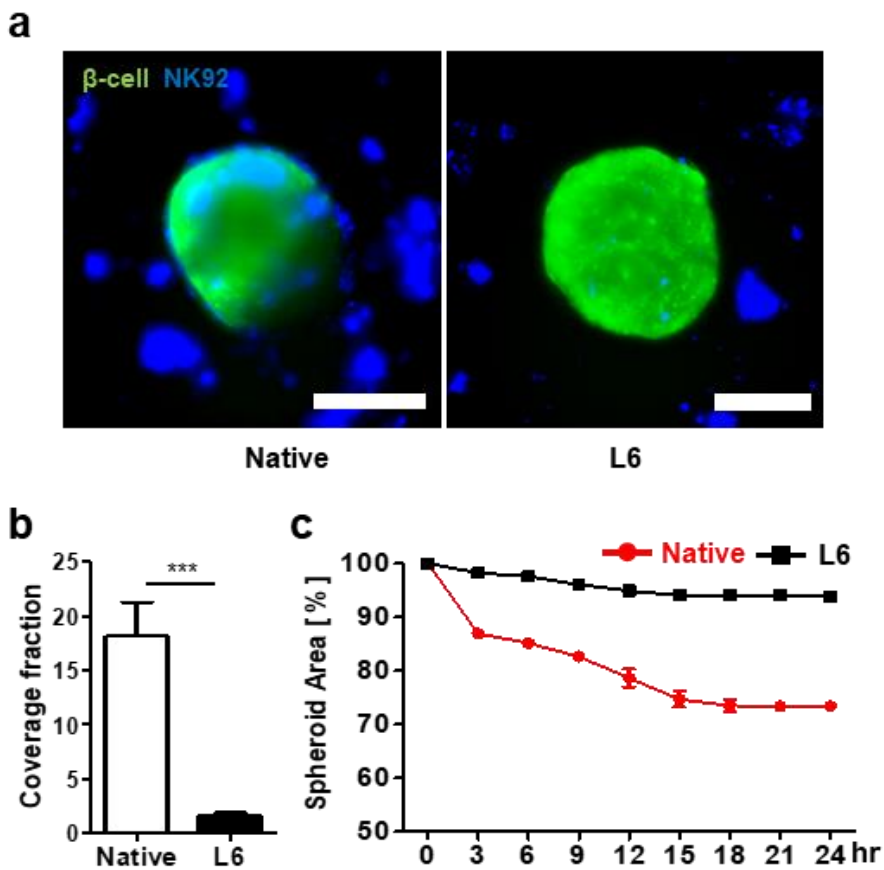

Figure 5. 17 Immune-protection assay. a) Confocal microscopic images of β-cell spheroids with/without hydrogel nanofilm co-cultured with NK92 cell. b) Comparison of the coverage fraction of NK cells on each β-cell spheroid groups (***$p < 0.01$). c) Percentage reduction of β-cell spheroids area by NK cells dissociating β-cells from the spheroid.

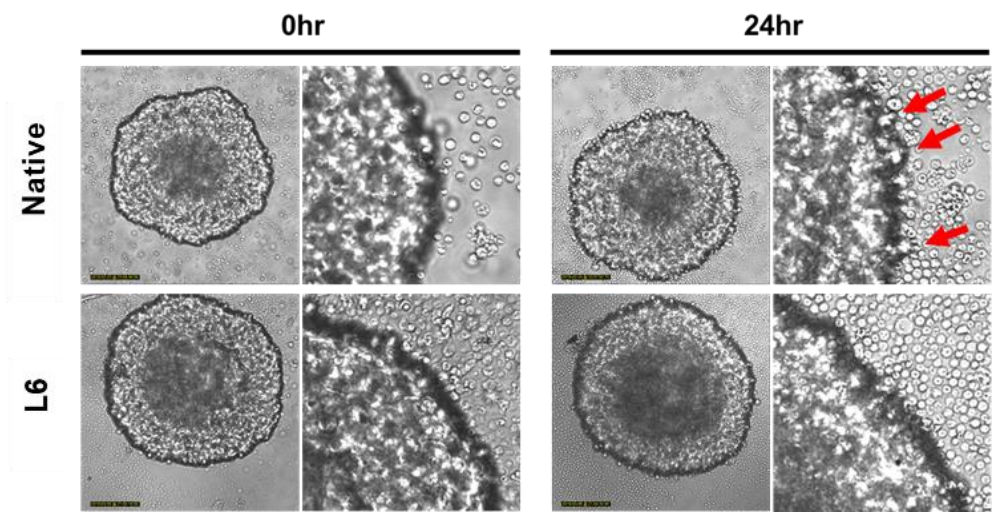

Figure 5. 18 Cell-cell interaction of between primary splenocytes to Native or L6 coated β-cell spheroid.

5.3.6 In vivo evaluation of glycemic control in diabetic mice.

We further examined the functional effects of L6 hydrogel nanofilm encapsulated β-cell spheroid to reverse hyperglycemia and regulate blood glucose levels in a streptozotocin (STZ)-induced type 1 diabetic mouse model **(Figure 5.19)**. The 150 L6 spheroids were homogeneously transplanted into the capsule membrane of kidney. For 3 control groups, sham, Native spheroid, L6 spheroid without SA-Ty mediated crosslinking were also injected. Transplantation of L6 spheroids with SA-Ty crosslinking efficiently declined blood glucose level from hyperglycemic condition to normoglycemic level, and maintained its state for up to 30 days. In contrast, without SA-Ty crosslinking, L6 spheroids did not stably retained blood glucose level to normoglycemic level, and other control groups showed elevated blood glucose levels throughout the transplant time. Moreover, removal of kidney raised the blood glucose level upto hyperglycemic level in L6 spheroid with SA-Ty crosslinking group, representing regulation of blood glucose level in T1D mouse was controlled by the transplanted L6 spheroids. Weight of treated mice followed the opposite trend of blood glucose level, as L6 spheroid with SA-Ty crosslinking group gained weight, on the other hand, other control groups lost its weight because of uncontrolled blood glucose levels **(Figure 5.20)**. After nephrectomy, mice transplanted with L6 spheroid with SA-Ty crosslinking started to lost weight. In vivo glucose-responsive ability of spheroids was also confirmed by performing IPGTT. 16 h after transplantation, L6 spheroids with SA-Ty crosslinking group sufficiently restored glucose tolerance when challenged with a bolus dose of glucose. Histological analysis and expression of insulin confirmed the stable engraftment and sufficient functionality of transplanted spheroids **(Figure 5.21)**. These results provide evidence that encapsulation of β-cell spheroid with L6 hydrogel

nanofilm with SA-ty crosslinking can maintain blood glucose level regulation function in vivo and restore euglycemia in diabetic mice.

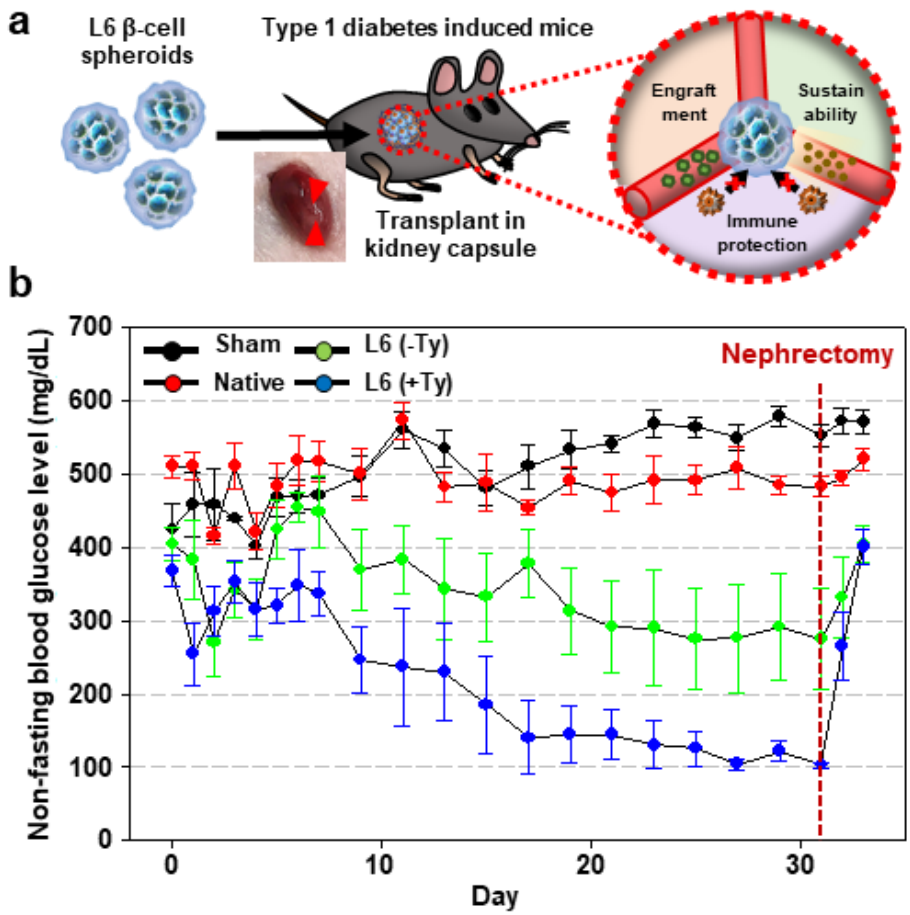

Figure 5. 19 Transplantation of L6 encapsulated β-cell spheroids. a) Schematic image of transplantation of β-cell spheroids into the kidney capsule of BALB/C mice. Non-fasting blood glucose level. b) Non-fasting blood glucose level of mice in each group were monitored periodically.

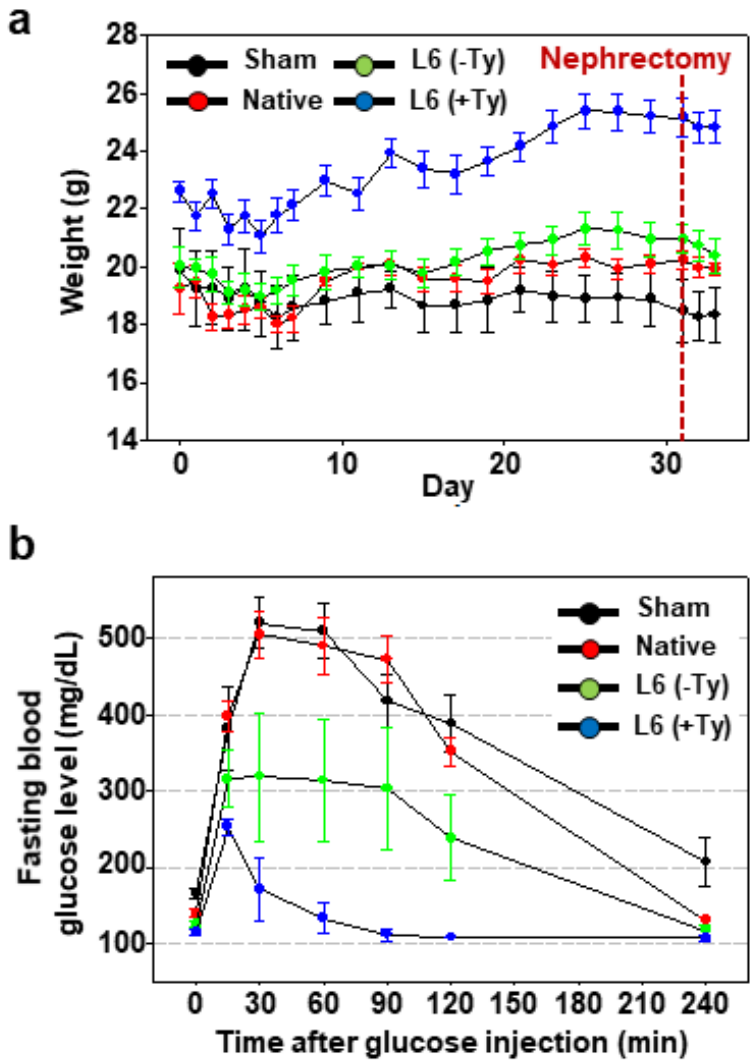

Figure 5. 20 Regulation effects of blood glucose level by L6 encapsulated β-cell spheroids. a) Body weight of mice in each group were monitored periodically. b) Measurement of blood glucose level of mice that were subjected to intraperitoneal glucose tolerance test after implantation.

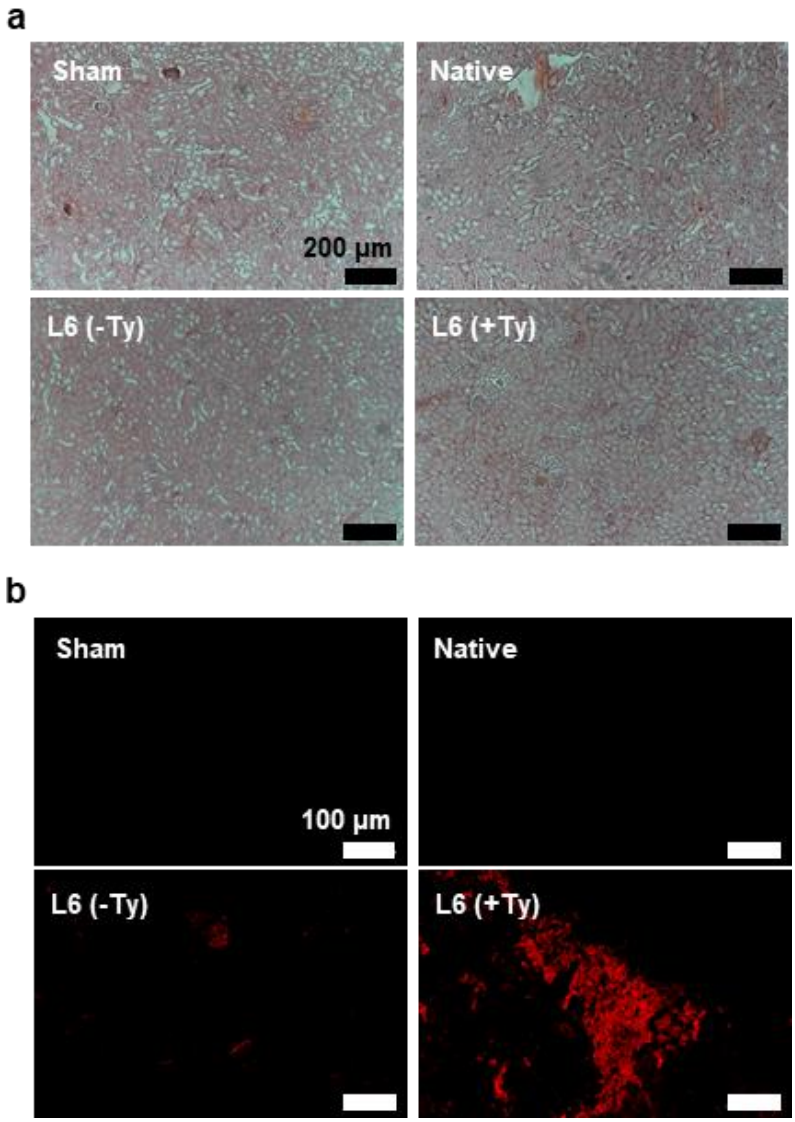

Figure 5. 21 Histological analysis of implants retrieved 30 d after implantation from the STZ-treated BALB/C mice, represented a) H & E staining and b) immunostaining of insulin in each group. Scale bar, 200 µm for upper images and 100 µm for lower images.

5.4 Summary

We have developed a novel enzymatic crosslinking-based hydrogel nanofilm on the surface of pancreatic β-cell spheroids using two polysaccharides with opposite charges and tyrosinase enzyme. The hydrogel nanofilm was fabricated LbL by electrostatically stacking of monophenol group conjugated polyelectrolytes on the surface of β-cell spheroid. Crosslinking of each phenol groups by tyrosinase induced hydrogel nanofilm to be more stable and advanced displayed in vitro and in vivo analysis. In particular, hydrogel nanofilm act as a physical barrier against external environment that endure higher external pressure, and reduce acute host immune response base on cell-cell interaction with NK cells. For the therapeutic application, we implanted L6 coated β-cell spheroids into T1D mice to regulate blood glucose level in vivo, and achieved significant result compare to non-coated β-cell spheroids group. The hydrogel nanofilm formation, we further hypothesize that this approach may be applicable to xenografts in immunocompetent animals over long periods.

CHAPTER SIX:

CONCLUDING REMARKS

6.1 Summary

In this thesis, I investigated the potential of cell surface modification and its applications for tissue engineering in order to develop the new types of cell surface coating for translational medicine. The concepts of surface modification including redox microenvironment and enzyme mediated hydrogel nanofilm formation are based on multi-disciplinary efforts that imparts the conception of biomaterial, chemical and biological engineering. I tried to provide our novel cell coating method with detailed chemical analysis, and biological effects in order to inspire and induce subsequent studies of other researchers to further develop the unique cell surface modification for translational medicine.

In the first part of this dissertation, I have presented current technologies and approaches of cell surface modification for developing ideal stem cell therapy along with clinical studies.

In the second part, I utilized disulfide bond of cell surface protein to react with maleimide-conjugated biomolecules by reducing the bond into reactive thiol groups. Reduction of disulfide bond was induced by mild reductant which in suitable concentration did not affect cell viability and function. Then, various biomolecules with maleimide functional group were attached on the cell surface. Coated cells represented

biomaterials characteristics that allowed rapid assembly of coated cells, layer-by-layering of cells, enhanced interaction between cell-matrix, and localized drug delivery. Although the coating was not stable for a long period of time because of the proliferation of coated cells and harsh microenvironment, it showed its effectiveness well when freshly treated. With this ability, it might be suitable for primary stem cell therapy which treatment should be rapid and simple, but show significant effects of coated biomaterials. This demonstrates that surface reduction-based cell coating might provide a robust platform in the field of both material science and translational medicine.

In the third part, I analyzed the biological effect of reduced microenvironment on stem cell function. Redox change effected cell surface proteins to be reduced, and it surely influenced the internal cell signaling. Reduction by mild reductant increased the focal adhesion of mesenchymal stem cells, which led to increased osteogenic differentiation. By bottom-up analysis, I investigated which cell signaling pathway has been influenced by the increment of focal adhesion and surface protein reduction, the surface protein endoglin, one of the receptors in TGF-β signaling pathway and activated by dimerizing with disulfide bonding. Endoglin depletion suppressed the phosphorylation of Smad2, which resulted in transcription of RUNX-2 early osteogenic marker. Due to the synergistic effect of increased focal adhesion and decreased TGF-β signaling early osteogenic differentiation has been achieved. This demonstrated that reduction of surface protein does not always give adverse effect to stem cell, rather in some ways it can positively influence the cell function by regulating internal cell signaling pathway.

In the last part of the thesis, I fabricated hydrogel nanofilm on the cell surface based on chitosan and hyaluronic acid crosslinked by novel recombinant tyrosinase.

With mono-phenol group conjugated chitosan and hyaluronic acid, it was easily oxidized to form hydrogel within 10 minutes with novel tyrosinase derived form *Streptomyces avermitilis*. When applied to the cell surface, by the electrostatic force between negative charged cell surface and hyaluronic acid, and positive charged chitosan, layer-by-layering of biomolecules were available. Additionally, crosslinking of layered biomolecules enhanced the physical properties of hydrogel nanofilm formed on the cell surface. To broaden the application field, hydrogel nanofilm was applied to β-cell spheroid for type 1 diabetes treatment. Spheroids encapsuled with hydrogel nanofilm showed enhanced ability of enduring higher external pressure against external environment, and reducing acute host immune response based on cell-cell interaction with immune cells. Moreover, when applied to type 1 diabetes mouse model, hydrogel nanofilm encapsulated β-cell spheroid regulated blood glucose level stay stable at normoglycemia level. Thus, I demonstrated that the novel enzyme-based crosslinking hydrogel nanofilm on the cell surface has a robust potential in stem cell therapy.

Cell surface modification method, biomaterials and chemistry in this thesis will be useful to understand the critical cues for ideal stem cell therapy in the aspect of tissue engineering and translational medicine. I believe that this study will significantly contribute to develop more cell surface modification methods and provide inspiration to the other various research fields.

6. 2 References

(1) Ratcliffe, E.; Glen, K. E.; Naing, M. W.; Williams, D. J., Current status and perspectives on stem cell-based therapies undergoing clinical trials for regenerative medicine: case studies. *Br Med Bull* **2013,** *108*, 73-94.

(2) Hwang, Y.; Phadke, A.; Varghese, S., Engineered microenvironments for self-renewal and musculoskeletal differentiation of stem cells. *Regen Med* **2011,** *6* (4), 505-24.

(3) Strauer, B. E.; Kornowski, R., Stem cell therapy in perspective. *Circulation* **2003,** *107* (7), 929-34.

(4) Brunt, K. R.; Weisel, R. D.; Li, R. K., Stem cells and regenerative medicine - future perspectives. *Can J Physiol Pharmacol* **2012,** *90* (3), 327-35.

(5) Chang, C. W.; Hwang, Y.; Brafman, D.; Hagan, T.; Phung, C.; Varghese, S., Engineering cell-material interfaces for long-term expansion of human pluripotent stem cells. *Biomaterials* **2013,** *34* (4), 912-21.

(6) Wu, S. M.; Hochedlinger, K., Harnessing the potential of induced pluripotent stem cells for regenerative medicine. *Nat Cell Biol* **2011,** *13* (5), 497-505.

(7) Pessina, A.; Gribaldo, L., The key role of adult stem cells: therapeutic perspectives. *Curr Med Res Opin* **2006,** *22* (11), 2287-300.

(8) Hwang, N. S.; Zhang, C.; Hwang, Y. S.; Varghese, S., Mesenchymal stem cell differentiation and roles in regenerative medicine. *Wiley Interdiscip Rev Syst Biol Med* **2009,** *1* (1), 97-106.

(9) Trounson, A.; Baum, E.; Gibbons, D.; Tekamp-Olson, P., Developing a case study model for successful translation of stem cell therapies. *Cell Stem Cell* **2010,** *6* (6), 513-6.

(10) Llufriu, S.; Sepulveda, M.; Blanco, Y.; Marin, P.; Moreno, B.;

Berenguer, J.; Gabilondo, I.; Martinez-Heras, E.; Sola-Valls, N.; Arnaiz, J. A.; Andreu, E. J.; Fernandez, B.; Bullich, S.; Sanchez-Dalmau, B.; Graus, F.; Villoslada, P.; Saiz, A., Randomized placebo-controlled phase II trial of autologous mesenchymal stem cells in multiple sclerosis. *PLoS One* **2014,** *9* (12), e113936.

(11) Vacanti, C. A.; Vacanti, J. P., The science of tissue engineering. *Orthop Clin North Am* **2000,** *31* (3), 351-6.

(12) Lodi, D.; Iannitti, T.; Palmieri, B., Stem cells in clinical practice: applications and warnings. *J Exp Clin Cancer Res* **2011,** *30*, 9.

(13) Herberts, C. A.; Kwa, M. S.; Hermsen, H. P., Risk factors in the development of stem cell therapy. *J Transl Med* **2011,** *9*, 29.

(14) Wu, R.; Hu, X.; Wang, J., Concise Review: Optimized Strategies for Stem Cell-Based Therapy in Myocardial Repair: Clinical Translatability and Potential Limitation. *Stem Cells* **2018,** *36* (4), 482-500.

(15) Perin, E. C.; Geng, Y. J.; Willerson, J. T., Adult stem cell therapy in perspective. *Circulation* **2003,** *107* (7), 935-8.

(16) Yang, J. M.; Yang, Y. J.; Kawazoe, N.; Chen, G. P., Encapsulation of individual living cells with enzyme responsive polymer nanoshell. *Biomaterials* **2019,** *197*, 317-326.

(17) Michel, J. B., Anoikis in the cardiovascular system: known and unknown extracellular mediators. *Arterioscler Thromb Vasc Biol* **2003,** *23* (12), 2146-54.

(18) Taddei, M. L.; Giannoni, E.; Fiaschi, T.; Chiarugi, P., Anoikis: an emerging hallmark in health and diseases. *J Pathol* **2012,** *226* (2), 380-93.

(19) Mooney, D. J.; Vandenburgh, H., Cell delivery mechanisms for tissue repair. *Cell Stem Cell* **2008,** *2* (3), 205-13.

(20) Hofmann, M.; Wollert, K. C.; Meyer, G. P.; Menke, A.; Arseniev, L.;

Hertenstein, B.; Ganser, A.; Knapp, W. H.; Drexler, H., Monitoring of bone marrow cell homing into the infarcted human myocardium. *Circulation* **2005,** *111* (17), 2198-202.

(21) Abbina, S.; Siren, E. M. J.; Moon, H.; Kizhakkedathu, J. N., Surface Engineering for Cell-Based Therapies: Techniques for Manipulating Mammalian Cell Surfaces. *Acs Biomater Sci Eng* **2018,** *4* (11), 3658-3677.

(22) Teramura, Y.; Iwata, H., Cell surface modification with polymers for biomedical studies. *Soft Matter* **2010,** *6* (6), 1081-1091.

(23) Sampathkumar, S. G.; Jones, M. B.; Yarema, K. J., Metabolic expression of thiol-derivatized sialic acids on the cell surface and their quantitative estimation by flow cytometry. *Nat Protoc* **2006,** *1* (4), 1840-51.

(24) Wilson, J. T.; Cui, W.; Kozlovskaya, V.; Kharlampieva, E.; Pan, D.; Qu, Z.; Krishnamurthy, V. R.; Mets, J.; Kumar, V.; Wen, J.; Song, Y.; Tsukruk, V. V.; Chaikof, E. L., Cell surface engineering with polyelectrolyte multilayer thin films. *J Am Chem Soc* **2011,** *133* (18), 7054-64.

(25) Lingwood, D.; Simons, K., Lipid rafts as a membrane-organizing principle. *Science* **2010,** *327* (5961), 46-50.

(26) Lee, D. Y.; Cha, B. H.; Jung, M.; Kim, A. S.; Bull, D. A.; Won, Y. W., Cell surface engineering and application in cell delivery to heart diseases. *J Biol Eng* **2018,** *12*, 28.

(27) Torres, A. G.; Gait, M. J., Exploiting cell surface thiols to enhance cellular uptake. *Trends Biotechnol* **2012,** *30* (4), 185-90.

(28) Matsusaki, M.; Kadowaki, K.; Nakahara, Y.; Akashi, M., Fabrication of cellular multilayers with nanometer-sized extracellular matrix films. *Angew Chem Int Ed Engl* **2007,** *46* (25), 4689-92.

(29) Krol, S.; del Guerra, S.; Grupillo, M.; Diaspro, A.; Gliozzi, A.; Marchetti, P., Multilayer nanoencapsulation. New approach for immune protection of human pancreatic islets. *Nano Lett* **2006,** *6* (9), 1933-9.

(30) Miura, S.; Teramura, Y.; Iwata, H., Encapsulation of islets with ultra-thin polyion complex membrane through poly(ethylene glycol)-phospholipids anchored to cell membrane. *Biomaterials* **2006,** *27* (34), 5828-35.

(31) Stephan, M. T.; Irvine, D. J., Enhancing cell therapies from the outside in: Cell surface engineering using synthetic nanomaterials. *Nano Today* **2011,** *6* (3), 309-325.

(32) Shi, P.; Ju, E.; Yan, Z.; Gao, N.; Wang, J.; Hou, J.; Zhang, Y.; Ren, J.; Qu, X., Spatiotemporal control of cell-cell reversible interactions using molecular engineering. *Nat Commun* **2016,** *7*, 13088.

(33) Xu, J.; Jung, K.; Atme, A.; Shanmugam, S.; Boyer, C., A robust and versatile photoinduced living polymerization of conjugated and unconjugated monomers and its oxygen tolerance. *J Am Chem Soc* **2014,** *136* (14), 5508-19.

(34) Niu, J.; Lunn, D. J.; Pusuluri, A.; Yoo, J. I.; O'Malley, M. A.; Mitragotri, S.; Soh, H. T.; Hawker, C. J., Engineering live cell surfaces with functional polymers via cytocompatible controlled radical polymerization. *Nat Chem* **2017,** *9* (6), 537-545.

(35) Lord, M. S.; Foss, M.; Besenbacher, F., Influence of nanoscale surface topography on protein adsorption and cellular response. *Nano Today* **2010,** *5* (1), 66-78.

(36) Jiang, W.; Kim, B. Y. S.; Rutka, J. T.; Chan, W. C. W., Nanoparticle-mediated cellular response is size-dependent. *Nat Nanotechnol* **2008,** *3* (3), 145-150.

(37) Stephan, M. T.; Moon, J. J.; Um, S. H.; Bershteyn, A.; Irvine, D. J., Therapeutic cell engineering with surface-conjugated synthetic nanoparticles. *Nature Medicine* **2010,** *16* (9), 1035-U135.

(38) Su, G. X.; Zhou, H. Y.; Mu, Q. X.; Zhang, Y.; Li, L. W.; Jiao, P. F.; Jiang, G. B.; Yan, B., Effective Surface Charge Density Determines the Electrostatic Attraction between Nanoparticles and Cells. *J Phys Chem C* **2012,** *116* (8), 4993-4998.

(39) Huebsch, N.; Arany, P. R.; Mao, A. S.; Shvartsman, D.; Ali, O. A.; Bencherif, S. A.; Rivera-Feliciano, J.; Mooney, D. J., Harnessing traction-mediated manipulation of the cell/matrix interface to control stem-cell fate. *Nat Mater* **2010,** *9* (6), 518-26.

(40) Mao, A. S.; Shin, J. W.; Utech, S.; Wang, H.; Uzun, O.; Li, W.; Cooper, M.; Hu, Y.; Zhang, L.; Weitz, D. A.; Mooney, D. J., Deterministic encapsulation of single cells in thin tunable microgels for niche modelling and therapeutic delivery. *Nat Mater* **2017,** *16* (2), 236-243.

(41) Kircher, M. F.; Gambhir, S. S.; Grimm, J., Noninvasive cell-tracking methods. *Nat Rev Clin Oncol* **2011,** *8* (11), 677-88.

(42) Babic, M.; Horak, D.; Trchova, M.; Jendelova, P.; Glogarova, K.; Lesny, P.; Herynek, V.; Hajek, M.; Sykova, E., Poly(L-lysine)-modified iron oxide nanoparticles for stem cell labeling. *Bioconjug Chem* **2008,** *19* (3), 740-50.

(43) Lee, S.; Yoon, H. I.; Na, J. H.; Jeon, S.; Lim, S.; Koo, H.; Han, S. S.; Kang, S. W.; Park, S. J.; Moon, S. H.; Park, J. H.; Cho, Y. W.; Kim, B. S.; Kim, S. K.; Lee, T.; Kim, D.; Lee, S.; Pomper, M. G.; Kwon, I. C.; Kim, K., In vivo stem cell tracking with imageable nanoparticles that bind bioorthogonal chemical receptors on the stem cell surface. *Biomaterials* **2017,** *139*, 12-29.

(44) Mangi, A. A.; Noiseux, N.; Kong, D.; He, H.; Rezvani, M.; Ingwall, J. S.; Dzau, V. J., Mesenchymal stem cells modified with Akt prevent remodeling and restore performance of infarcted hearts. *Nat Med* **2003,** *9* (9), 1195-201.

(45) Laflamme, M. A.; Chen, K. Y.; Naumova, A. V.; Muskheli, V.; Fugate,

J. A.; Dupras, S. K.; Reinecke, H.; Xu, C.; Hassanipour, M.; Police, S.; O'Sullivan, C.; Collins, L.; Chen, Y.; Minami, E.; Gill, E. A.; Ueno, S.; Yuan, C.; Gold, J.; Murry, C. E., Cardiomyocytes derived from human embryonic stem cells in pro-survival factors enhance function of infarcted rat hearts. *Nat Biotechnol* **2007,** *25* (9), 1015-24.

(46) Fakhrullin, R. F.; Zamaleeva, A. I.; Minullina, R. T.; Konnova, S. A.; Paunov, V. N., Cyborg cells: functionalisation of living cells with polymers and nanomaterials. *Chem Soc Rev* **2012,** *41* (11), 4189-206.

(47) Huang, X.; Zhang, F.; Wang, H.; Niu, G.; Choi, K. Y.; Swierczewska, M.; Zhang, G.; Gao, H.; Wang, Z.; Zhu, L.; Choi, H. S.; Lee, S.; Chen, X., Mesenchymal stem cell-based cell engineering with multifunctional mesoporous silica nanoparticles for tumor delivery. *Biomaterials* **2013,** *34* (7), 1772-80.

(48) Wilson, J. T.; Krishnamurthy, V. R.; Cui, W.; Qu, Z.; Chaikof, E. L., Noncovalent cell surface engineering with cationic graft copolymers. *J Am Chem Soc* **2009,** *131* (51), 18228-9.

(49) Fliervoet, L. A. L.; Mastrobattista, E., Drug delivery with living cells. *Adv Drug Deliv Rev* **2016,** *106* (Pt A), 63-72.

(50) Stephan, M. T.; Moon, J. J.; Um, S. H.; Bershteyn, A.; Irvine, D. J., Therapeutic cell engineering with surface-conjugated synthetic nanoparticles. *Nat Med* **2010,** *16* (9), 1035-41.

(51) Hayashi, T.; Yasueda, Y.; Tamura, T.; Takaoka, Y.; Hamachi, I., Analysis of Cell-Surface Receptor Dynamics through Covalent Labeling by Catalyst-Tethered Antibody. *J Am Chem Soc* **2015,** *137* (16), 5372-80.

(52) Rossi, N. A.; Constantinescu, I.; Brooks, D. E.; Scott, M. D.; Kizhakkedathu, J. N., Enhanced cell surface polymer grafting in concentrated and

nonreactive aqueous polymer solutions. *J Am Chem Soc* **2010,** *132* (10), 3423-30.

(53) Takaoka, Y.; Ojida, A.; Hamachi, I., Protein organic chemistry and applications for labeling and engineering in live-cell systems. *Angew Chem Int Ed Engl* **2013,** *52* (15), 4088-106.

(54) Rabuka, D.; Forstner, M. B.; Groves, J. T.; Bertozzi, C. R., Noncovalent cell surface engineering: incorporation of bioactive synthetic glycopolymers into cellular membranes. *J Am Chem Soc* **2008,** *130* (18), 5947-53.

(55) Sampathkumar, S. G.; Li, A. V.; Jones, M. B.; Sun, Z.; Yarema, K. J., Metabolic installation of thiols into sialic acid modulates adhesion and stem cell biology. *Nat Chem Biol* **2006,** *2* (3), 149-52.

(56) Cheng, H.; Kastrup, C. J.; Ramanathan, R.; Siegwart, D. J.; Ma, M.; Bogatyrev, S. R.; Xu, Q.; Whitehead, K. A.; Langer, R.; Anderson, D. G., Nanoparticulate cellular patches for cell-mediated tumoritropic delivery. *ACS Nano* **2010,** *4* (2), 625-31.

(57) Dutta, D.; Pulsipher, A.; Luo, W.; Yousaf, M. N., Synthetic chemoselective rewiring of cell surfaces: generation of three-dimensional tissue structures. *J Am Chem Soc* **2011,** *133* (22), 8704-13.

(58) Rossi, N. A.; Constantinescu, I.; Kainthan, R. K.; Brooks, D. E.; Scott, M. D.; Kizhakkedathu, J. N., Red blood cell membrane grafting of multi-functional hyperbranched polyglycerols. *Biomaterials* **2010,** *31* (14), 4167-78.

(59) Kang, K.; Joo, S.; Choi, J. Y.; Geum, S.; Hong, S. P.; Lee, S. Y.; Kim, Y. H.; Kim, S. M.; Yoon, M. H.; Nam, Y.; Lee, K. B.; Lee, H. Y.; Choi, I. S., Tissue-based metabolic labeling of polysialic acids in living primary hippocampal neurons. *Proc Natl Acad Sci U S A* **2015,** *112* (3), E241-8.

(60) Laughlin, S. T.; Baskin, J. M.; Amacher, S. L.; Bertozzi, C. R., In vivo

imaging of membrane-associated glycans in developing zebrafish. *Science* **2008,** *320* (5876), 664-7.

(61) Mahal, L. K.; Yarema, K. J.; Bertozzi, C. R., Engineering chemical reactivity on cell surfaces through oligosaccharide biosynthesis. *Science* **1997,** *276* (5315), 1125-8.

(62) Yu, K. R.; Shin, J. H.; Kim, J. J.; Koog, M. G.; Lee, J. Y.; Choi, S. W.; Kim, H. S.; Seo, Y.; Lee, S.; Shin, T. H.; Jee, M. K.; Kim, D. W.; Jung, S. J.; Shin, S.; Han, D. W.; Kang, K. S., Rapid and Efficient Direct Conversion of Human Adult Somatic Cells into Neural Stem Cells by HMGA2/let-7b. *Cell Rep* **2015,** *10* (3), 441-452.

(63) Ackerman, G. A., Substituted naphthol AS phosphate derivatives for the localization of leukocyte alkaline phosphatase activity. *Lab Invest* **1962,** *11*, 563-7.

(64) Kaplow, L. S., A histochemical procedure for localizing and evaluating leukocyte alkaline phosphatase activity in smears of blood and marrow. *Blood* **1955,** *10* (10), 1023-9.

(65) Creczynski-Pasa, T. B.; Millone, M. A.; Munford, M. L.; de Lima, V. R.; Vieira, T. O.; Benitez, G. A.; Pasa, A. A.; Salvarezza, R. C.; Vela, M. E., Self-assembled dithiothreitol on Au surfaces for biological applications: phospholipid bilayer formation. *Phys Chem Chem Phys* **2009,** *11* (7), 1077-84.

(66) Pan, L.; He, Q.; Liu, J.; Chen, Y.; Ma, M.; Zhang, L.; Shi, J., Nuclear-targeted drug delivery of TAT peptide-conjugated monodisperse mesoporous silica nanoparticles. *J Am Chem Soc* **2012,** *134* (13), 5722-5.

(67) Han, J. C.; Han, G. Y., A procedure for quantitative determination of tris(2-carboxyethyl)phosphine, an odorless reducing agent more stable and effective than dithiothreitol. *Anal Biochem* **1994,** *220* (1), 5-10.

(68) Kirley, T. L., Reduction and fluorescent labeling of cyst(e)ine-containing proteins for subsequent structural analyses. *Anal Biochem* **1989,** *180* (2), 231-6.

(69) Gong, P. Y.; Zheng, W. F.; Huang, Z.; Zhang, W.; Xiao, D.; Jiang, X. Y., A Strategy for the Construction of Controlled, Three-Dimensional, Multilayered, Tissue-Like Structures. *Adv Funct Mater* **2013,** *23* (1), 42-46.

(70) Hwang, N. S.; Kim, M. S.; Sampattavanich, S.; Baek, J. H.; Zhang, Z. J.; Elisseeff, J., Effects of three-dimensional culture and growth factors on the chondrogenic differentiation of murine embryonic stem cells. *Stem Cells* **2006,** *24* (2), 284-291.

(71) Kim, H. D.; Heo, J.; Hwang, Y.; Kwak, S. Y.; Park, O. K.; Kim, H.; Varghese, S.; Hwang, N. S., Extracellular-Matrix-Based and Arg-Gly-Asp-Modified Photopolymerizing Hydrogels for Cartilage Tissue Engineering. *Tissue Eng Pt A* **2015,** *21* (3-4), 757-766.

(72) Uccelli, A.; Moretta, L.; Pistoia, V., Mesenchymal stem cells in health and disease. *Nat Rev Immunol* **2008,** *8* (9), 726-36.

(73) Nombela-Arrieta, C.; Ritz, J.; Silberstein, L. E., The elusive nature and function of mesenchymal stem cells. *Nat Rev Mol Cell Biol* **2011,** *12* (2), 126-31.

(74) Duijvestein, M.; Vos, A. C.; Roelofs, H.; Wildenberg, M. E.; Wendrich, B. B.; Verspaget, H. W.; Kooy-Winkelaar, E. M.; Koning, F.; Zwaginga, J. J.; Fidder, H. H.; Verhaar, A. P.; Fibbe, W. E.; van den Brink, G. R.; Hommes, D. W., Autologous bone marrow-derived mesenchymal stromal cell treatment for refractory luminal Crohn's disease: results of a phase I study. *Gut* **2010,** *59* (12), 1662-9.

(75) Connick, P.; Kolappan, M.; Crawley, C.; Webber, D. J.; Patani, R.; Michell, A. W.; Du, M. Q.; Luan, S. L.; Altmann, D. R.; Thompson, A. J.; Compston, A.; Scott, M. A.; Miller, D. H.; Chandran, S., Autologous mesenchymal

stem cells for the treatment of secondary progressive multiple sclerosis: an open-label phase 2a proof-of-concept study. *Lancet Neurol* **2012,** *11* (2), 150-6.

(76) Kim, H. D.; Jang, H. L.; Ahn, H. Y.; Lee, H. K.; Park, J.; Lee, E. S.; Lee, E. A.; Jeong, Y. H.; Kim, D. G.; Nam, K. T.; Hwang, N. S., Biomimetic whitlockite inorganic nanoparticles-mediated in situ remodeling and rapid bone regeneration. *Biomaterials* **2017,** *112*, 31-43.

(77) Caplan, A. I.; Correa, D., The MSC: an injury drugstore. *Cell Stem Cell* **2011,** *9* (1), 11-5.

(78) Watt, F. M.; Hogan, B. L., Out of Eden: stem cells and their niches. *Science* **2000,** *287* (5457), 1427-30.

(79) Yin, H.; Price, F.; Rudnicki, M. A., Satellite cells and the muscle stem cell niche. *Physiol Rev* **2013,** *93* (1), 23-67.

(80) Scadden, D. T., Nice neighborhood: emerging concepts of the stem cell niche. *Cell* **2014,** *157* (1), 41-50.

(81) Wagers, A. J., The stem cell niche in regenerative medicine. *Cell Stem Cell* **2012,** *10* (4), 362-9.

(82) Nelson, C. M.; Jean, R. P.; Tan, J. L.; Liu, W. F.; Sniadecki, N. J.; Spector, A. A.; Chen, C. S., Emergent patterns of growth controlled by multicellular form and mechanics. *Proc Natl Acad Sci U S A* **2005,** *102* (33), 11594-9.

(83) Hwang, N. S.; Varghese, S.; Zhang, Z.; Elisseeff, J., Chondrogenic differentiation of human embryonic stem cell-derived cells in arginine-glycine-aspartate-modified hydrogels. *Tissue Eng* **2006,** *12* (9), 2695-706.

(84) Kloxin, A. M.; Kasko, A. M.; Salinas, C. N.; Anseth, K. S., Photodegradable hydrogels for dynamic tuning of physical and chemical properties. *Science* **2009,** *324* (5923), 59-63.

(85) Hamilton, D. W.; Maul, T. M.; Vorp, D. A., Characterization of the response of bone marrow-derived progenitor cells to cyclic strain: implications for vascular tissue-engineering applications. *Tissue Eng* **2004,** *10* (3-4), 361-9.

(86) Loye, A. M.; Kinser, E. R.; Bensouda, S.; Shayan, M.; Davis, R.; Wang, R.; Chen, Z.; Schwarz, U. D.; Schroers, J.; Kyriakides, T. R., Regulation of Mesenchymal Stem Cell Differentiation by Nanopatterning of Bulk Metallic Glass. *Sci Rep* **2018,** *8* (1), 8758.

(87) Tang, J.; Peng, R.; Ding, J., The regulation of stem cell differentiation by cell-cell contact on micropatterned material surfaces. *Biomaterials* **2010,** *31* (9), 2470-6.

(88) Kim, H.; Shin, K.; Park, O. K.; Choi, D.; Kim, H. D.; Baik, S.; Lee, S. H.; Kwon, S. H.; Yarema, K. J.; Hong, J.; Hyeon, T.; Hwang, N. S., General and Facile Coating of Single Cells via Mild Reduction. *J Am Chem Soc* **2018,** *140* (4), 1199-1202.

(89) Cha, J.; Kim, H.; Hwang, N. S.; Kim, P., Mild Reduction of the Cancer Cell Surface as an Anti-invasion Treatment. *ACS Appl Mater Interfaces* **2018,** *10* (42), 35676-35680.

(90) Dominici, M.; Le Blanc, K.; Mueller, I.; Slaper-Cortenbach, I.; Marini, F.; Krause, D.; Deans, R.; Keating, A.; Prockop, D.; Horwitz, E., Minimal criteria for defining multipotent mesenchymal stromal cells. The International Society for Cellular Therapy position statement. *Cytotherapy* **2006,** *8* (4), 315-7.

(91) Maleki, M.; Ghanbarvand, F.; Reza Behvarz, M.; Ejtemaei, M.; Ghadirkhomi, E., Comparison of mesenchymal stem cell markers in multiple human adult stem cells. *Int J Stem Cells* **2014,** *7* (2), 118-26.

(92) Titushkin, I.; Cho, M., Regulation of cell cytoskeleton and membrane

mechanics by electric field: role of linker proteins. *Biophys J* **2009,** *96* (2), 717-28.

(93) Ryu, K. H.; Cho, K. A.; Park, H. S.; Kim, J. Y.; Woo, S. Y.; Jo, I.; Choi, Y. H.; Park, Y. M.; Jung, S. C.; Chung, S. M.; Choi, B. O.; Kim, H. S., Tonsil-derived mesenchymal stromal cells: evaluation of biologic, immunologic and genetic factors for successful banking. *Cytotherapy* **2012,** *14* (10), 1193-202.

(94) Jung, J.; Choi, J. H.; Lee, Y.; Park, J. W.; Oh, I. H.; Hwang, S. G.; Kim, K. S.; Kim, G. J., Human placenta-derived mesenchymal stem cells promote hepatic regeneration in CCl4 -injured rat liver model via increased autophagic mechanism. *Stem Cells* **2013,** *31* (8), 1584-96.

(95) Park, M.; Kim, Y. H.; Woo, S. Y.; Lee, H. J.; Yu, Y.; Kim, H. S.; Park, Y. S.; Jo, I.; Park, J. W.; Jung, S. C.; Lee, H.; Jeong, B.; Ryu, K. H., Tonsil-derived mesenchymal stem cells ameliorate CCl4-induced liver fibrosis in mice via autophagy activation. *Sci Rep* **2015,** *5*, 8616.

(96) Biggs, M. J.; Dalby, M. J., Focal adhesions in osteoneogenesis. *Proc Inst Mech Eng H* **2010,** *224* (12), 1441-53.

(97) Mathieu, P. S.; Loboa, E. G., Cytoskeletal and focal adhesion influences on mesenchymal stem cell shape, mechanical properties, and differentiation down osteogenic, adipogenic, and chondrogenic pathways. *Tissue Eng Part B Rev* **2012,** *18* (6), 436-44.

(98) Hu, J.; Liao, H.; Ma, Z.; Chen, H.; Huang, Z.; Zhang, Y.; Yu, M.; Chen, Y.; Xu, J., Focal Adhesion Kinase Signaling Mediated the Enhancement of Osteogenesis of Human Mesenchymal Stem Cells Induced by Extracorporeal Shockwave. *Sci Rep* **2016,** *6*, 20875.

(99) Miron, R. J.; Zhang, Y. F., Osteoinduction: a review of old concepts with new standards. *J Dent Res* **2012,** *91* (8), 736-44.

(100) Rosu-Myles, M.; Fair, J.; Pearce, N.; Mehic, J., Non-multipotent stroma inhibit the proliferation and differentiation of mesenchymal stromal cells in vitro. *Cytotherapy* **2010,** *12* (6), 818-30.

(101) Anderson, P.; Carrillo-Galvez, A. B.; Garcia-Perez, A.; Cobo, M.; Martin, F., CD105 (endoglin)-negative murine mesenchymal stromal cells define a new multipotent subpopulation with distinct differentiation and immunomodulatory capacities. *PLoS One* **2013,** *8* (10), e76979.

(102) Levi, B.; Wan, D. C.; Glotzbach, J. P.; Hyun, J.; Januszyk, M.; Montoro, D.; Sorkin, M.; James, A. W.; Nelson, E. R.; Li, S.; Quarto, N.; Lee, M.; Gurtner, G. C.; Longaker, M. T., CD105 protein depletion enhances human adipose-derived stromal cell osteogenesis through reduction of transforming growth factor beta1 (TGF-beta1) signaling. *J Biol Chem* **2011,** *286* (45), 39497-509.

(103) Farina, M.; Alexander, J. F.; Thekkedath, U.; Ferrari, M.; Grattoni, A., Cell encapsulation: Overcoming barriers in cell transplantation in diabetes and beyond. *Adv Drug Deliv Rev* **2019,** *139*, 92-115.

(104) Mitrousis, N.; Fokina, A.; Shoichet, M. S., Biomaterials for cell transplantation. *Nat Rev Mater* **2018,** *3* (11), 441-456.

(105) Foster, G. A.; Garcia, A. J., Bio-synthetic materials for immunomodulation of islet transplants. *Adv Drug Deliver Rev* **2017,** *114*, 266-271.

(106) Hasturk, O.; Kaplan, D. L., Cell armor for protection against environmental stress: Advances, challenges and applications in micro- and nanoencapsulation of mammalian cells. *Acta Biomater* **2019,** *95*, 3-31.

(107) Orive, G.; Hernandez, R. M.; Gascon, A. R.; Calafiore, R.; Chang, T. M. S.; De Vos, P.; Hortelano, G.; Hunkeler, D.; Lacik, I.; Shapiro, A. M. J.; Pedraz, J. L., Cell encapsulation: Promise and progress. *Nat Med* **2003,** *9* (1), 104-107.

(108) Kozlovskaya, V.; Zavgorodnya, O.; Chen, Y.; Ellis, K.; Tse, H. M.; Cui, W. X.; Thompson, J. A.; Kharlampieva, E., Ultrathin Polymeric Coatings Based on Hydrogen-Bonded Polyphenol for Protection of Pancreatic Islet Cells. *Adv Funct Mater* **2012,** *22* (16), 3389-3398.

(109) Pham-Hua, D.; Padgett, L. E.; Xue, B.; Anderson, B.; Zeiger, M.; Barra, J. M.; Bethea, M.; Hunter, C. S.; Kozlovskaya, V.; Kharlampieva, E.; Tse, H. M., Islet encapsulation with polyphenol coatings decreases pro-inflammatory chemokine synthesis and T cell trafficking. *Biomaterials* **2017,** *128*, 19-32.

(110) Stabler, C. L.; Li, Y.; Stewart, J. M.; Keselowsky, B. C., Engineering immunomodulatory biomaterials for type 1 diabetes. *Nat Rev Mater* **2019,** *4* (6), 429-450.

(111) Bose, S.; Volpatti, L. R.; Thiono, D.; Yesilyurt, V.; McGladrigan, C.; Tang, Y. Y.; Facklam, A.; Wang, A.; Jhunjhunwala, S.; Veiseh, O.; Hollister-Lock, J.; Bhattacharya, C.; Weir, G. C.; Greiner, D. L.; Langer, R.; Anderson, D. G., A retrievable implant for the long-term encapsulation and survival of therapeutic xenogeneic cells. *Nat Biomed Eng* **2020**.

(112) Vegas, A. J.; Veiseh, O.; Gurtler, M.; Millman, J. R.; Pagliuca, F. W.; Bader, A. R.; Doloff, J. C.; Li, J.; Chen, M.; Olejnik, K.; Tam, H. H.; Jhunjhunwala, S.; Langan, E.; Aresta-Dasilva, S.; Gandham, S.; McGarrigle, J. J.; Bochenek, M. A.; Hollister-Lock, J.; Oberholzer, J.; Greiner, D. L.; Weir, G. C.; Melton, D. A.; Langer, R.; Anderson, D. G., Long-term glycemic control using polymer-encapsulated human stem cell-derived beta cells in immune-competent mice (vol 22, pg 306, 2016). *Nature Medicine* **2016,** *22* (4), 446-446.

(113) Desai, T.; Shea, L. D., Advances in islet encapsulation technologies (vol 16, pg 367, 2017). *Nat Rev Drug Discov* **2017,** *16* (5).

(114) Gibly, R. F.; Graham, J. G.; Luo, X.; Lowe, W. L.; Hering, B. J.; Shea, L. D., Advancing islet transplantation: from engraftment to the immune response. *Diabetologia* **2011,** *54* (10), 2494-2505.

(115) Shapiro, A. M. J.; Pokrywczynska, M.; Ricordi, C., Clinical pancreatic islet transplantation. *Nat Rev Endocrinol* **2017,** *13* (5), 268-277.

(116) Shapiro, A. M. J.; Ricordi, C.; Hering, B. J.; Auchincloss, H.; Lindblad, R.; Robertson, P.; Secchi, A.; Brendel, M. D.; Berney, T.; Brennan, D. C.; Cagliero, E.; Alejandro, R.; Ryan, E. A.; DiMercurio, B.; Morel, P.; Polonsky, K. S.; Reems, J. A.; Bretzel, R. G.; Bertuzzi, F.; Froud, T.; Kandaswamy, R.; Sutherland, D. E. R.; Eisenbarth, G.; Segal, M.; Preiksaitis, J.; Korbutt, G. S.; Barton, F. B.; Viviano, L.; Seyfert-Margolis, V.; Bluestone, J.; Lakey, J. R. T., International trial of the edmonton protocol for islet transplantation. *New Engl J Med* **2006,** *355* (13), 1318-1330.

(117) Mao, A. S.; Shin, J. W.; Utech, S.; Wang, H. N.; Uzun, O.; Li, W. W.; Cooper, M.; Hu, Y. B.; Zhang, L. Y.; Weitz, D. A.; Mooney, D. J., Deterministic encapsulation of single cells in thin tunable microgels for niche modelling and therapeutic delivery. *Nat Mater* **2017,** *16* (2), 236-243.

(118) Colton, C. K., Oxygen supply to encapsulated therapeutic cells. *Adv Drug Deliver Rev* **2014,** *67-68*, 93-110.

(119) Velasco, D.; Tumarkin, E.; Kumacheva, E., Microfluidic Encapsulation of Cells in Polymer Microgels. *Small* **2012,** *8* (11), 1633-1642.

(120) Ryan, A. J.; O'Neill, H. S.; Duffy, G. P.; O'Brien, F. J., Advances in polymeric islet cell encapsulation technologies to limit the foreign body response and provide immunoisolation. *Curr Opin Pharmacol* **2017,** *36*, 66-71.

(121) Fukuda, Y.; Akagi, T.; Asaoka, T.; Eguchi, H.; Sasaki, K.; Iwagami,

Y.; Yamada, D.; Noda, T.; Kawamoto, K.; Gotoh, K.; Kobayashi, S.; Mori, M.; Doki, Y.; Akashi, M., Layer-by-layer cell coating technique using extracellular matrix facilitates rapid fabrication and function of pancreatic beta-cell spheroids. *Biomaterials* **2018,** *160*, 82-91.

(122) Hwang, J.; Choi, D.; Choi, M.; Seo, Y.; Son, J.; Hong, J.; Choi, J., Synthesis and Characterization of Functional Nanofilm-Coated Live Immune Cells. *Acs Appl Mater Inter* **2018,** *10* (21), 17685-17692.

(123) Wilson, J. T.; Cui, W. X.; Kozovskaya, V.; Kharlampieva, E.; Pan, D.; Qu, Z.; Krishnamurthy, V. R.; Mets, J.; Kumar, V.; Wen, J.; Song, Y. H.; Tsukruk, V. V.; Chaikof', E. L., Cell Surface Engineering with Polyelectrolyte Multilayer Thin Films. *J Am Chem Soc* **2011,** *133* (18), 7054-7064.

(124) Kim, S. H.; Lee, S. H.; Lee, J. E.; Park, S. J.; Kim, K.; Kim, I. S.; Lee, Y. S.; Hwang, N. S.; Kim, B. G., Tissue adhesive, rapid forming, and sprayable ECM hydrogel via recombinant tyrosinase crosslinking. *Biomaterials* **2018,** *178*, 401-412.

(125) Faure, E.; Falentin-Daudre, C.; Jerome, C.; Lyskawa, J.; Fournier, D.; Woisel, P.; Detrembleur, C., Catechols as versatile platforms in polymer chemistry. *Prog Polym Sci* **2013,** *38* (1), 236-270.

(126) Land, E. J.; Ramsden, C. A.; Riley, P. A., Tyrosinase autoactivation and the chemistry of ortho-quinone amines. *Accounts Chem Res* **2003,** *36* (5), 300-308.

(127) Bal, T.; Oran, D. C.; Sasaki, Y.; Akiyoshi, K.; Kizilel, S., Sequential Coating of Insulin Secreting Beta Cells within Multilayers of Polysaccharide Nanogels. *Macromol Biosci* **2018,** *18* (5).

(128) Perez-Armendariz, E. M., Connexin 36, a key element in pancreatic beta cell function. *Neuropharmacology* **2013,** *75*, 557-566.

(129) Shyr, Z. A.; Wang, Z. Y.; Wyork, N.; Nichols, C. G.; Remedi, M. S., The role of membrane excitability in pancreatic beta-cell glucotoxicity. *Sci Rep-Uk* **2019,** *9*.

(130) Kyluik-Price, D. L.; Scott, M. D., Effects of methoxypoly (Ethylene glycol) mediated immunocamouflage on leukocyte surface marker detection, cell conjugation, activation and alloproliferation. *Biomaterials* **2016,** *74*, 167-177.

6.3 Bibliography

1. Journal Publication (* denotes co-first authors)

1) **Hyunbum Kim***, Yunhye Kim*, Jihyun Park, Nathaniel S. Hwang, Yun Kyung Lee and Yongsung Hwang, "Recent Advances in Engineered Cell Sheets for Tissue Regeneration", ***Polymers***, 2019

2) **Hyunbum Kim***, Kwangsoo Shin*, Ok Kyu Park*, Daheui Choi, Hwan D. Kim, Seungmin Baik, Soo Hong Lee, Seung-Hae Kwon, Kevin J. Yarema, Jinkee Hong, Taeghwan Hyeon and Nathaniel S. Hwang, "General and Facile Coating of Single Cells via Mild Reduction", ***Journal of the American Chemical Society***, 2018

3) Seungmi Ryu*, **Hyunbum Kim***, Seokyung Kang, Kwangsoo Shin, Seon-Yeop Jung, Jiwoong Heo, Jin Han, Jeong-Kee Yoon, Ju-Ro Lee, Jinkee Hong, Kyung Hyun Ahn, Taeghwan Hyeon, Nathaniel S. Hwang and Byung-Soo Kim, "Reversible Cell Layering for Heterogenous Cell Assembly Mediated by Ionic Crosslinking of Chitosan and Functionalized Cell Surface Membrane", ***Chemistry of Materials***, 2017

4) Junghwa Cha, **Hyunbum Kim**, Nathaniel S. Hwang and Philnam Kim, "Mild Reduction of the Cancer Cell Surface as an Anti-invasion Treatment", ***ACS Appl. Mater. Interfaces***, 2018

5) Hwan D. Kim, Jiseung Heo, Yongsung Hwang, Seon-Yeong Kwak, Ok Kyu Park, **Hyunbum Kim**, Shyni Varghese and Nathaniel S. Hwang, "Cell responsive ECM-based hydrogels for functional cartilage tissue engineering", ***Tissue Engineering Part A***, 2015

2. Book chapter

1) **Hyunbum Kim**, Yunhye Kim, Mona Fendereski, Nathaniel S. Hwang and Yongsung Hwang, "Recent Advancements in Decellularized Matrix-Based Biomaterials for Musculoskeletal Tissue Regeneration", ***Novel Biomaterials for Regenerative Medicine. Advances in Experimental Medicine and Biology***, Springer, 2018

2) **Hyunbum Kim**, Seung-Hyun L. Kim, Young-Hwan Choi, Young-Hyun Ahn and Nathaniel S. Hwang, "Biomaterials for Stem Cell Therapy for Cardiac Disease", ***Biomimetic Medical Materials. Advances in Experimental Medicine and Biology***, Springer, 2018

3. Patent

1) Nathaniel S. Hwang, Taeghwan Hyeon, **Hyunbum Kim**, Kwangsoo shin "Surface modified cell and its formation method", **2015**
Korea patent, Application number: 10-2015- 0007166

2) Nathaniel S. Hwang, Byungsoo Kim, **Hyunbum Kim**, Seungmi Ryu "Co-culturing method of multi-cell", **2018**
Korea patent, Application number: 10-2018-0000508

국문 초록

세포 표면 개질을 통한 효과적인 줄기세포 치료제 개발

줄기 세포 치료제는 다양한 퇴행성 질환 및 손상된 기관을 치료하기위한 유망한 접근법으로 주목을 받고 있다. 줄기 세포의 이식 및 직접 주사는 선천성 결함 치료를 위한 실용적인 해결책을 또한 제공하고 있다. 그러나, 주사 시 또는 투여 후 외부 스트레스와 동종 숙주 면역 거부 반응에 따른 투여된 세포의 생존율 및 치료 효과의 감소는 세포 치료제의 광범위한 활용을 제한되고 있다. 결과적으로, 이식 전에 줄기 세포 치료제의 효능을 결정하고 치료 결과를 향상시키기 위해서는 일반적인 접근성 및 다목적 성을 갖는 다양한 전략이 필요하다.

이러한 요구에 따라, 천연 또는 합성 생체 재료를 이용한 세포 표면 개질 방법은 줄기 세포 치료 기술로서 광범위하게 연구되고 있다. 세포 기능은 공유결합, 소수성 상호 작용 및 정전 기적 상호 작용을 통해 세포 표면에 도입된 다양한 활성 작용기를 활용함으로써 조절될 수 있다. 세포 표면에 외인성 물질을 결합시키면 세포가 보다 복잡한 생물학적 환경에 이식될 때 일반세포 보다 안정적으로 생체 내에서 활성화될 수 있다. 추가적으로, 생체 고분자를 활용해서 세포 표면을 개질 할 경우, 세포 표면의 항원을 고분자로 덮게 됨으로써 면역 세포가 이식된 세포를

제대로 인식하지 못해 적응면역계를 억제하는 결과를 가져올 수 있다. 따라서, 이 논문에서 소개될 세포 표면 개질 전략은 조직 공학 및 병역의학 측면에서 이상적인 줄기 세포 치료제 개발을 위한 중요한 초석이 될 수 있다.

논문의 제1장에서는 세포막 단백질의 이황화 결합을 환원시켜 티올기로 전환하여 이를 활용하는 손쉽고 보편적인 세포 표면 개질 방법을 제시한다. 표면이 개질 된 세포는 말레이미드-티올 화학 접합에 의해 효과적으로 생체고분자들을 세포 표면에 코팅 할 수 있다. 이렇게 코팅된 세포들은 세포 시각화, 신속한 세포 조립, 세포 층 형성, 주변 물질들과 상호 작용 및 국소화 된 세포 기반 약물 전달에 활용된다. 세포 형태, 생존력, 증식 및 대사에 대한 부작용은 관찰되지 않았다. 더 나아가, 폴리에틸렌 글라이콜 생체고분자와 면역억제제가 주입된 나노 입자들로 코팅된 세포들을 마우스에 주입하였을 시에 급성 면역 반응을 견뎌내어 향상된 세포 활동을 관찰할 수 있다.

논문의 제2장에서는 세포 표면 단백질을 환원시키는 미세환경이 중간엽 줄기세포에 미치는 생물학적 효과를 분석하였다. 세포 표면 단백질 수용체들의 환원은 결과적으로 세포 생존력에는 악영향을 미치지 않으면서 초점 접착력의 현저한 증가를 보였다. 결국, 이러한 초점 부착의 상승은 중간엽 줄기세포의 골 형성 분화의 초기 단계를 향상시켰다. 더하여, 세포 표면의 TGF-β 신호 전달 경로의 근본적인 수용체 중 하나인 엔도글린이 환원됨으로써 신호 전달 경로의 하향 조절이 검출되었다. 이 두 효과의 상호 작용을 통해, 줄기 세포의 초점 부착은 상승시키는 반면, 세포 내 신호 전달을 감소하게 유도함으로 초기 골 형성 분화를 상향 조절했다.

마지막으로 논문의 제3장에서는 높은 전단 응력으로부터 세포를

보호하고 세포-세포 상호 작용을 방해하여 면역 반응을 줄일 수 있는 다층 하이드로 겔 나노 필름 형성 방법을 고안했다. 페놀 작용기를 갖도록 2 개의 반대 대전 된 다당류를 개질하고 이를 타이로신 효소를 사용하여 가교 시킴으로 강인하고 탄력 있는 하이드로 겔 나노 필름을 제작하였다. 이 하이드로 겔 나노 필름으로 코팅된 β-세포 스페로이드는 이자 섬 이식에 활용되었다. 코팅된 β-세포 스페로이드 표편의 얇지만 균일하고 치밀한 필름층은 물리적 스트레스와 생체내 면역에 대한 세포 보호 효과를 가졌다. 이렇게 코팅된 스페로이드들을 제1형 당뇨 쥐 모델에 주입하였을 때에 효과적으로 혈당을 조절하는 것을 확인할 수 있다.

종합적으로 세포 표면의 단백질의 이황화결합을 개질 함으로서 다양한 세포 표면에 다양한 생체 물질들을 결합시킬 수 있다는 것을 토대로 이 개질 방법이 줄기세포에 어떠한 영향을 끼치는지를 알아보았다. 그러나, 이황화결합을 환원시키는 방법은 몇 가지 단점들이 있었고, 이를 보완하기 위해 개발된 효소 가교 기반 하이드로 겔 나노 필름 코팅 방법은 제1형 당뇨병 치료에 우수한 성능을 보였으므로 앞으로의 임상 응용 프로그램에 새로운 플랫폼을 제공할 것으로 기대하며 세포 표면 개질을 통한 효과적인 줄기세포 치료제의 가능성을 확인할 수 있다.

주요어: 세포 표면 개질, 생체고분자, 미세환경, 세포 분화, 세포 캡슐화

학번: 2014-21517

감사의 글

끝이 보이지 않았던 석박사과정의 길을 6년 반의 시간을 들여 완주하게 되었습니다. 뒤돌아보면 막상 길게만 느껴 지진 않았던 것 같습니다. 대학원 생활을 하면서 기억에 남는 많은 추억들이 있기에 이 박사학위라는 것이 단순히 지식적인 측면에서만 의미를 지니는 것이 아니라 그 과정 간의 희로애락이 담겨 있어 더욱 의미가 깊었습니다. 석박사과정동안 저와 함께 희로애락으로 인연을 맺은 수많은 사람들께 감사를 드립니다.

먼저, 부족한 저를 지도해주신 지도교수님 황석연 교수님께 감사드립니다. 교수님의 통찰력과 연구에 대한 열정이 없었으면 제 연구들이 이러한 좋은 결과로 나타나지 않았을 것입니다. 교수님을 처음 뵙던 날, 줄기세포나 생체재료에 대해 아무것도 모르는 학부생을 데리고 1시간 넘게 자신의 연구실이 어떠한 연구들을 하는지, 앞으로는 어떠한 방향으로 연구를 할 것인지, 김현범 학생이 연구실에 들어오면 어떠한 연구들을 할 수 있다는 지, 말씀해 주셨던 교수님의 열정이 아직도 생생히 기억납니다. 그런 교수님의 통찰력, 열정, 저의 성장에 대한 믿음을 보았기에 대학원 생활동안 자신감 있게 연구들을 수행해 나갈 수 있었습니다. 항상 건승하시길 진심으로 바라며 저 또한 주신 가르침을 되새겨 훌륭한 연구자가 되도록 노력하겠습니다.

다음으로, 2년의 짧은 기간이었지만 제가 추구하는 진정한 스승이자 연구자에 제일 가까운 이미지를 보여주셨던 황용성 교수님께 감사의 말을 드립니다. 단순히 저에게 급했던 군대 문제를 해결하기 위해 교수님 연구실에 들어갔지만, 제가 그 곳에서 최선을 다해 연구하고 연구실 선배로서 후배들을 대하는 법을 알게 된 것은 교수님의 덕망 때문이었다고 생각합니다. 끝임없이 탐구하시고 항상 열정적이시지만

학생들에게 친절하시고 도움이 되기 위해 노력하시는 교수님을 통해 인격적으로도 많은 성장을 이룰 수 있었습니다.

그리고, 제 연구 내외로 가장 많은 도움을 주었던 신광수 박사님께 감사를 드립니다. 너무나도 많이 부족했던 신입생 때부터 지금에까지, 연구계획수립부터 논문작성법까지 하나하나 알려주시고, 저에게 올바른 '박사'란 어떻게 연구해야 하는지를 알려주시고 직접 보여주셔서 감사합니다. 또한, 매번 어려운 동물실험 부탁을 흔쾌히 수락해주시고 최상의 결과를 도출해 주신 박옥규 박사님, 새로운 아이디어로 제 연구 범위와 생각의 반경을 넓혀 주신 류승미 박사님께도 감사를 드립니다.

제가 있었던 서울대 BMSCE 연구실 식구들에게 또한 감사를 전합니다. 초창기 연구실을 이끌어 주시고 많은 것들을 후배들을 위해 애써 주신 환형과 은지누나, 언제나 든든하고 실험에 있어서는 진지한 모습으로 연구실 남자들의 리더와 같았던 수환형, 같은 무도팬으로서 공감대도 나누고 석사생의 표본이 되어 주신 민의누나, 만날 때마다 항상 긍정적인 에너지를 나눠 주신 이해심 많은 은서누나, 연구실 동기로 들어와서 군대부터 졸업, 포닥 문제까지, 모든 과정마다 함께 했고 항상 도움을 많이 준 영환이형, 연구실 전반을 관리해 주시면서 같이 정보교환도 하고 어려울 때마다 친절하게 도와 주신 희승누나, 동갑의 나이로 같이 수학하고 이번에 다 같이 박사 졸업하고 서로 많은 추억들을 가지고 앞으로도 각자의 길에서 잘되길 항상 응원하는 영현이와 승현이, 좋은 사수의 모습을 보여주지 못해 미안한 마음이 큰 인선이, 많은 시간 사수의 역할을 제대로 해주지 못했지만 떳떳한 석사로 성장해준 민지, 이후의 이어질 연구들을 책임져줄 성실한 영선이, 이 외의 저에게 많은 도움을 준 BMSCE 연구실 다른 모든 학생들에게도 감사함을 전합니다.

마찬가지로 제가 속했던 순천향의생명연구원 연구실 식구들에게도 감사함으로 전합니다. 랩장으로서, 같은 믿음의 사람으로서 책임감이 컸던 윤혜, 모든 분야에서 잘해야 한다는 부담감을 내려놓고 마음 편히 한

단계씩 밟아 나갔으면 좋겠다. 나를 어느 순간에나 형으로서 믿고 따라준 지훈이, 몇 번 말했지만 너의 그 성실함을 토대로 자신감을 더한다면 분명 꽃 필 날이 올 거라 믿어 의심치 않는다. 그리고 타국에 와서도 기운차게 분위기를 띄워주고 연구에 진지하고 열심히 임하는 로렌시아, 타국에서의 박사과정이 더 힘들 수 있겠지만 분명 원하는 결과를 얻을 거라 생각한다. 이 외의 거쳐갔던 몇 명의 인턴들, 그리고 다른 연구실 학생들까지 제가 타지서 연구 및 생활할 때에 적응에 많은 도움을 줘서 감사를 전합니다.

언제나 따뜻한 사랑과 응원을 아끼지 않는 저희 가족들께 진심으로 사랑한다는 말을 전하고 싶습니다. 집에서는 티를 내지도 않고, 마음을 내보이지 않는 아들이지만, 부모님께서 제가 스스로 당당하게 사회에서 설 수 있도록, 제가 앞만 보고 나아갈 수 있게 물심양면으로 도와주시고, 저를 위해 희생해주신 많은 것들에 항상 감사함을 잊지 않고 있습니다. 이제 세상에 나가 더욱 성장한 모습을 보여드릴 테니 항상 강건하시고 꽃 길만 걸으시길 바랍니다.

그리고 이제 함께 인생을 걸어가길 바라는 혜지에게 감사함을 전합니다. 같은 믿음의 동역자로서 항상 내 편이 되어주고, 응원해줬기에 더 좋은 결과로 박사과정을 마무리할 수 있었습니다. 졸업과 동시에 바로 우리 앞에 힘든 길이 놓였지만, 서로가 의지하고, 격려하고, 합심하여 지혜롭게 능히 이 이후에 있을 더 큰 행복을 소망하며 잘 헤쳐 나갈 수 있을 거라 생각해 큰 힘이 됩니다.

마지막으로 저에게 박사가 되는 진로를 내려 주시고, 모든 과정, 순간마다 저와 동행하여 주시고 지혜주시고 힘주신 주님께 감사드립니다.

2020 년 07 월

김현범 드림